A Review of Aeronautical Fatigue Investigations in Brazil

36th Conference - International Committee on Aeronautical Fatigue and Structural Integrity
Krakow – Poland – 3-4 June 2019

Prepared by:

Carlos E. Chaves

On behalf of:

Fatigue, Fracture and Structural Integrity Committee

Brazilian Society of Engineering and Mechanical Sciences - ABCM

SUMMARY

This report presents the review of fatigue investigations related to aeronautics performed in Brazil during the years 2017 to 2019. Its contents will be presented during the 36th ICAF (International Committee on Aeronautical Fatigue and Structural Integrity) Conference to be held in Krakow, Poland, in June 3-4, 2019.

All papers, dissertations, theses and conference proceedings presented in this document were directly supplied by their authors, co-authors or advisors to the author of this review, and some of the works were previously presented in other conferences or are available from public sources.

COVER: EMB-314 (Super Tucano)

CONTENTS

ABBREVIATIONS

3-ENF	Three Point Bend End-notched Flexure
4-ENF	Four Point Bend End-notched Flexure
ABCM	Associação Brasileira de Engenharia e Ciências Mecânicas (Brazilian Society of Engineering and Mechanical Sciences)
ANAC	Agência Nacional de Aviação Civil (Brazilian Civil Aviation Agency)
AR	Augmented Reality
ASTM	American Society for Testing and Materials
CFRP	Carbon Fiber Reinforced Plastics
CB	Co-bonding (related to composites)
CC	Co-curing (related to composites)
CPOF	Cumulative Probability of Failure
CVM	Comparative Vacuum Monitoring
CZM	Cohesive Zone Model
DAH	Design Approval Holder
DCB	Double Cantilever Beam
DCT	Displacement Correction Technique
DCTA	Departamento de Ciência e Tecnologia Aeroespacial (Department of Aerospace Science and Technology)
DEN	Double Edge Notched (Specimen)
DIC	Digital Image Correlation
DMA	Dynamic Mechanical Analysis
DSC	Differential Scanning Calorimetry
EMB	Embraer
ERJ	Embraer Regional Jet
ETW	Elevated Temperature Wet
FAB	Força Aérea Brasileira (Brazilian Air Force)
FCG	Fatigue Crack Growth
FDG	Fatigue Disbond Growth
FEM	Finite Element Method
FML	Fiber Metal Laminate

FRF	Frequency Response Function
FSFT	Full-Scale Fatigue Test
FS	Friction Surfacing
FSW	Friction Stir Welding
GA	Genetic Algorithm
GFEM	Global Finite Element Method
HLUP	Hand Lay-Up
HZG	Helmholtz-Zentrum Geesthacht
ITA	Instituto Tecnológico de Aeronáutica (Aeronautical Institute of Technology)
ISP	Inspection Starting Point (related to WFD)
LOV	Limit of Validity (related to WFD)
LVDT	Linearly Variable Displacement Transducer
LVI	Low Velocity Impact
LW	Lamb Waves
MIM	Metal Injection Molding
MMB	Mixed-Mode Bending
MSD	Multi-Site Damage
M(T)	Middle Tension (Specimen)
MWCM	Modified Wöhler Curve Method
NCF	Non Crimp Fabrics
NDT	Non Destructive Test
NEVF	Nastran Embedded Vibration Fatigue
NRMSE	Normalized Root Mean Square Error
OEM	Original Equipment Manufacturer
POD	Probability of Detection
PSD	Power Spectrum Density
R&D	Research and Development
RH	Relative Humidity
RIFT	Infusion Under Flexible Tooling
RTA	Room Temperature Ambient
RVE	Representative Volume Element
SB	Secondary Bonding (related to composites)
S/A	Sociedade Anônima (Corporation)

SEM	Scanning Electron Microscopy
SERR	Strain Energy Release Rate
SENB	Single Edge Notched (Specimen) in Bending
SFO	Sunflower Optimization Algorithm
SFPF	Single Flight Probability of Failure
SG	Strain Gage
SHM	Structural Health Monitoring
SIF	Stress Intensity Factor
SLJ	Single Lap Joint
SMP	Structural Modification Point (related to WFD)
SP	São Paulo (State)
S-SHM	Scheduled Structural Health Monitoring
TCD	Theory of Critical Distances
TSL	Traction-Separation Law
TTR	Through-the-thickness Reinforcement
UEPG	Universidade Estadual de Ponta Grossa (State University of Ponta Grossa)
UFSCAR	Universidade Federal de São Carlos (Federal University of São Carlos)
ULSF	Ultimate Lap Shear Force
UnB	Universidade de Brasília (Federal University of Brasília)
UNIFEI	Universidade Federal de Itajubá (Federal University of Itajubá)
UNESP	Universidade Estadual Paulista (State University of São Paulo)
USP	Universidade de São Paulo (University of São Paulo)
VCCT	Virtual Crack Closure Technique
WFD	Widespread Fatigue Damage
XFEM	eXtended Finite Element Method

INDEX OF FIGURES

INDEX OF TABLES

1. INTRODUCTION

This document was prepared to summarize fatigue and fracture investigations related to aerospace structures performed in Brazil during the past two years. Its contents will be presented during the 36th ICAF (International Committee on Aeronautical Fatigue and Structural Integrity) Conference to be held in Krakow, Poland, during June 03 and 04, 2019. The document contains the third brazilian national review and the first one presented while Brazil is a member country of the ICAF. Some of the research works presented along this review are follow on research activities related to the ones previously presented in References [1] and [2].

During this period other institutions - and other research teams from the previous institutions - joined the network of ICAF activities, and consequently the number of contributions nearly doubled if compared to the previous periods. While there is a significant increase in research activities being reported, on the other hand a steady pace in industrial activities was observed.

The following brazilian institutions have collaborated during this period with research works on fatigue and fracture mechanics related to aeronautical products, and had scientific or technological research works added to this review:

- Brazilian Society of Engineering and Mechanical Sciences (ABCM) – Rio de Janeiro - RJ
- Department of Aerospace Science and Technology (DCTA) – São José dos Campos - SP
- University of São Paulo (USP) – Campus of São Carlos – São Carlos – SP
- State University of São Paulo (UNESP) – Campus of Guaratinguetá – Guaratinguetá – SP
- State University of São Paulo (UNESP) – Campus of São José dos Campos – SP
- Federal University of Brasília (UnB) – Brasília - DF
- Federal University of Itajubá (UNIFEI) – Itajubá – MG
- Federal University of São Carlos (UFSCAR) – São Carlos - SP
- State University of Ponta Grossa (UEPG) – Ponta Grossa - PR
- Aeronautical Institute of Technology (ITA) – São José dos Campos – SP
- Embraer S/A – São José dos Campos – SP

Further, some works to be presented were developed in cooperation with foreign institutions, from which some are mentioned here:

- TU-Delft University of Technology– The Netherlands
- NLR – National Aerospace Laboratory – The Netherlands

- Technical University of Graz – Austria
- Sandia National Laboratories – USA

The author would like to thank to all partners from the Academy and the research institutes that have collaborated with this compilation, some of which will be cited along the report.

The author is also very grateful to the two other members of the present brazilian ICAF delegation, Mr. Fernando F. Fernandez and to Dr. Giorgia T. Aleixo, from Embraer R&D Department, for their help and continuous support during the organization of this work.

2. CONCEPTS

The first two works presented in this review describe theoretical failure models developed by researchers from the Aeronautical Institute of Technology (ITA).

A Multiaxial Fatigue Damage Model for Isotropic Materials (Ref. [3])

This paper presents a novel failure model for the prediction of low cycle fatigue life and residual strength of isotropic structures under multiaxial loading.

The approach proposed does not discretize every load cycle, using instead a loading envelope whereby the load value remains constant at a maximum level while the number of cycles is obtained from a given elapsed time defined within a pseudo-time framework. The proposed formulation is based on the smeared cracking approach accounting for damage propagation due to static and fatigue loadings, where the static component is based on the Von-Mises yield criterion and Prandtl-Reuss stress flow rule; whereas the crack propagation in cyclic loading component is based on the Paris law. Furthermore, the formulation combines damage mechanics and fracture mechanics within a unified approach enabling to control the energy dissipated in each loading cycle.

The proposed constitutive model accounts for the static damage followed by fatigue induced damage accumulation, depicted in Figure 2-1.

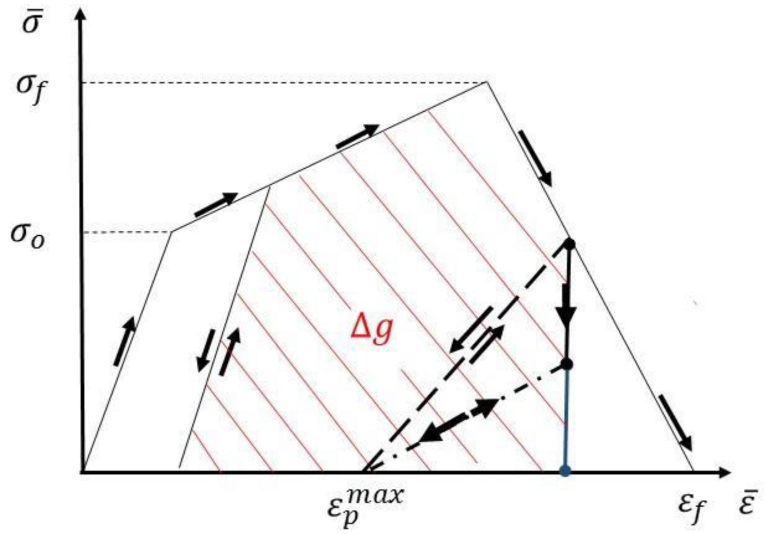

Figure 2-1 - Constitutive model behavior for isotropic material under static followed by damage induced by cyclic loading.

The model has been implemented as a user defined material model within S4R shell elements available in ABAQUS/Explicit© finite element code. An accurate prediction between numerical model and experimental results is observed in Figure 2-2, considering in terms of Paris law plots for the single element simulation and real structures.

The full research work will be presented during the 30th ICAF Symposium.

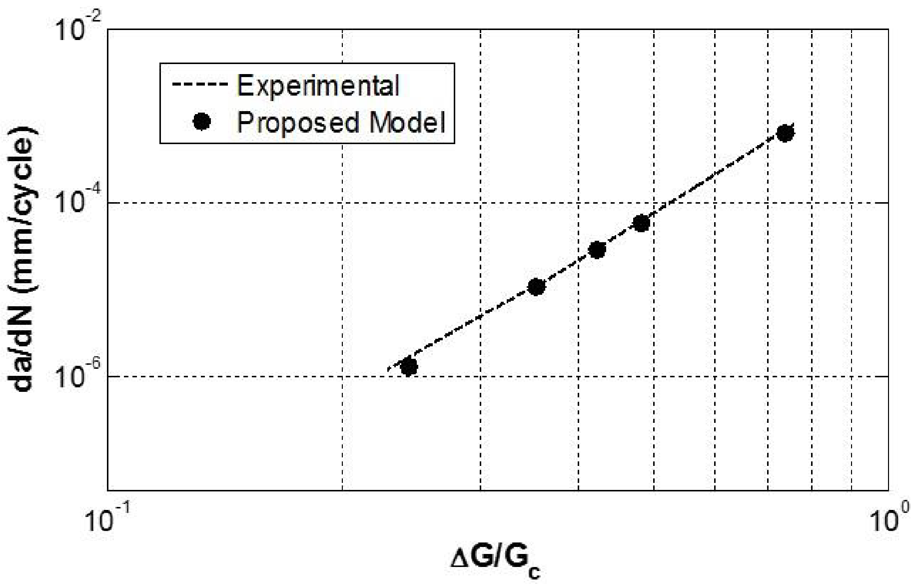

Figure 2-2 - Single element validation.

Fatigue-driven Delamination Modelling in Composites and Adhesives (Ref. [4])

In this paper, a constitutive damage model is proposed to predict static and high-cycle fatigue-induced interlaminar damage in carbon/epoxy composite laminates. This model accounts for fatigue-induced delamination in Modes I, II and III, either individually or combined without knowing the modes ratios *a priori*. The constitutive law used in this model to represent the behavior of the interface between two adjacent layers is based on the Cohesive Zone Model (CZM - Ref. [5]), where the fatigue damage evolution is derived from a modified Paris law (Ref. [6]) written in terms of Strain Energy Release Rate (SERR).

The SERR is computed using a J-integral, and a new J-integral strategy is proposed to improve the accuracy of SERR estimation by mitigating its variation during element degradation. The constitutive model proposed by Donadon et al. (Ref. [7]) for quasi-static loading is modified to include the proposed fatigue-induced damage model.

In this CZM, the damage state is represented by a single variable independently of the mode ratio and the constitutive law has the form of a bilinear Traction-Separation Law (TSL). The bilinear TSL combines two behaviours shown in Figure 2-3. First, starting from zero displacement the material presents a linear elastic response until the onset point (where the displacement δ is equal to the damage onset displacement δ^0 and the stress σ is equal to the material strength S). After this point, there is a linear softening response, where the fully failed displacement δ^f is chosen in a way that the area below the curve is equal to the fracture toughness Gc. After the fully failed displacement, the stiffness remains zero, and the material can no longer sustain loads. A crack-tip tracking algorithm identifies the elements in which the damage may nucleate and the elements at the crack front. This algorithm works in two different stages. In the damage fatigue nucleation stage, it tracks the SERR peaks within the elements and set them as crack initiation elements. The fatigue propagation stage is characterized by the presence of at least one entirely failed element. In this case, the algorithm tracks the elements adjacent to the failed one. After the crack-tip and nucleation elements are identified and their stiffnesses are degraded by fatigue.

The SERR is estimated using the J-integral method applied on the cohesive zone boundary, where the integration contour is taken at the cohesive elements surface, as shown in Figure 2-4.

The proposed formulation is implemented into ABAQUS/Explicit™ FE code within solid elements. The material properties are obtained from experimental data published by Asp, Sjögren and Greenhalg (Ref. [8]). In this paper, three loading conditions were simulated, namely Mode I, Mode II and Mixed-mode, using DCB, 4-ENF and MMB specimen configurations, respectively. Figure 2-5 presents a comparison of the crack growth rate predicted by the proposed model and experimental results.

More details about this work will be presented during the 30th ICAF Symposium.

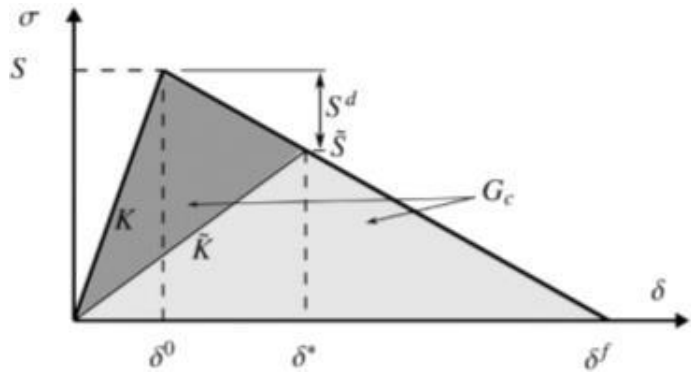

Figure 2-3 - Bi-linear TSL for a generic mode loading.

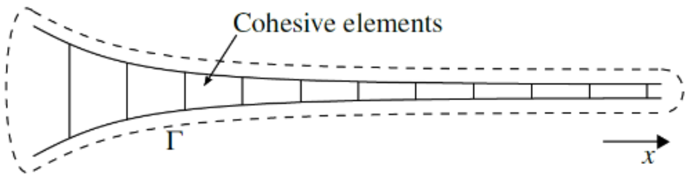

Figure 2-4 - Definition of the J integral surrounding the cohesive zone.

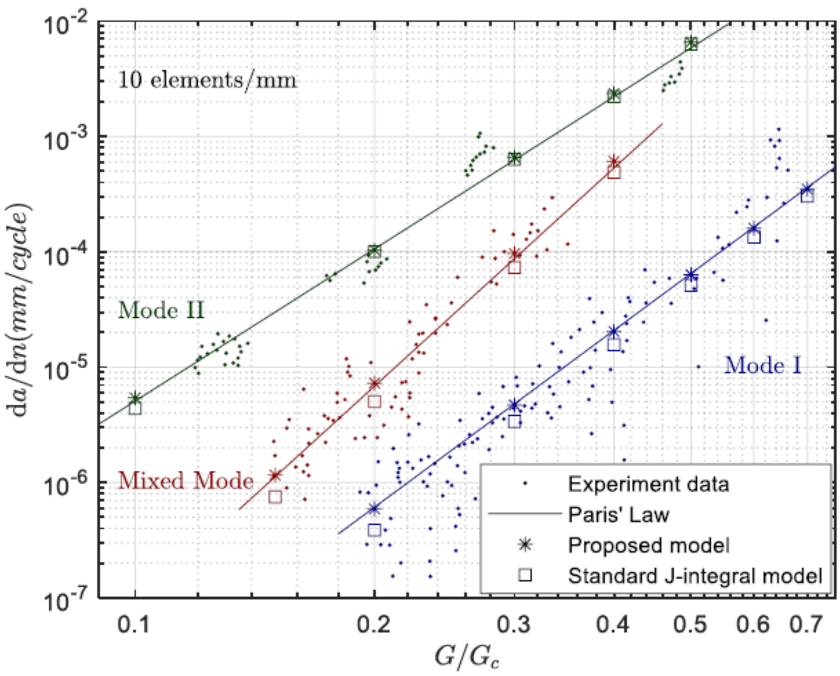

Figure 2-5 - Comparison between numerical prediction for the crack growth rate and experimental results.

3. ANALYSIS AND SIMULATION

There were three selected contributions related to fatigue and fracture analysis in metallic and mainly composite materials. These works were developed by the Aeronautical Institute of Technology (ITA) under supervision of Professor Mariano Arbelo, and by the University of São Paulo (USP), under the supervision of Professor Volnei Tita.

A Numerical Tool for Fatigue Induced Failure Analysis in the Frequency Domain (Ref. [9])

The use of life estimation methods is essential to engineers when designing structures that will be subjected to time-varying loadings, resulting in more reliable products with lower development cost. When the loadings are caused by random processes a frequency domain approach is preferable over the traditional time domain methods. The irregular loading is modelled as a stationary ergodic Gaussian random process, represented in the form of a Power Spectral Density (PSD). It means that instead of performing time-consuming measurements to obtain the necessary data, or performing expensive transient analysis, it is possible to simulate equivalent time histories with the same statistical properties and apply efficient methods in the frequency domain to compute fatigue life.

This work presents the implementation of an analysis tool that can be used in a FE-based environment to perform Stress-Life fatigue analysis in the frequency domain for random loadings. Some case studies taken from MSC™ Nastran Embedded Vibration Fatigue (2017) were used for verification of the code implemented in the proposed tool. The results obtained showed a good agreement between the implemented Python module and MSC™ NEVF, such that the tool developed and verified is a valid alternative for fatigue analysis.

Figure 3-1 shows a flowchart outlining the general analysis process for the frequency domain based approach developed in this work.

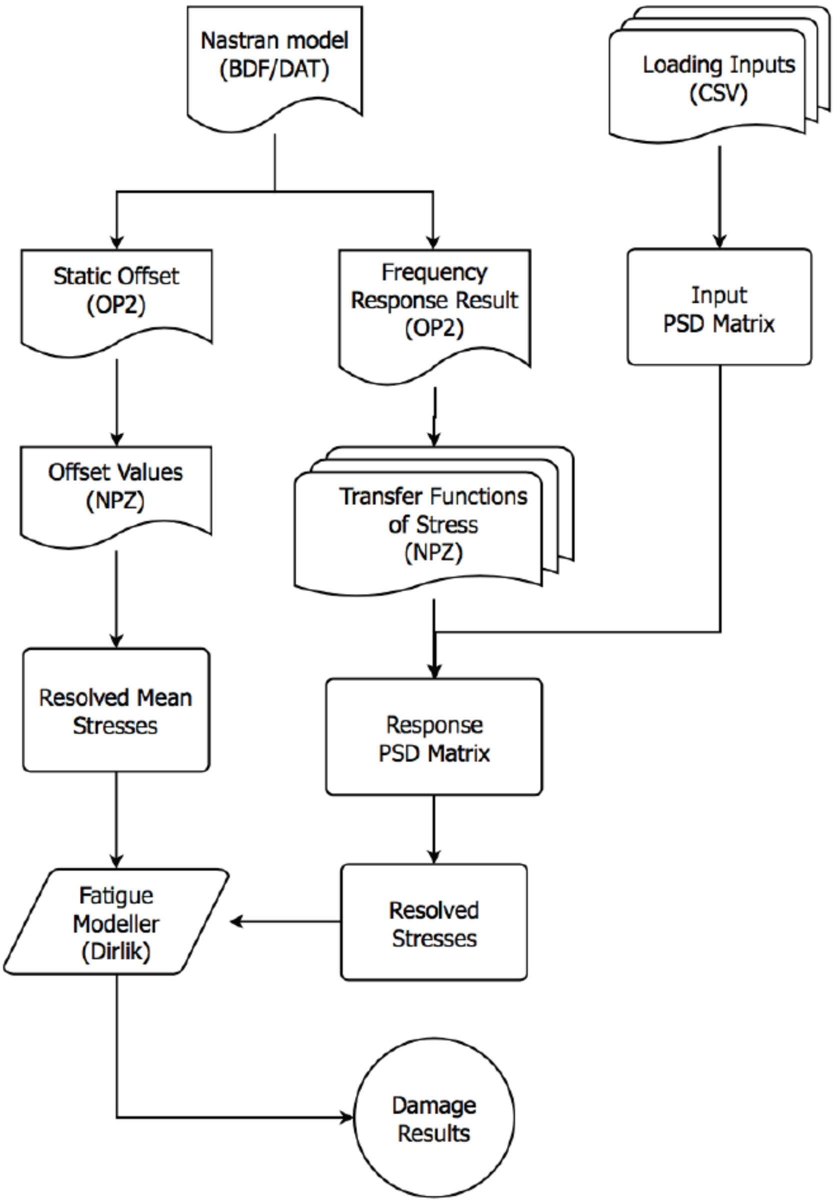

Figure 3-1 - General analysis flowchart.

A Computational Framework for Predicting Onset and Crack Propagation in Composite Structures via EXtended Finite Element Method - XFEM (Refs. [10] and [11])

The eXtended Finite Element Method (XFEM) has been reliably used for analyzing crack growth in 3D structural elements over last years. However, although many researchers have worked in this field, there are few scientific contributions about 3D XFEM models applied to the failure of non-standard composite parts, such as tapered structures and thick laminated composites.

In this work a new computational framework is developed, which is based on a new enhanced golden section search algorithm and 3D Puck's action plane principle in order to define the crack initiation direction. This information is integrated into XFEM and used to enrich elements which have failed during analysis. Compared to the traditional algorithm that have been used for this purpose, the new methodology has convergence one order of magnitude higher than the former, and it is about 20 times computationally more efficient. Therefore, if more precision is needed, then higher gains are achieved combined to lower computational cost by using the proposed framework.

Moreover, thick laminated composites with layers mainly oriented to 90° were simulated under tension and compression via the computational framework, displaying results as reported in the literature. Also, compact tension tests with 0°, 90° and 45° specimens were evaluated, and numerical results were qualitatively coherent with experimental data.

Figure 3-2 shows the experimental results used for validation and obtained from Reference [12]. Figure 3-3 shows the analysis results for these three conditions. More detailed validation of the numerical approach (including other examples) may be found in Reference [11].

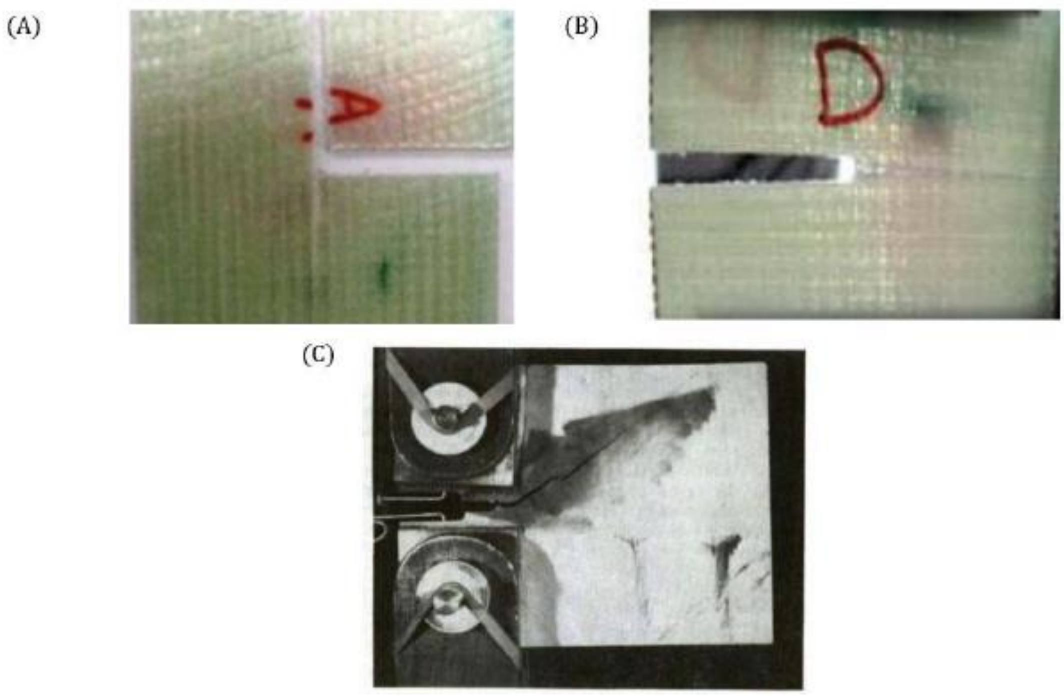

Figure 3-2 - Compact tension experimental results observed from the literature: layer orientations are (a) 0°, (b) 90° and (c) 45°.

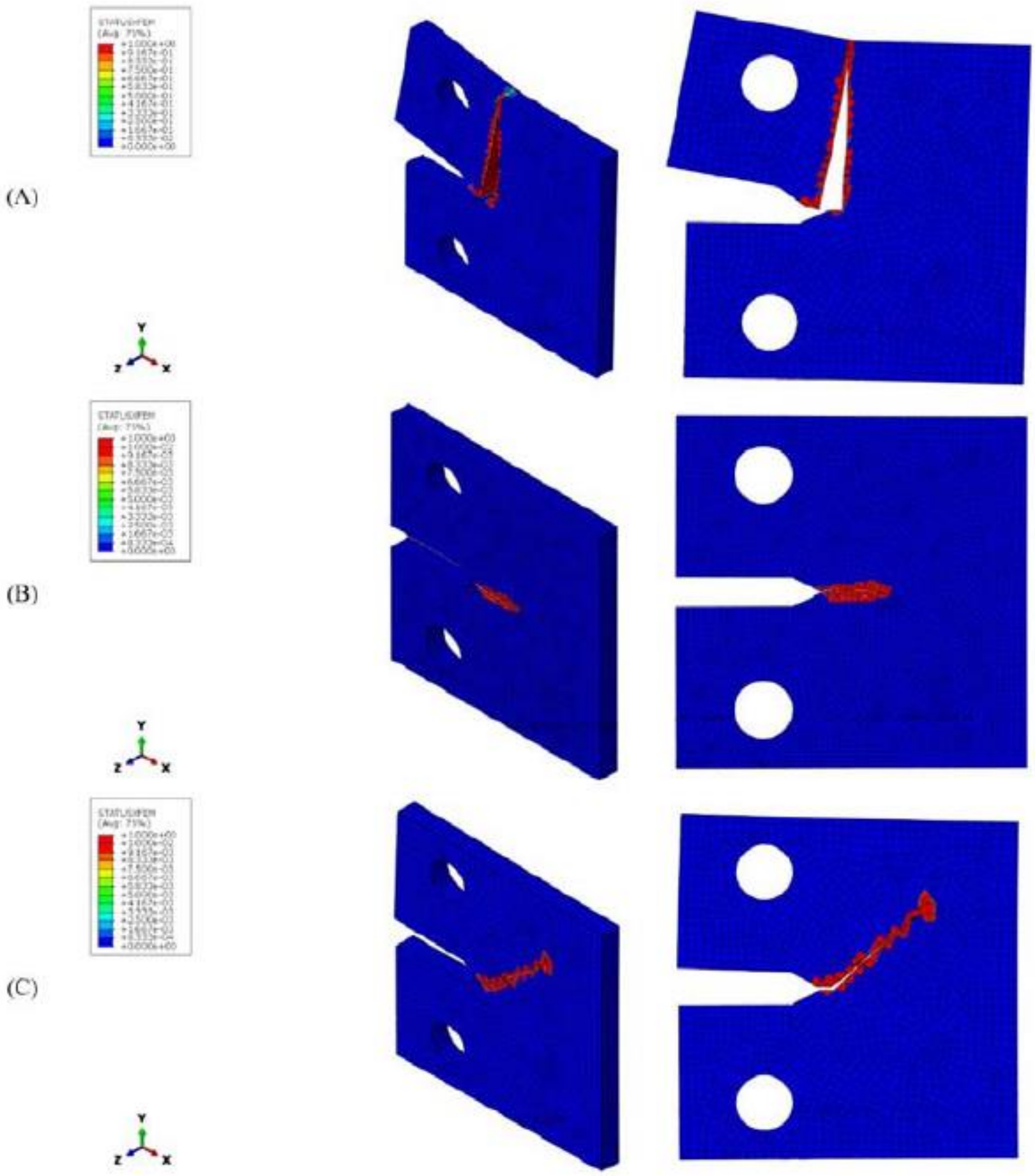

Figure 3-3 - Compact tension FEM analysis results: (A) 0°, (B) 90° and (C) 45° specimen.

Micro and Macroscale Analyses for Prognosis of Composite Structures: A New Physics Based Multiscale Methodology (Ref. [13])

Currently, one of the greatest challenges for the areas of Material Sciences and Structural Engineering is to perform accurate analysis for prediction of damage in composite materials, the evolution of damage and failure. Although several models and failure criteria already exist for the simulation of damage in composite materials, most models do not produce acceptable results for detailed designs. The models currently in use often under or overestimate loads required for the degradation and failure. This occurs as most of these models are based on phenomenological or semi-empirical data, which adjust failure surfaces or failure envelopes to experiments. This approach neglects the inherent anisotropy and heterogeneity of composite materials, which cause several failure mechanisms to occur simultaneously in different material scales and phases.

One possible solution to this problem is to use and/or develop new damage and failure models based on multiscale approaches and physical failure mechanisms based on Continuum Fracture Mechanics.

In this scenario, the main objective of this work consists on studying and developing multiscale based damage models applied to composite structures manufactured with unidirectional fibers under different load conditions: pure tensile, pure bending, mixed tensile-bending and multiaxial.

The basic methodology is based on using homogenization techniques to obtain degenerated elastic properties from damaged Representative Volume Elements (RVEs). The damage profile of the RVE is defined as intralaminar cracks parallel to the fiber directions and is calculated using a multiscale approach. The multiscale approach comprehends three separate models, one in the macroscale for the calculation of accurate stress/strain states in the critical points, and two in the microscale for the prediction of intralaminar damage (matrix cracking). These models interact between themselves, as the results from each one are used as boundary conditions for the other in a computational analysis loop over load steps via an iterative process.

The models developed were implemented either stand-alone in Python codes or into the finite element analysis package Abaqus™ using its automation capabilities with Python scripts, as well as subroutines in Fortran linked to Abaqus™.

Figure 3-4 summarizes, in a very high level, the computational procedure that was developed in this work.

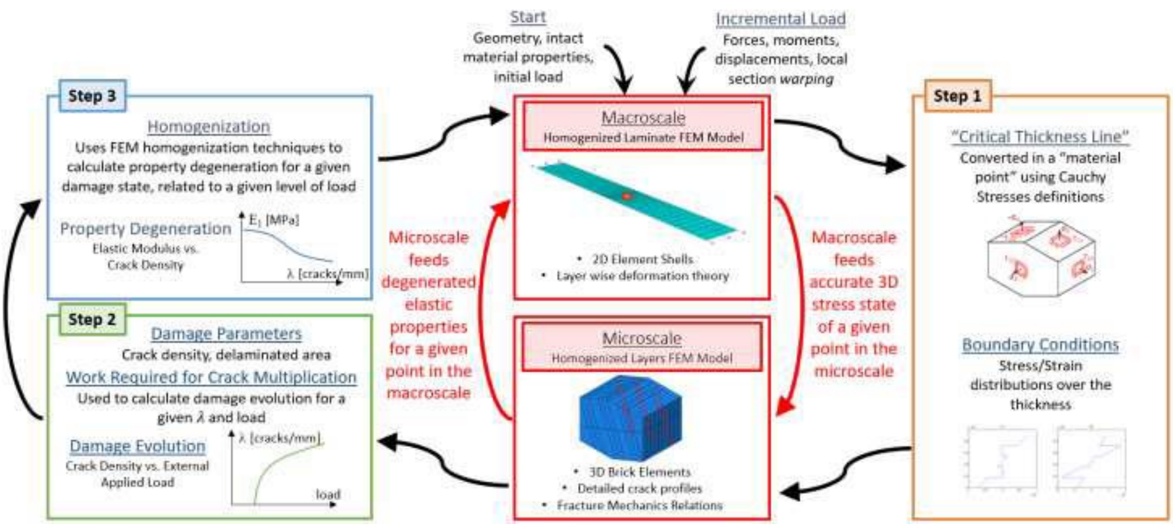

Figure 3-4 – Summary of the computational procedure developed in Ref. [13].

4. METALLIC MATERIALS – FATIGUE AND FRACTURE PROPERTIES

There are two contributions with respect to the development of fatigue and fracture properties. The first contribution is the result of a work developed by Professor Alex Araújo and co-workers, from the University of Brasília, and the second is a work on material properties of a Magnesium alloy, developed by Professor Waldek Bose Filho and co-workers, from the University of São Paulo.

The Role of the Shear and Normal Stress Gradients on Life Estimation of Notched Al7050-T7451 Under Multiaxial Loadings(Ref. [14])

The aim of this work was to investigate the role of the normal and shear stress gradients on the life estimation of notched Al 7050-T7451 components under multiaxial stress states. In this setting, a new concept of an equivalent critical distance, Leq, was proposed.

To validate the analysis, a wide number of experimental fatigue data were generated for smooth and notched specimens under push–pull, torsion and combined in phase axial–torsional loadings. From these data, critical distance versus life curves ($L–N_f$) were obtained under torsion and push–pull loading conditions.

The Modified Wöhler Curve Method (MWCM) critical plane based multiaxial model was used in conjunction with these curves and with the new $Leq–N_f$ relationship to estimate lives. The results showed that the $L–N_f$ curves obtained from the fully reversed torsion and push–pull tests had opposite behaviours. The best life estimates for the notched specimens under combined in phase axial–torsional loadings were obtained considering the new $L_{eq}–N_f$ relationship curve proposed in this work.

Figure 4-1 shows an overview of the procedure adopted to obtain the $L\text{-}N_f$ diagram, while Figure 4-2 summarizes the methodology proposed for life estimation in multiaxial fatigue. Figure 4-3 and Figure 4-4 bring some selected experimental results from this work.

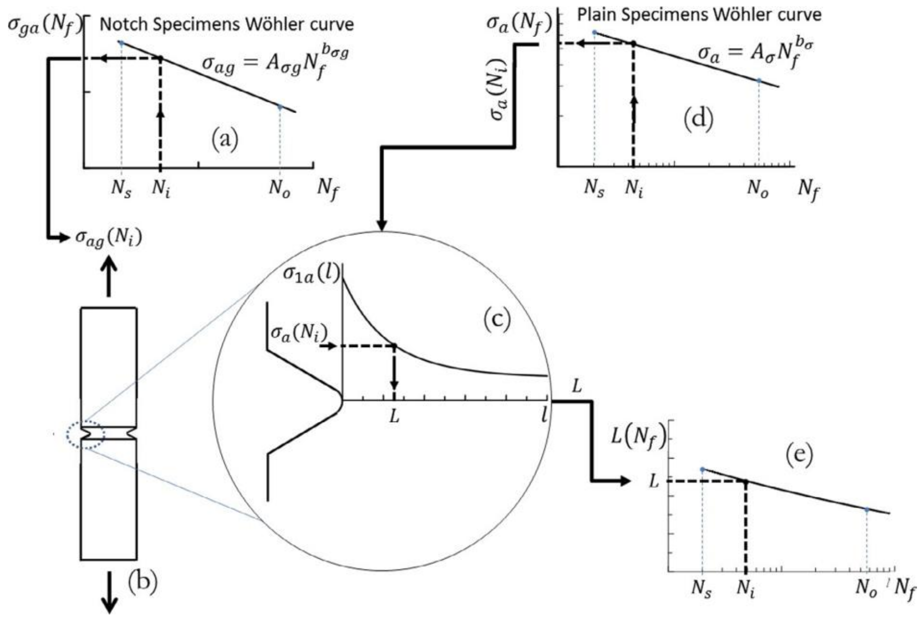

Figure 4-1 - Schematic view of the procedure to obtain the L−N_f diagram.

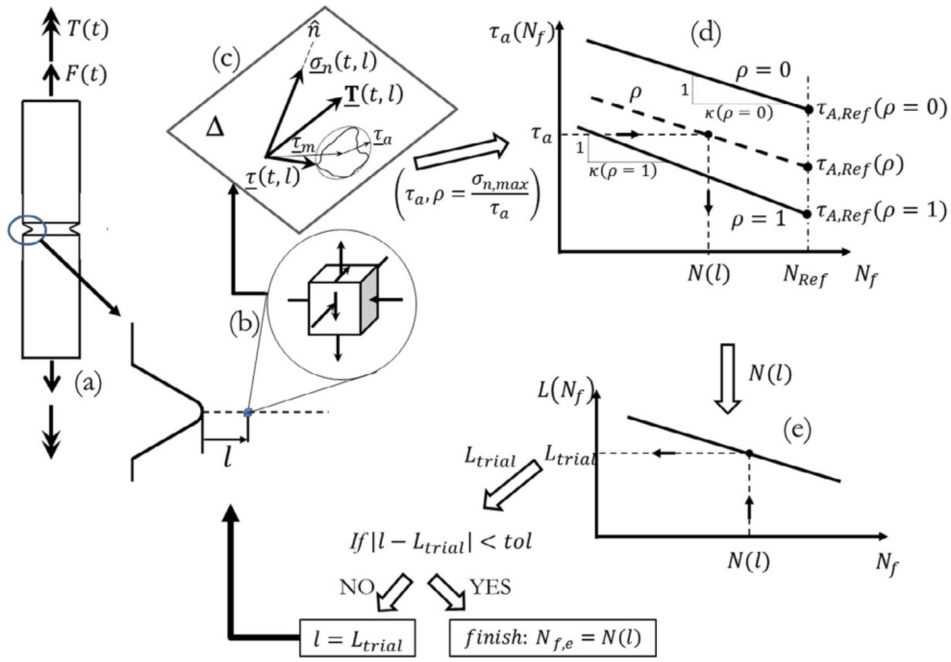

Figure 4-2 - Summary of a methodology proposed for life estimation in multiaxial fatigue using TCD and MWCM.

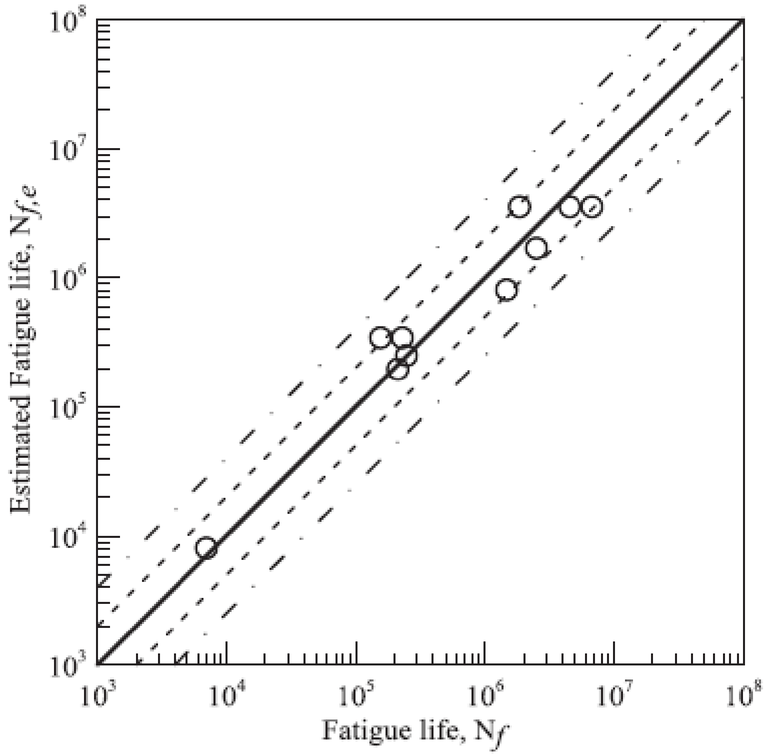

Figure 4-3 - Accuracy of the MWCM model in predicting fatigue lifetime of the plain specimens tested under axial-torsional loading.

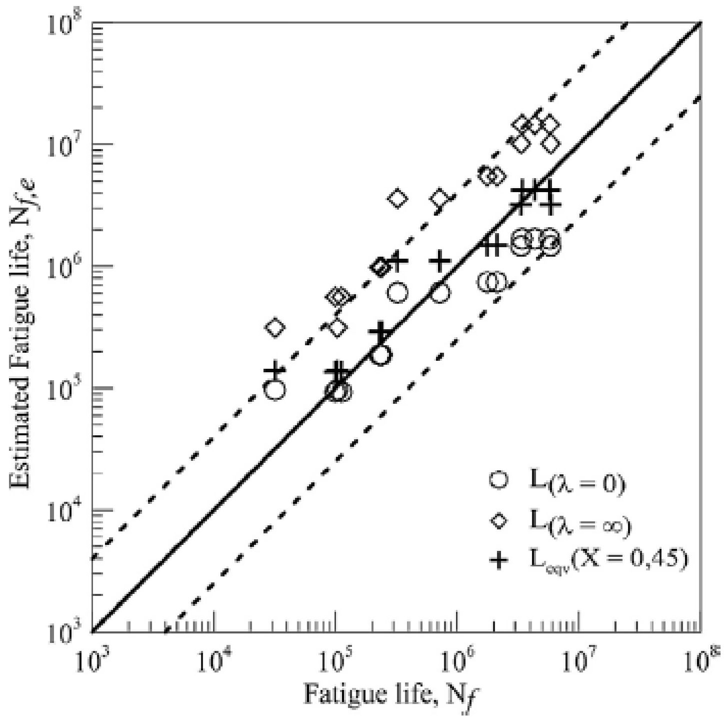

Figure 4-4 - Accuracy of the life estimates for the notched specimens of Al7050-T7451 subjected to combined in phase axial-torsional loading considering the use of the MWCM coupled with different measures of the critical distance.

Microstructural and Mechanical Characterization of WE43 Magnesium Alloy (Ref. [15])

New lighter metal alloys have been developed recently to replace the traditional alloys, aiming mainly structural weight reduction without compromising mechanical strength and corrosion resistance. In this context, the scope of this project was to study the microstructural and mechanical properties of the non-flammable magnesium alloy named as WE43 (Mg-Y-Nd-Zr).

The material used in the study was a plate with 28.0 mm thickness (aerospace specification AMS 4371). This Mg alloy was microstructurally analyzed by optical and scanning electron microscopies and the tensile, fracture toughness and fatigue properties were evaluated.

The results obtained showed that the WE43 has low microstructural and mechanical anisotropies due to the grains being morphologically quite equiaxial with the precipitates finally dispersed at the boundaries and inside the grains.

Figure 4-5 shows as an example the da/dN x ΔK curves obtained for R=0.1 in the T-L and L-T directions.

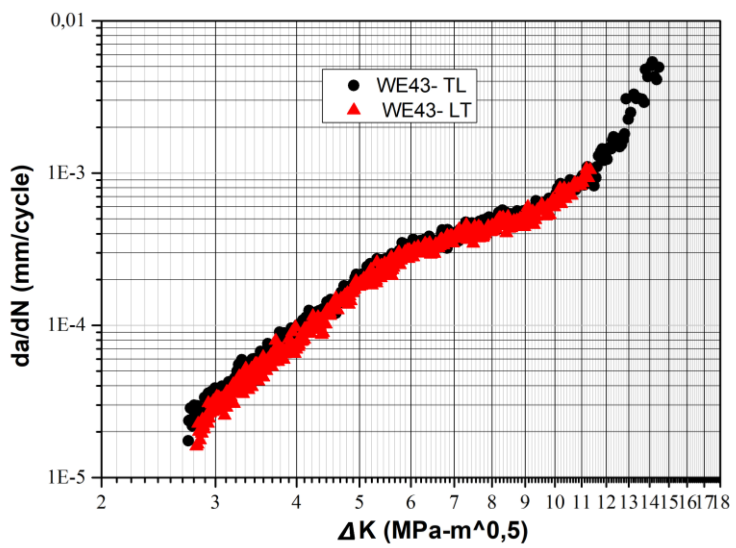

Figure 4-5 - Fatigue crack growth rate curve (log da / dN x log ΔK) for the WE43 alloy in the T-L and L-T grain directions.

5. METALLIC MATERIALS - FRETTING

Many aircraft structural details subject to cyclic loading, such as lugs and shear joints, may be prone to fretting as part of a damage process that leads to cracking. There is a research team in the University of Brasília, coordinated by Professor Alex Araújo, who has been developing many works on fretting over the last years. They have been working with some aerospace industries, like the Safran group.

Two contributions from this team are being included in this review. Although the materials analyzed are not necessarily for aerospace applications, it is believed that the work results and their conclusions may be applied for a variety of applications.

Early Cracking Orientation Under High Stress Gradients: The Fretting Case (Ref. [16])

Many fretting contacts experience a rapid variation of the magnitude and relative contribution of the stress components away from the surface. This feature of the fretting problem poses an additional difficulty for the modeling of the early cracking orientation. In this work, critical plane approaches associated with a process zone are evaluated by taking into account the fretting crack behavior observed in two different steels. The results show that the conventional approaches may provide inconsistent cracking directions.

A new method for early cracking orientation prediction is developed by employing the average values of the normal and shear stresses along a critical direction. This method is simpler to implement and improves the estimates when compared to the other approaches.

In this work, available fretting experiments on two different steels have been used to evaluate the accuracy of three methods for early cracking orientation prediction. For Methods 1 and 2, the shear-based criteria (Fatemi–Socie and MWCM) associated with a material characteristic length yield cracking directions opposite to the observed ones.

When applied together with Method 3 the MWCM is able to correctly estimate a crack direction oriented towards the inside of the contact, but the accuracy of the calculated orientation is not adequate. Similar behavior has been observed for the 35NCD16 steel but not for the AISI 1034 considering the application of the Fatemi–Socie model.

The critical direction method (Method 3) combined with the SWT criterion provided the most reliable results for the estimation of the crack initiation path under complex stress fields. Experimental evaluations considering different contact configurations and materials are required to further challenge the methodologies.

Figure 5-1 shows schematically a typical fretting problem, where the normal and tangential loads are applied and there is a contact point where cracks are like to initiate. Figure 5-2 shows three possible methods for cracking orientation prediction.

Figure 5-3 presents the observed and predicted crack directions using Method 1, while Figure 5-4 shows similar results based on Method 3.

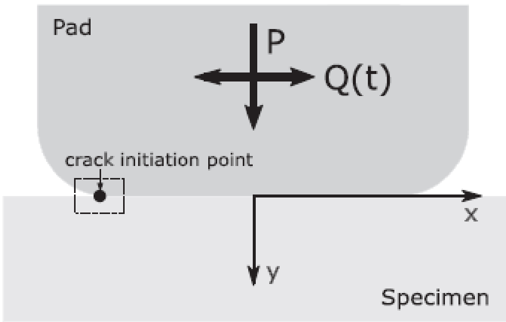

Figure 5-1 - Fretting problem under normal and tangential loading.

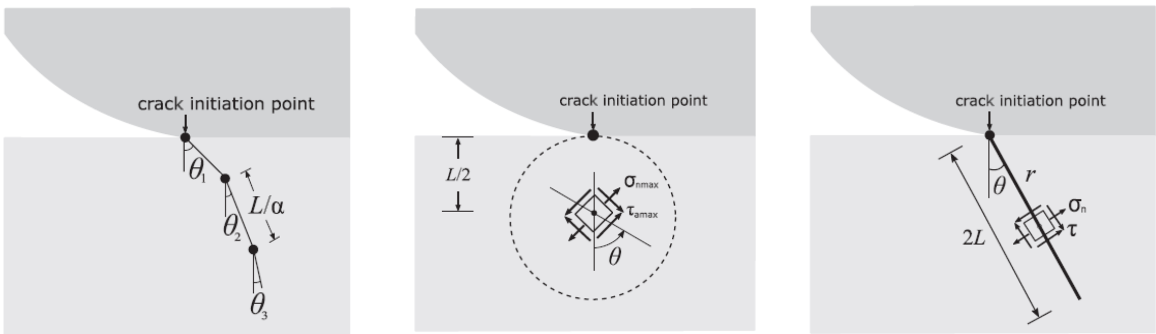

Method 1: Critical plane search for each stress point

Method 2: Center of the structural volume

Method 3: The critical direction method

Figure 5-2 - Schematic representation of Methods 1, 2 and 3 at the trailing edge of the contact. The angle θ is positive in the counterclockwise direction.

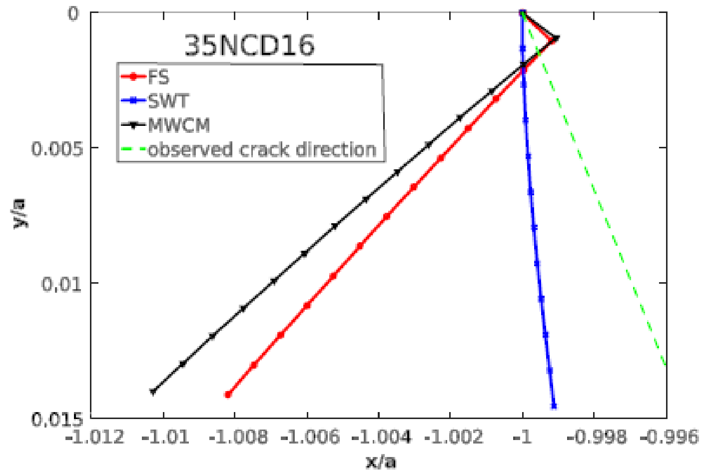

Figure 5-3 - Observed crack directions and predictions based on Method 1 (for 35NCD16 material samples).

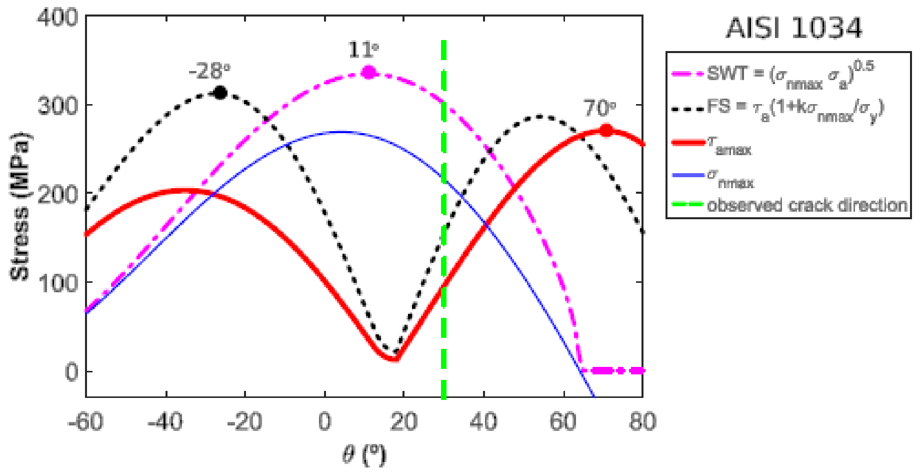

Figure 5-4 - Observed crack directions and predictions based on Method 3 (for AISI 1034 samples). The angle θ is positive in the counterclockwise direction.

A Multiaxial Stress-based Critical Distance Methodology to Estimate Fretting Fatigue Life [17])

This work presents a methodology for fretting fatigue life estimation based on the evaluation of a multiaxial fatigue parameter at a critical distance below the contact surface. The fatigue parameter is defined using the Modified Wöhler Curve Method (MWCM) together with a measure of shear stress amplitude based on the Maximum Rectangular Hull concept. To apply the approach in the medium-cycle fatigue regime, the critical distance is assumed to depend on the fatigue life.

Available fretting fatigue experiments conducted on a cylinder-on-flat contact configuration made of Al–4%Cu alloy were used to evaluate the methodology. Most of the fatigue life estimates were within factor-of-two boundaries.

The methodology does not take into account a number of features of the fretting fatigue problem as, for example, the surface modification due to wear. A more detailed description of fretting fatigue could be formulated by using a wear law or a crystal plasticity model. However, it is found that the simple approach used in this work can correlate well fretting fatigue data for Al–4%Cu alloy.

The methodology can be easily incorporated into existing FEM analysis software and be used in the fatigue life prediction of mechanical couplings with complex geometry. Further experimental evaluations of the methodology considering different contact configurations and materials are required.

Figure 5-5 shows an overview of the procedure, while Figure 5-6 shows a comparison between the estimated life according to the simplified procedure and experimental data obtained from the literature.

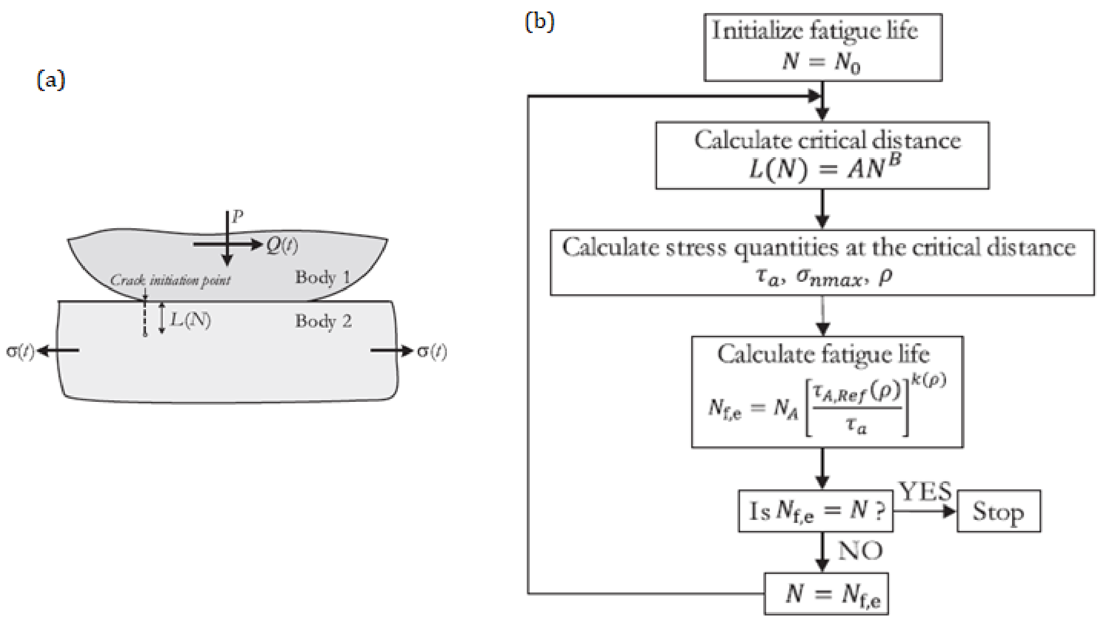

Figure 5-5 - Procedure to estimate fretting fatigue life: (a) definition of the critical distance L(N) and (b) flowchart of the algorithm for fatigue life calculation.

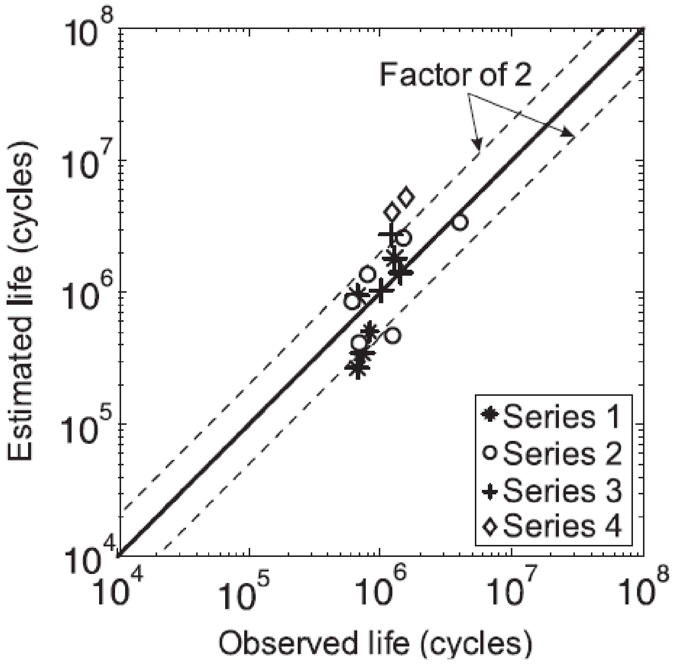

Figure 5-6 - Observed and estimated fatigue lives for the fretting fatigue tests reported by Carpinteri et. al. (Ref. [18]).

6. METALLIC MATERIALS – PROCESSES

From the contributions received this year regarding metallic material processes, two works are follow on activities from a previous investigation presented in Reference [2]. Additionally, there is one work about friction surfacing in aluminum. Both processes aim to increase crack growth intervals by retarding the crack growth rate.

Laser-induced Heating for Enhanced Fatigue Life of Aerospace Aluminum Alloys (Refs. [19] and [20])

It is known that compressive residual stresses enhance the performance of structural components by retarding the crack propagation rate, extending the fatigue life of such components. For this reason aircraft manufacturers may apply some process like mechanical peening, ballburnishing and laser shock peening to improve the fatigue life of structural parts.

This contribution aims to propose the laser surface treatment of aerospace aluminum alloys as a possible way to retard the crack propagation rate, by using experimental data obtained via compact tension - C(T) - specimens. Since the laser technology has been already used in welding and cutting operations, the same setup could be used to produce discrete heating lines with low cost.

Three types of aluminum alloys were analyzed Al-Zn-Mg-Cu (AA7475-T761), pure aluminum-coated Al-Cu (AA2024-T3) and Al-Si-Mn-Cu-Mg (AA6013-T4), for better understanding of phenomena related to the crack propagation. A carbon coating was proved to allow good absorptivity of the laser beam, since the aluminum surface is highly reflective to the fiber laser 1 μm radiation.

It was verified that two laser tracks, with power 200 W, speed below 5 mm/s and beam diameter of about 2 mm, consistently results in a crack-retardant piece. According to the results, the laser processing barely doubled the fatigue life under some conditions.

The main mechanism of crack retardation was associated with the modification of stresses ahead of the crack tip, since the microstructure and hardness were almost unchanged after the laser treatment. The maximum measured compressive stresses ahead of the laser track for AA7475-T761, AA2024-T3 and AA6013-T4 were 30 MPa, 30 MPa and 67 MPa, respectively.

Figure 6-1 shows the two configurations evaluated in this study, with one and two laser lines positioned perpendicularly to the crack growth direction.

Figure 6-2 shows the residual stress profiles (due to the heated zones) ahead of the crack tip for the initial crack tip position. Figure 6-3 and Figure 6-4 show the crack propagation results for AA 2024-T3 and for AA 7475-T7351 for the same laser heat condition applied and with two heating lines, compared to the baseline unheated condition.

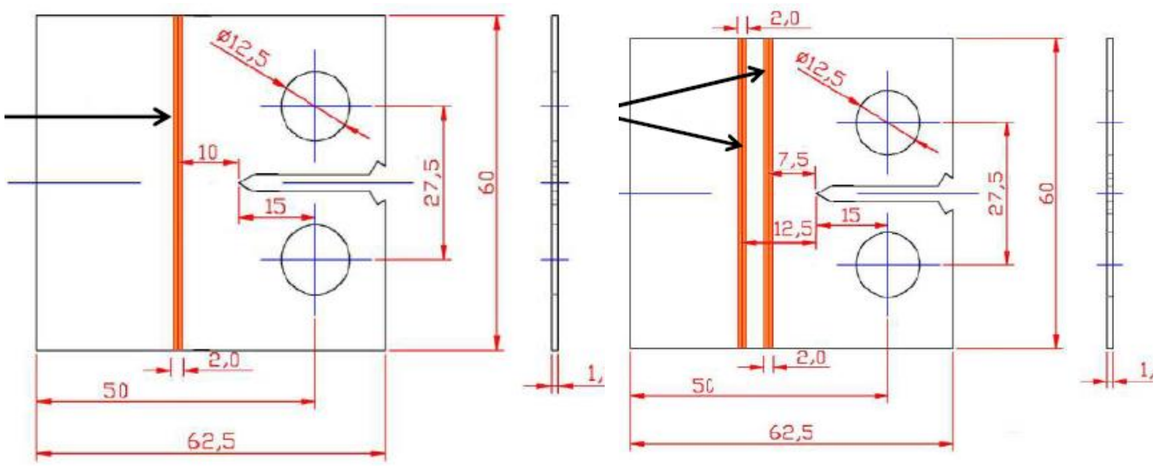

Figure 6-1 - C(T) specimens dimensions, with laser line positions indicated (dimensions in mm).

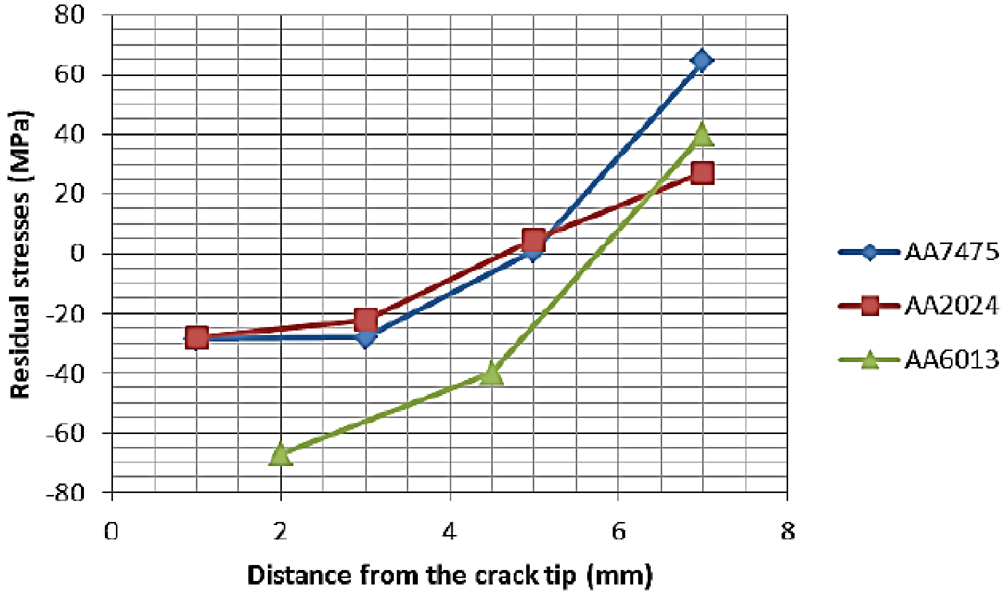

Figure 6-2 - Residual stresses between the initial crack tip and the laser heated region.

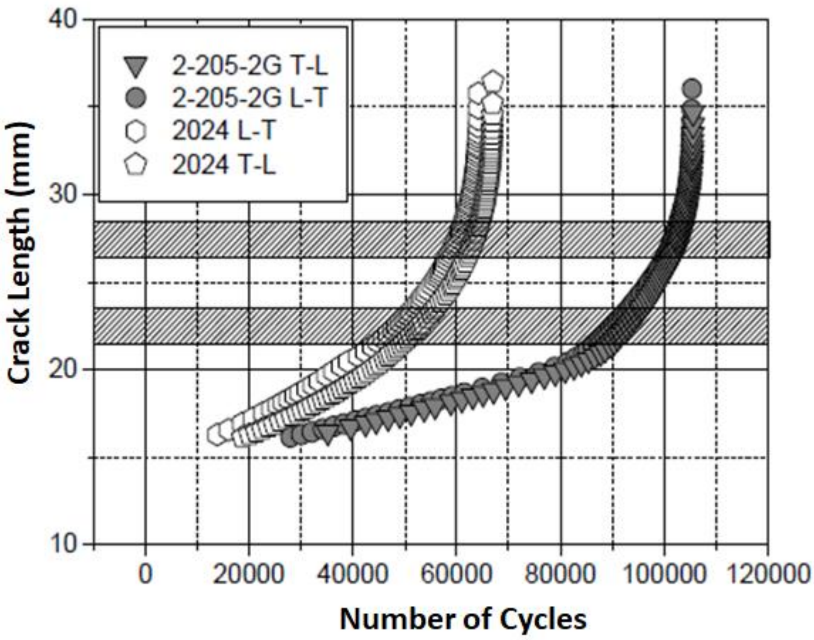

Figure 6-3 - Crack growth versus number of fatigue cycles for AA2024-T3 comparing base material (open symbols) to the lasered coupons (closed symbols). The rolling direction, L-T or T-L, is also indicated.

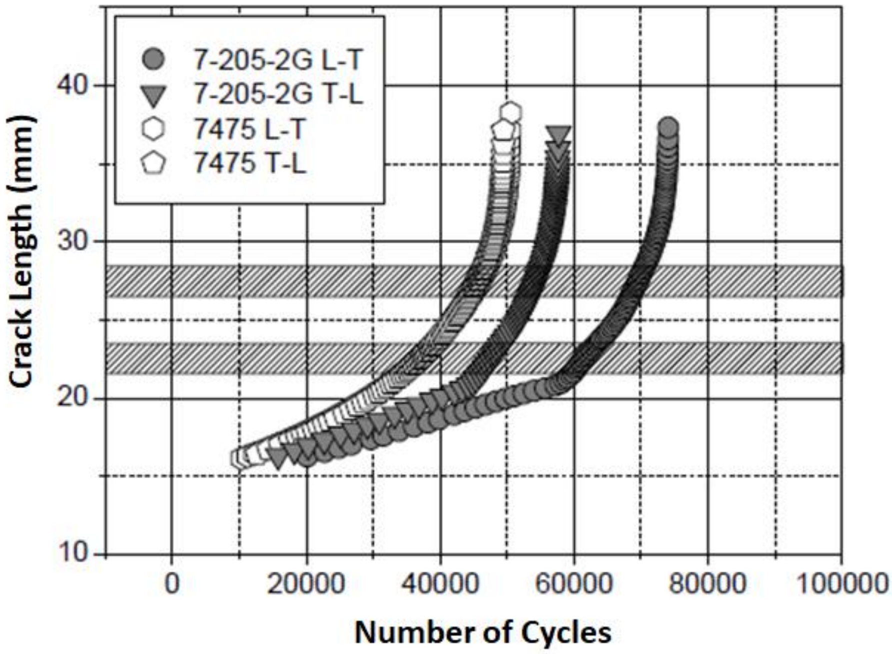

Figure 6-4 - Crack growth versus number of fatigue cycles for AA7475-T761 comparing base material (open symbols) to the lasered coupons (closed symbols). The rolling direction, L-T or T-L, is also indicated.

Application of Friction Surfacing to the Production of Aluminum Coatings on the Aeronautical Alloys (Ref. [21])

Selective reinforcement materials (GLARE, AA7075 and carbon-epoxy in a fibremetal laminate) on the wide aluminum panel as bonded reinforcement straps, may be used as crack growth retarders for aircraft structures, in order to provide a beneficial effect on both fatigue crack growth life and to increase the structure residual strength.

In this context, Friction Surfacing (FS) process enters in scene as one attractive option to be considered as a reinforcement on metallic fuselage in transport aircraft. FS is a deposition technique in state solid between a consumable rod and substrate. This process occurs by inter diffusion. All deformation process occurs only at the tip rod. FS produces refined grain coating. FS can be an excellent alternative as reinforcement on the aircraft structures, effectively working as crack growth retarders on the metallic structure.

This work describes an extensive research to find the best process parameters by Friction Surfacing. Three point bending testing was performed to verify the adhesion resistance of substrate/coating interface. Further, fatigue crack growth testing was carried-out to assess the efficiency of reinforcement with single and double layer AA-2024 on the AA2024-T3 substrate of fuselage application. Reinforcement was deposited on one side and on both sides of the plates.

Figure 6-5 shows an overview of the M(T) specimens used for the crack growth and residual strength experiments.

Figure 6-6 shows the profile of one specimen subject to bending, as part of a set of supplementary tests for verification of the possibility of delamination in the coating/substrate interface under both compression and tension conditions.

Figure 6-7 shows the crack propagation results for baseline specimens and for the specimens with layers added in one and two sides. The life increases observed for the latter conditions are indicated in the figure.

Figure 6-5 – Overview of test specimens (material deposition in one and two sides).

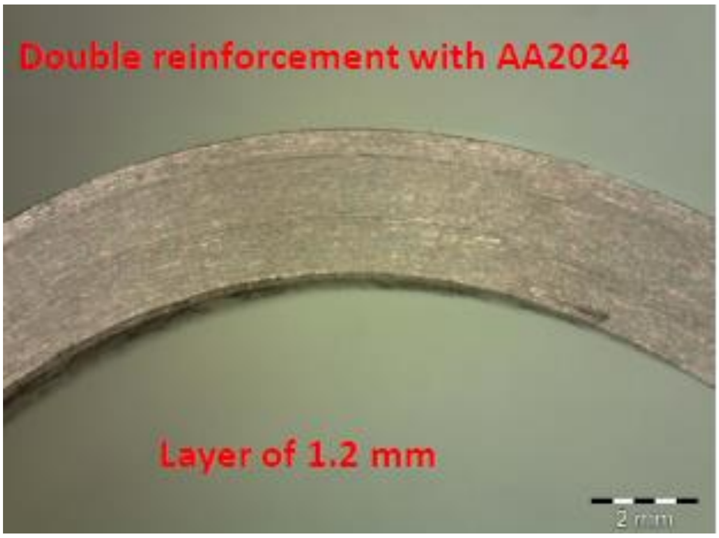

Figure 6-6 – Visual appearance of bent specimen, showing a good adhesion between the substrate and the coating interfaces.

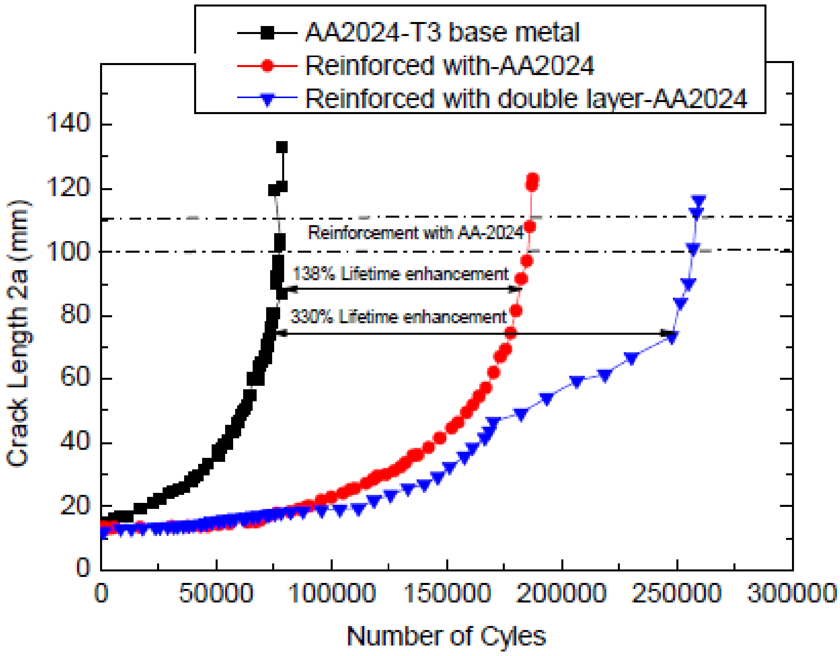

Figure 6-7 – Crack growth results for baseline specimens and specimens with layers added in one and two sides.

7. METALLIC MATERIALS – STRUCTURES

During the period 2017-2019, after certification of Embraer commercial and military aircraft, the main activities were related to development tests and monitoring the progress of full-scale fatigue tests.

Analysis Prediction and Correlation of Fiber Metal Laminate (FML) Crack Propagation in Semi-wing Full-scale Test (Ref. [22])

This study aims to demonstrate the correlation between the simulation and the experimental results obtained in terms of crack propagation for artificially cracks inserted in the semi-wing full-scale test developed by Embraer. The crack selected for this study was one of the several cracks inserted in the semi-wing lower wing cover. The crack under evaluation developed on the lower wing skin, which was manufactured in FML. These cracks were inserted for the development of the crack propagation analysis methodology in FML. In addition, the application of cracks in a Full-scale test allowed the evaluation of several damage scenarios that could hardly be reproduced with accuracy in tests with structural subcomponents, such as: design details in assemblies, geometric details without simplifications, redistribution of load flow among components structural and so on.

Several studies about crack propagation in FML have been published in the last decade, mostly related to propagation in coupons and subcomponents. Figure 7-1 illustrates the semi-wing used in the Full-Scale test and highlights the lower wing cover manufactured in FML with bonded stringers.

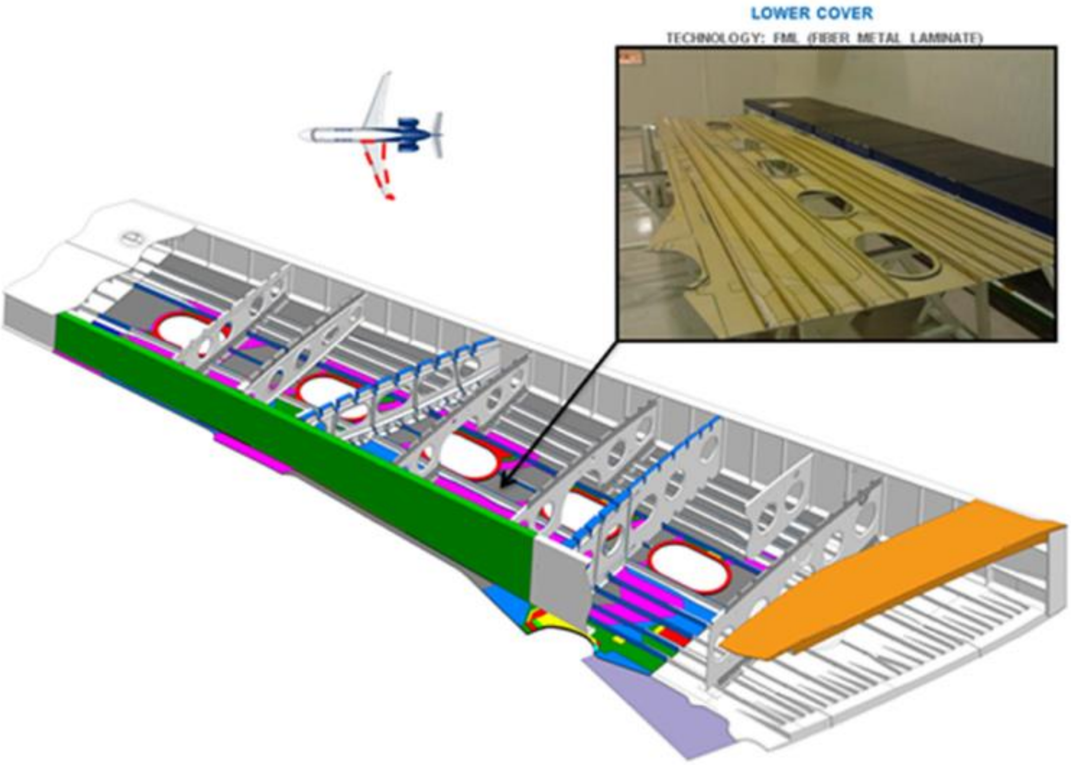

Figure 7-1 - Lower wing cover applied in semi-wing test specimen.

This semi-wing is similar in geometry to the semi-wing existing in the ERJ-145 aircraft and has been tested on fatigue prior to the propagation test. The fatigue test lasted 120,000 Flight Cycles (FC) which corresponds to two lives of the aircraft operation. It should be mentioned that no cracks initiated naturally in FML during the first 120,000 FC.

The results presented in this study were obtained from a damage that simulates a failure in the window frame, made of FML. Figure 7-2 shows this artificial damage. Figure 7-3 illustrates the structure in the surroundings of the crack; it is possible to visualize the crack inserted in the frame and the adjacent stringer in the lower wing cover.

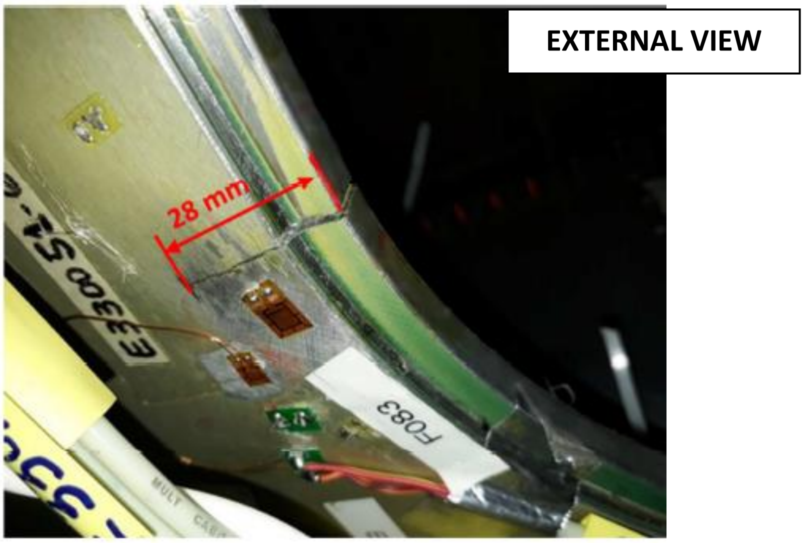

Figure 7-2 –Artificial damage and crack extension - external view.

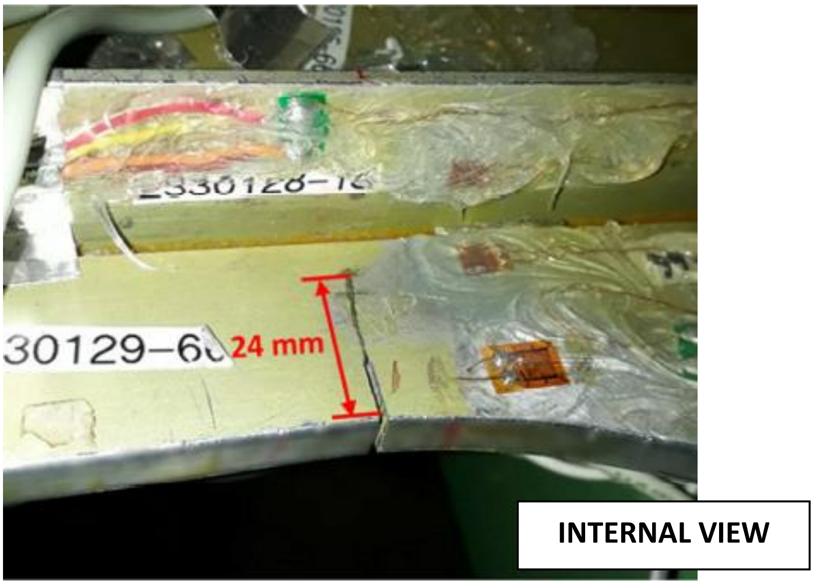

Figure 7-3 – Artificial damage and crack extension – internal view.

From this test the experimental results presented in Figure 7-4 were obtained, where it is also possible to observe the simulation of crack propagation. The experimental results were measured for each tip crack in FML, emphasizing that the FML in this region is composed of different layups along the crack path.

The propagation prediction analysis of this crack was based on an analytical methodology originally developed for thinner layers, which was adapted for a thick layer laminate, combined with Finite Elements Analysis (FEA), from which the stress field in the structure was obtained. The model used is illustrated in Figure

7-5. This procedure allowed to represent more complex structures with greater fidelity.

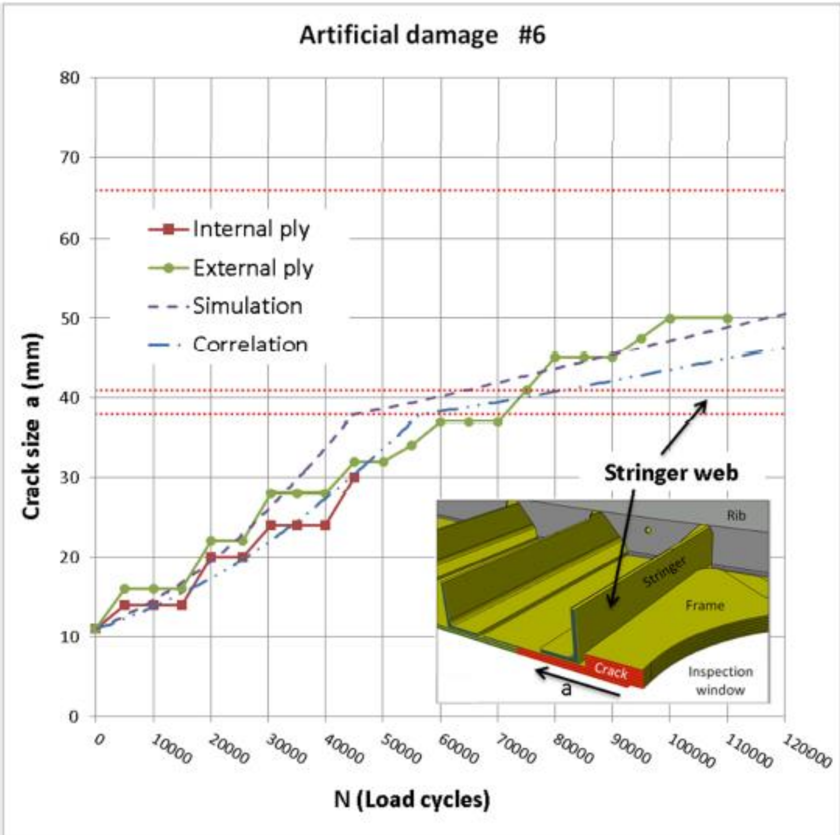

Figure 7-4 – Results correlation for damage evolution.

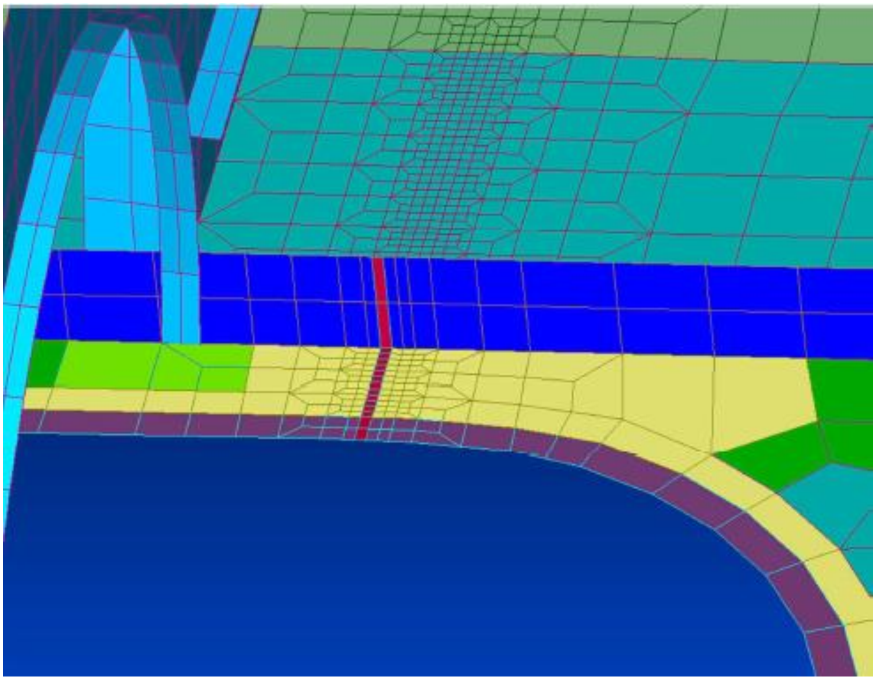

Figure 7-5 – FEA representation of the problem.

A good correlation between the analysis prediction and test results can be observed in Figure 7-4. Thus, the applied methodology was able to represent the structure complexity degree, which it contained layup changes in the skin and bonded stringers. These complexity means, locally, a secondary moment caused by the off-set differences, the stiffener disbond in addition to the delamination in the FML. This result is an indication of the robustness of methodology applied for crack propagation in the FML for wing structures and also contributes to increase the reliability that has been proved over the years in others researches for coupons and panels made of FML.

More details about this investigation will be presented during the 30th ICAF Symposium.

Crack Growth Analysis of Panels with Different Construction Methodologies (Ref. [23])

In order to compare different methods of built up construction and new materials under the context of damage tolerance, three stiffened panels were tested at the Aerospace Structures Laboratory (LAB-ESP) from ITA. The first panel had an aluminum plate with riveted stringers, the second an aluminum plate with bonded stringers and the third had a Glare plate with bonded stringers. The experiments conducted with these three panel configurations were reported in Reference [2].

The three panels portrayed significantly different results, with the FML having the best response both in crack propagation and residual strength.

With the objective to obtain reliable analysis tools for these three panels, filling a gap on available solutions available in softwares like Nasgro®, detailed FEM models were built aiming to use the VCCT technique in order to obtain Stress Intensity Factors (SIFs), with a special approach on Glare taking into account its delamination phenomenon during crack propagation.

Results have shown that the proposed technique demonstrates good accuracy, including the ones obtained for Glare panels, but care must be taken on these cases because the results are very sensitive to the chosen delamination shape. However, it was found that rigid modeling on bonded stringers held relatively imprecise results, thus calling for a better approach.

Figure 7-6 shows the comparison between the simulation and the experimental results for the panels with bonded strigers. A linear approach and a non-linear approach (accounting for the effect of stringer yielding, through NASTRAN 106 solution), the latter showing a better correlation with the experiments. Figure 7-7 once again shows the comparison between numerical and experimental results for the crack propagation, where the numerical analysis was performed for various delamination shapes (triangle, cosine, ellipse and parabola). The SIF is higher for shapes that lead to larger delamination areas, and that lead to higher bridging stresses. Results indicated a very good correlation of VCCT against analytical results. Furthermore, for the FML materials and loading conditions close to the ones tested on this work, delamination between aluminum and fiber glass layers seem to be well modeled with a triangular or cosine shape and a b/a proportion between 0.25-0.30, which is a value commonly found in literature (a = crack half length, b = maximum delamination length).

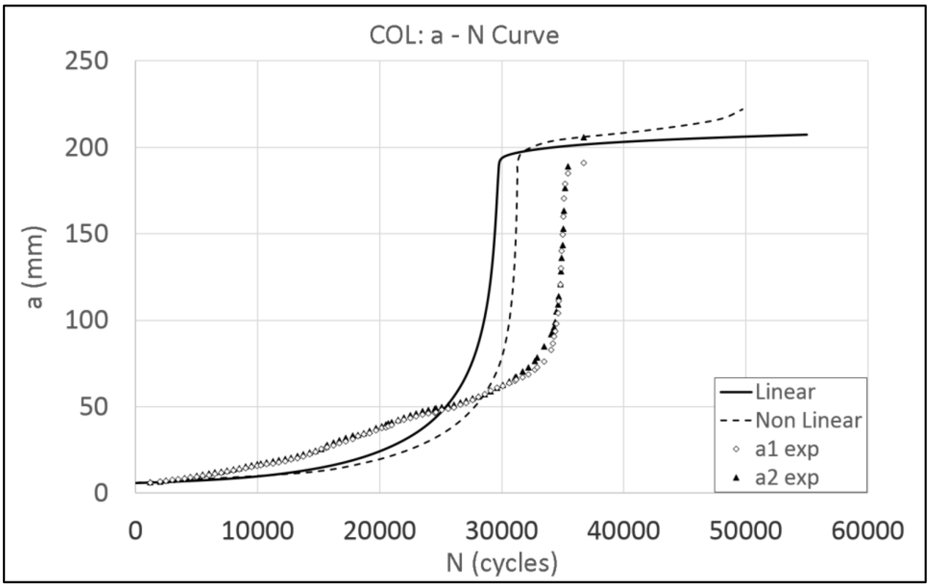

Figure 7-6 – Bonded stringers, comparison between numerical analysis and test results for linear and non-linear numerical approaches.

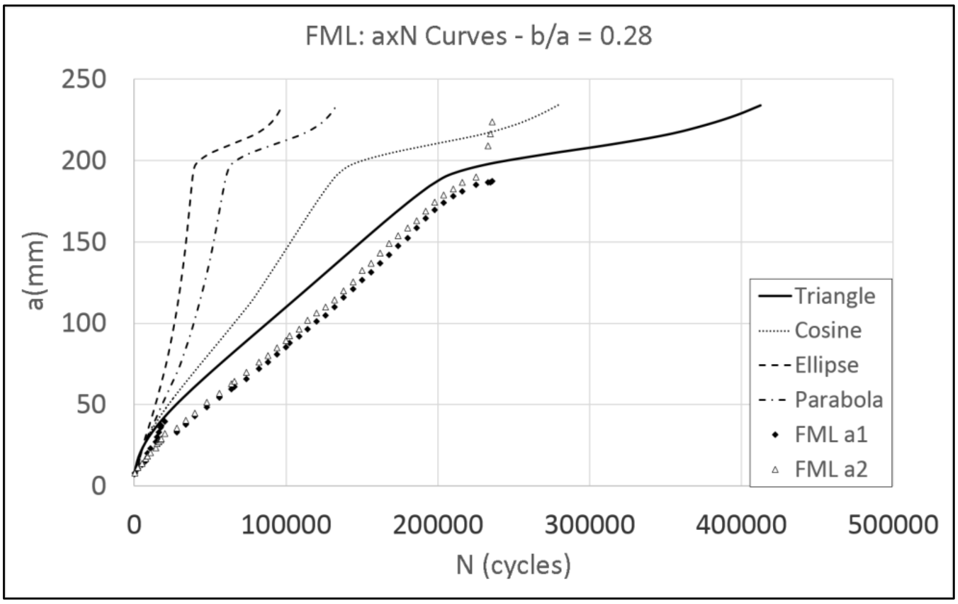

Figure 7-7 – FML panel, comparison between numerical analysis and test results accounting for four delamination shapes.

Development of Novel Methodologies for Crack Propagation Analysis of Pressurized Fuselages

This work is being developed by Embraer R&D team. Part of the information contained in this work is being applied to a project carried out in partnership between Embraer, the FAA Technical Center and Arconic, whose partial results are being presented in the 30th ICAF Symposium (Reference [24]).

In order to obtain robust methodologies able to simulate crack propagation, residual strength and Widespread Fatigue Damage (WFD) in pressurized fuselages, modeling adequately the complex effects in this type of analysis, Embraer is developing novel analyses techniques and experimental tests based on damage tolerance approach.

For cracks in a pressurized fuselage there are some dominant factors that affect the behavior of through-cracks in the fuselage skin, the out-of-plane deformation or bulging at crack edges, mixed modes of failure (I, II and III), influence of stiffness, crack propagation path and nonlinearities. In addition, the loss of residual strength in the presence of WFD has been studied to evaluate the structural integrity of damage structures.

All these factors are taken into consideration for the developing of this robust methodology. Figure 7-8 shows an example of a building-block applied to obtain this robust methodology able to calculate crack propagation in a full-scale fuselage. In this example, cruciform specimens (base of the building-block) were used to study crack propagation due to biaxial loads, crack propagation path, instability of the crack path and influence of stiffness. Pressurized curved panels (center of the building-block) were used to study the bulging phenomenon, mixed modes of failure (I, II and III) and crack flapping. Finally, at the top of the building block full-scale tests have been used to validate the methodology of analysis.

For studying the complex effects of this kind of analysis each parameter was validated by experimental tests, well known analytical models and different approaches for the numerical models (such as XFEM, J-Integral using standard FEM, VCCT etc.).

Figure 7-9 shows one example of validation, throughout the comparison for the pressurized curved panel regarding the crack flapping. For this example an experimental test, extended finite element method (XFEM) and two most common theories for predicting the crack propagation angle were used. Moreover, for this example a crack tip constraint was studied by the second term of the elastic asymptotic stress series near a crack tip (T-stress).

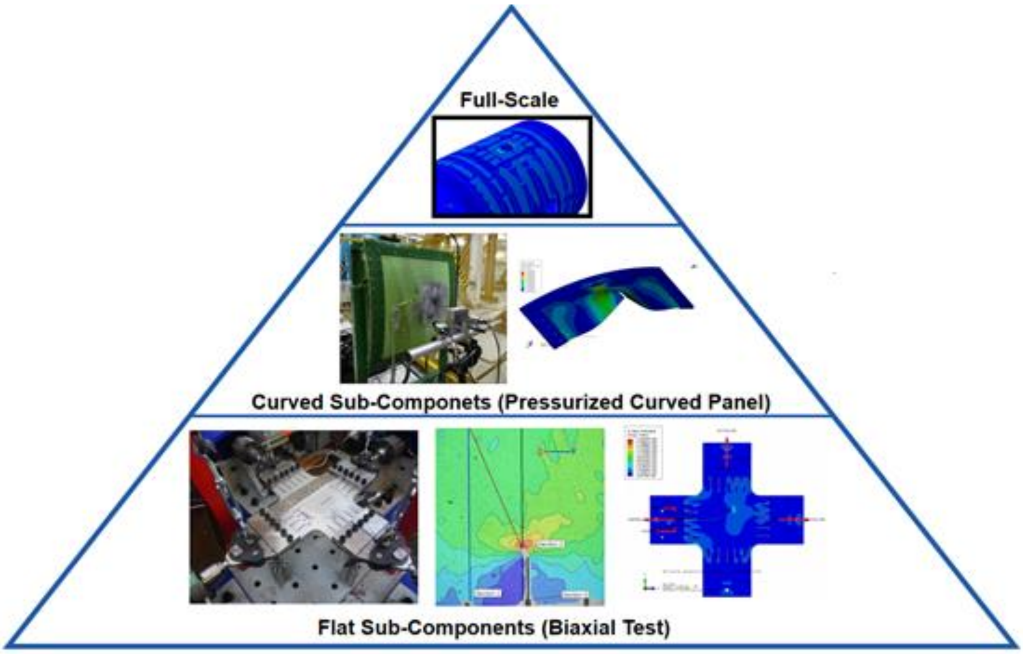

Figure 7-8 – Example of Building-Block applied to obtain a robust methodology to calculate crack propagation in a full-scale fuselage.

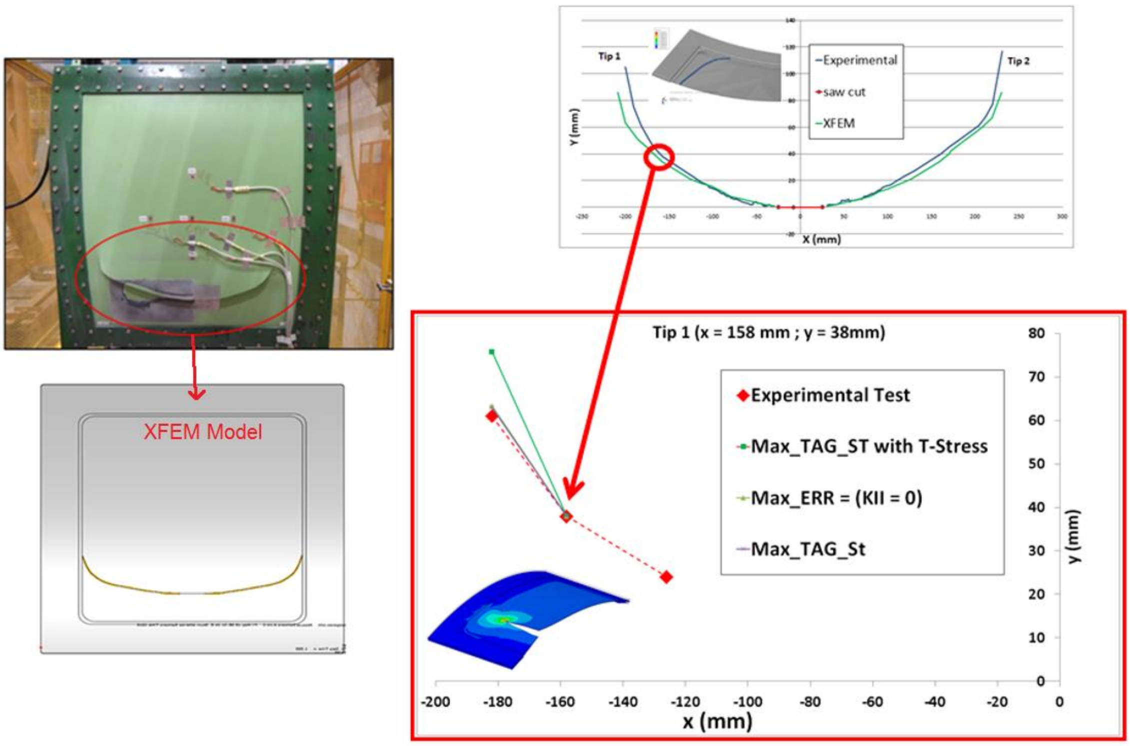

Figure 7-9 – Example of crack flapping validation approach.

To take advantage of the Finite Element Method (FEM) a parametric study was done to verify the influence of the parameters described before on crack behavior.

In addition, the damage tolerance design philosophy requires realistic stress state determination in the vicinity of cracks in airframe fuselages. Therefore, to validate the analytical and numerical models, some methodologies were used to obtain the stress intensity factor (SIF) directly from the experimental tests. Figure 7-10 shows a comparison between the numerical model and Digital Image Correlation (DIC) for the pressurized curved panel to obtain the strain along the crack surface and calculate the stress intensity factor in the asymptotic zone.

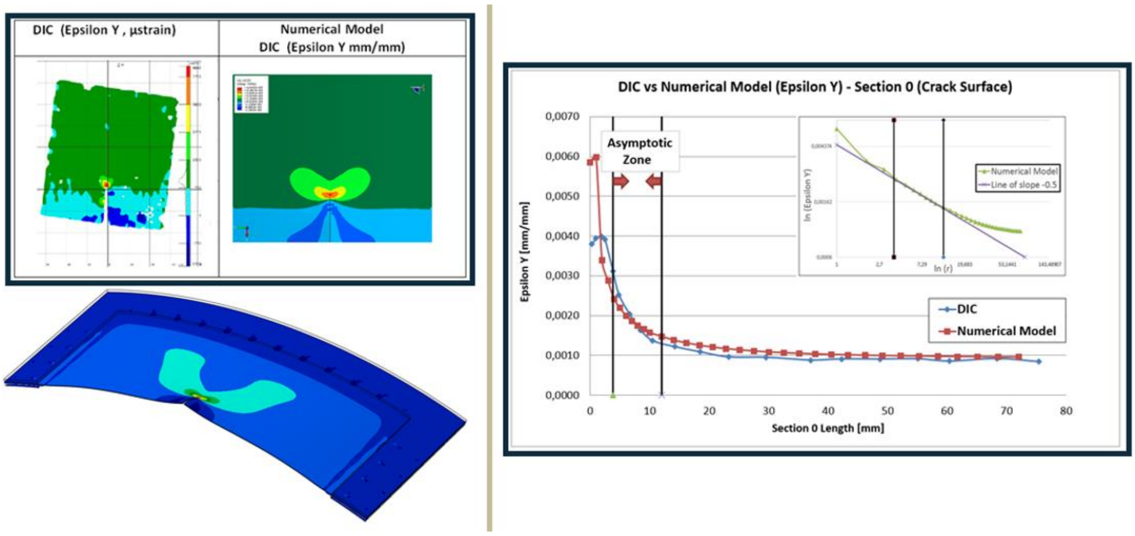

Figure 7-10 - Strain comparison along the crack surface between the numerical model and the DIC for the pressurized curved panel.

Full-scale Fatigue Tests

There are two Full-scale fatigue tests (FSFT) in progress at Embraer during this period (2017-2019).

The first one is related to the second generation of the E-Jets (previously mentioned in Ref. [2]). The first variant of this aircraft had a triple certification (ANAC/FAA/EASA) in February 28, 2018 and now is entering in service. The E2 FSFT is in progress, now simulating first design life of the aircraft.

The second FSFT that is in progress is dedicated to the KC-390. The KC-390 is a medium-size, twin-engine jet-powered military transport aircraft under development by Embraer during the last five years, and able to perform aerial refuelling and to transport cargo and troops. It is the heaviest aircraft that the company has made to date, and will be able to transport up to 26 tonnes (29 tons) of cargo, including wheeled armoured fighting vehicles.

The KC-390 has received a civil (Part 25) type certification from ANAC, the brazilian aviation agency, in October 23, 2018.

The KC-390 full-scale fatigue test is in progress (first lifetime).

Figure 7-11 and Figure 7-12 show an overview of the KC-390 and from the Full-scale Fatigue Test.

Figure 7-11 – Embraer KC-390.

Figure 7-12 – Embraer KC-390 Full-scale Fatigue Test overview.

8. COMPOSITE MATERIALS

During the last two years, there were many important contributions related to the development of fatigue and damage tolerance for composite materials and structures, mainly from the Aeronautical Institute of Technology (ITA) and from the University of São Paulo (USP).

Durability of Co-bonded Stiffened CFRP Panels Subjected to Post-bucking Fatigue (Ref. [25])

The research proposed in this work is part of the INOVA project. INOVA is a collaboration between the Technological Institute of Aeronautics (ITA) and Embraer. The goal of this project is to get a more thorough understanding of the behavior of bonded composite structures over the course of an aircraft's life cycle and what role the bonding techniques co-bonded, co-cured and secondary bonded play.

During the INOVA project coupon tests were carried out to determine the fracture toughness and the fatigue threshold of each bonding technique. Half of these coupons were subjected to hygrothermal aging and subsequently tested at these conditions to determine the infuence of hot-wet conditions on the mechanical properties of a bonded structure. Additionally, all bonding techniques were tested on subcomponent level in the form of stiffened bonded panels with an initial disbond subjected to post-buckling fatigue. Half of these panels were hygrothermally aged. Testing of these panels took place at room temperature conditions due to equipment restrictions and because this allows for the separation of effects caused by the hygrothermal aging and testing at elevated temperature. By performing these experiments for different bonding techniques the INOVA project aids aircraft manufacturers in choosing the right bonding type for each application.

The above described scope can be summarized in the following research objective: to numerically simulate the behavior of co-bonded composite stiffened panels loaded in compression post-buckling fatigue and to analyze the infuence of hygrothermal aging on the compression post-buckling fatigue behavior of these panels.

Additionally, the conditions for hygrothermal aging were determined by the agreements in the INOVA project. The panels were kept in a special oven until the start of the tests at 80^{0}C and 90% humidity. Total aging time varied due to the time of testing, but was in between 280 and 396 days. This was below the glass transition temperature of both the carbon fiber reinforced polymer adherent (166-204ºC) and the adhesive (95-150ºC).

Some selected information from this work is presented below. Figure 8-1 shows the front view of the panels tested, while Figure 8-2 shows the isometric view with the artificial damage inserted. Figure 8-3 shows how the specimens were assembled for the static, fatigue and residual strength tests, including some auxiliary devices, such as the anti-buckling, strain gages and LVDTs.

Figure 8-4 and Figure 8-5 show the disbond area and the disbond length growth respectively as function of the number of cycles for the post-buckling cyclic tests. Figure 8-6 and Figure 8-7 show the FEM model that was developed for this study, including the mesh and dimensions, and the comparison between numerical and experimental results for the static compression test in terms of axial and membrane strains.

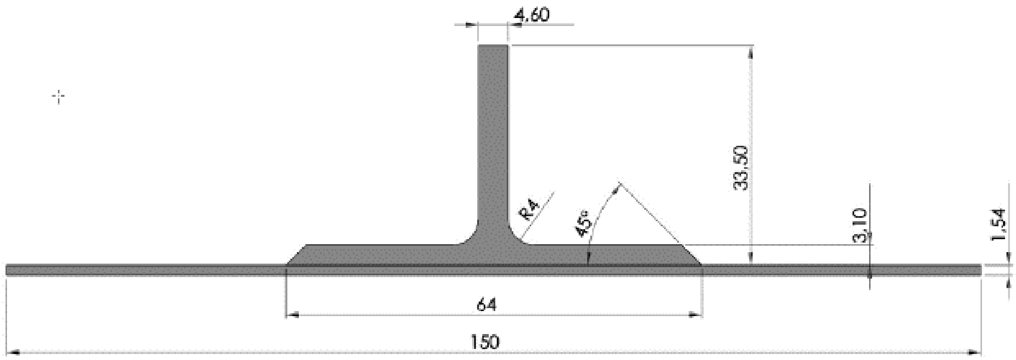

Figure 8-1 - Front view of the panels tested.

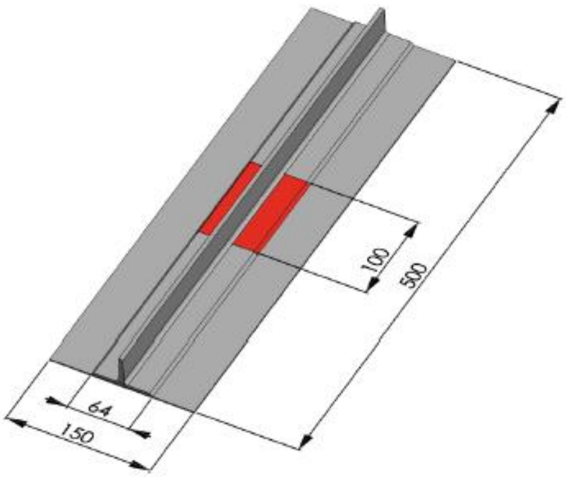

Figure 8-2 - Isometric view of the panels, with the Teflon™ insert depicted in red.

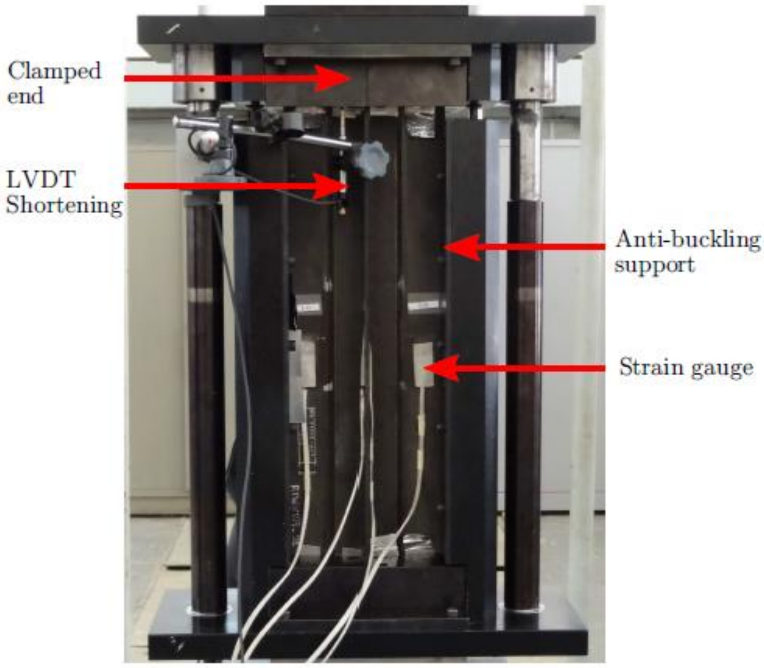

Figure 8-3 - Close-up of the test rig.

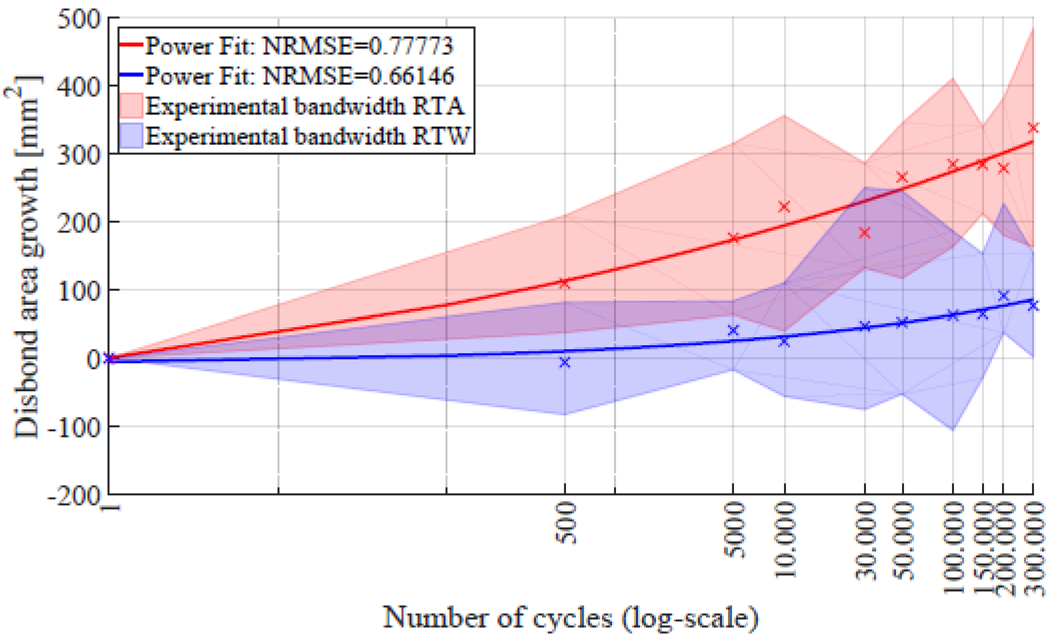

Figure 8-4 - Crack area growth.

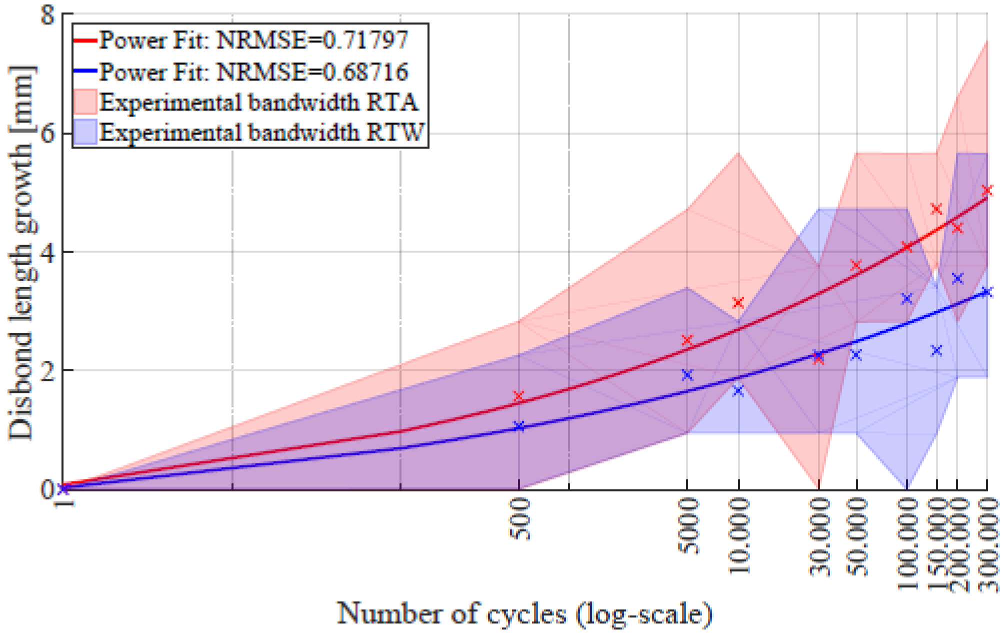

Figure 8-5 - Crack length growth.

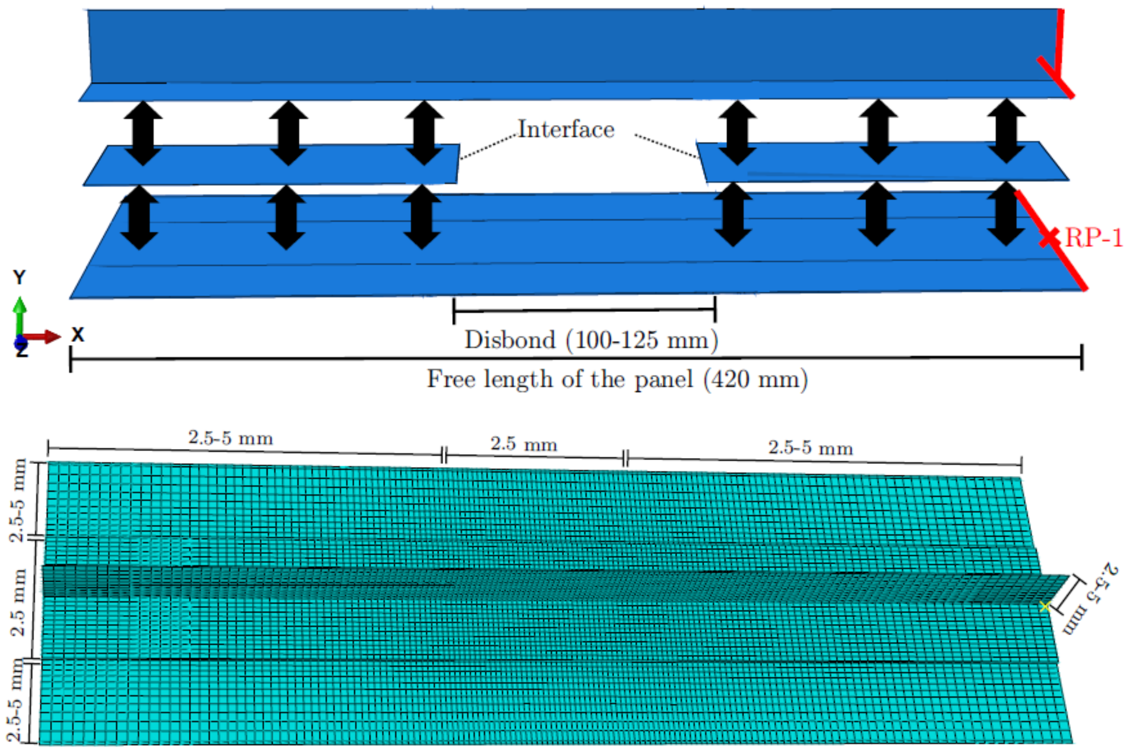

Figure 8-6 - FEM Model (a) schematic, (b) mesh and dimensions.

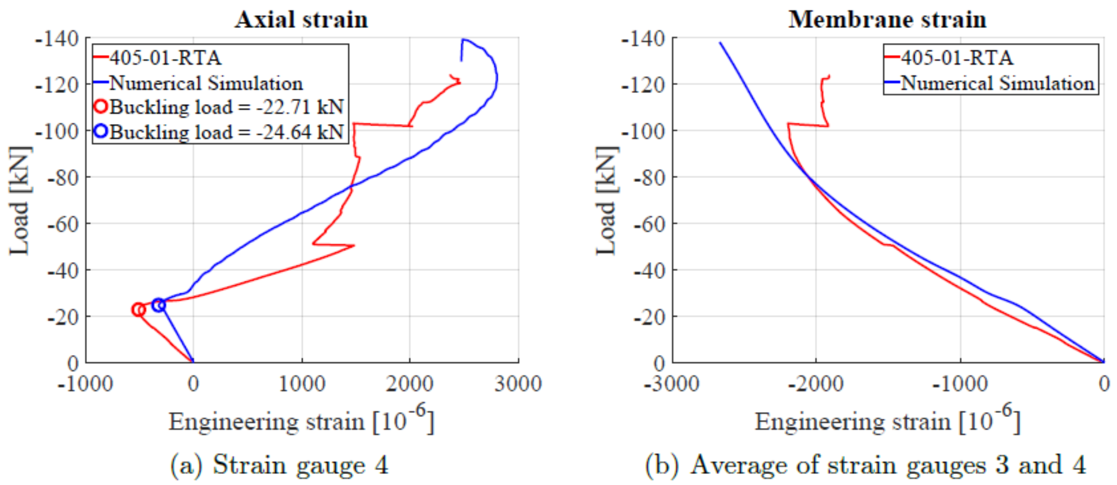

Figure 8-7 - Panel buckling behavior – experimental vs. numerical results.

Durability of Stiffened CFRP Panels with Initial Delaminations (Ref. [26])

This work was done in collaboration between TU-Delft and ITA, as part of the INOVA project, previously mentioned. The aim is to investigate the durability of bonded and co-cured joints in primary composite aerospace structures. Furthermore, the influence of elevated temperature and humidity on the joint properties was studied. The goal was ultimately to achieve a better understanding of the behaviour of bonded joints over a typical aircraft lifetime. This may then be further implemented in the damage tolerant design of a bonded composite structure for application within a primary aerospace structure.

The scope of the thesis is limited to co-cured composite (Carbon/Epoxy) panels at room temperature ambient (RTA) conditions. Bonding techniques and environmental affects were investigated to understand the broader scope of the whole project and how the research of this proposed MSc thesis would contribute to the larger aim of the INOVA project. The study of bonded joints is relevant to co-cured structures since the mechanisms of crack growth in a bonded joint are comparable to delamination growth in a co-cured interface.

The primary contributing members of the INOVA project are Technological Institute of Aeronautics (ITA) and Embraer. The stiffened panels investigated were produced (by Embraer) and introduced in the dissertation to give a better understanding of the physical problem at hand. The panel and the Teflon™ insert characteristics are the same as in Figure 8-1 and Figure 8-2.

The primary objective of the work was to experimentally validate a fatigue crack growth model, using a cohesive zone formulation, on the sub-assembly level by analyzing fatigue crack growth in artificially disbonded stiffened panels. Figure 8-8 shows an overview of the project work, including a numerical and an experimental work.

Additionally, some selected results are presented. Figure 8-9 shows one example of DIC measurement for a loaded panel. Figure 8-10 shows an overview of the laboratory facilities, while the test specimen and setup are the same as presented previously in Figure 8-3. Figure 8-11 shows the comparison of the numerical residual strength models with the pristine (i.e., undamaged) residual strength model and experimental data from residual strength tests for both pristine and damaged conditions. Figure 8-12 shows the disbond length growth measured for two of the tested panels.

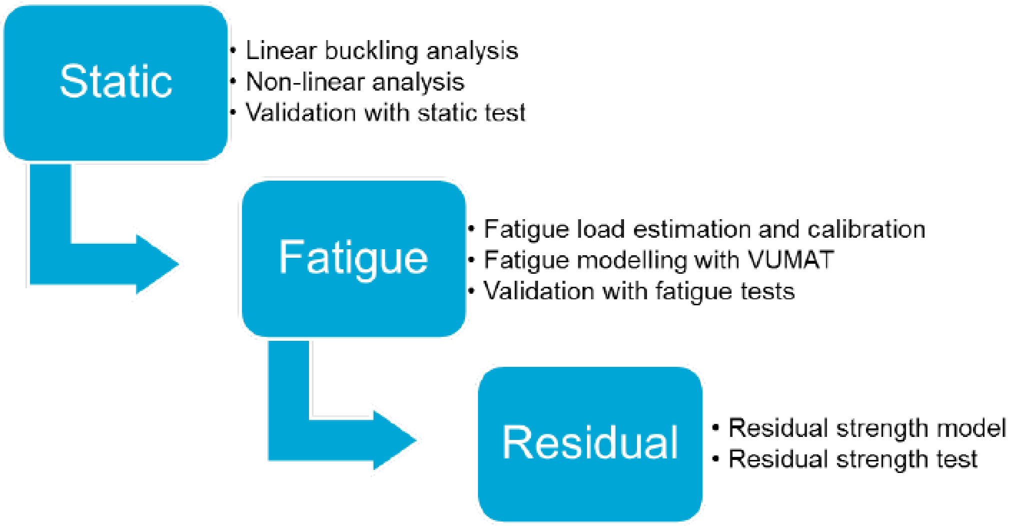

Figure 8-8 - Overview of the project work: modelling, testing and validation.

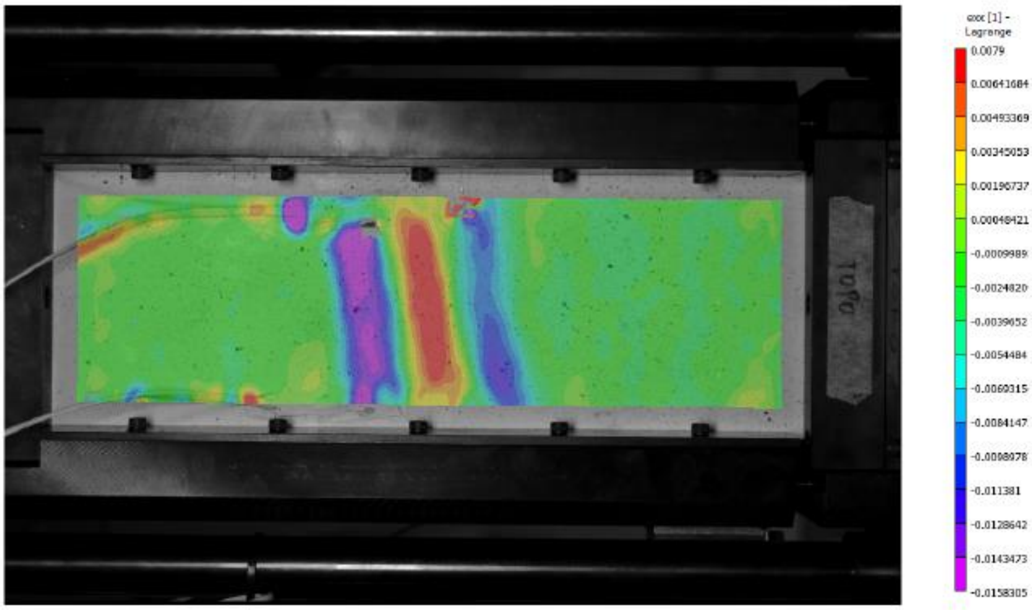

Figure 8-9 - Quasi-static tests: DIC analysis of panel skin, load = 80kN.

Figure 8-10 - Fatigue test setup. Left to right: Load frame with test rig, portable c-scan device, hydraulic control computer.

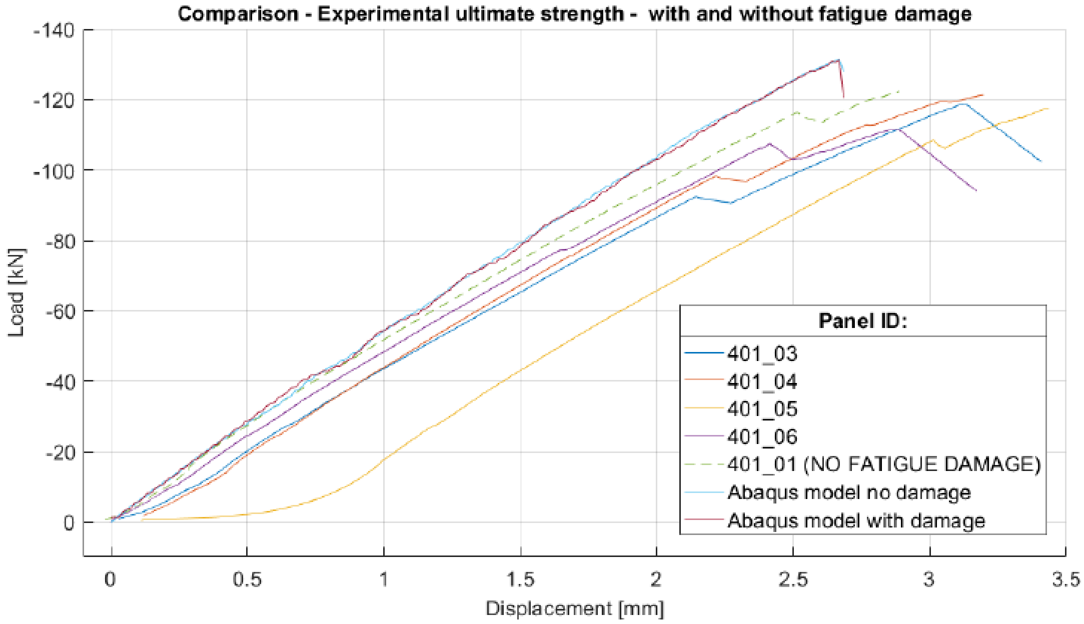

Figure 8-11 - Comparison of residual strength model with the pristine strength model and experimental data from residual strength tests.

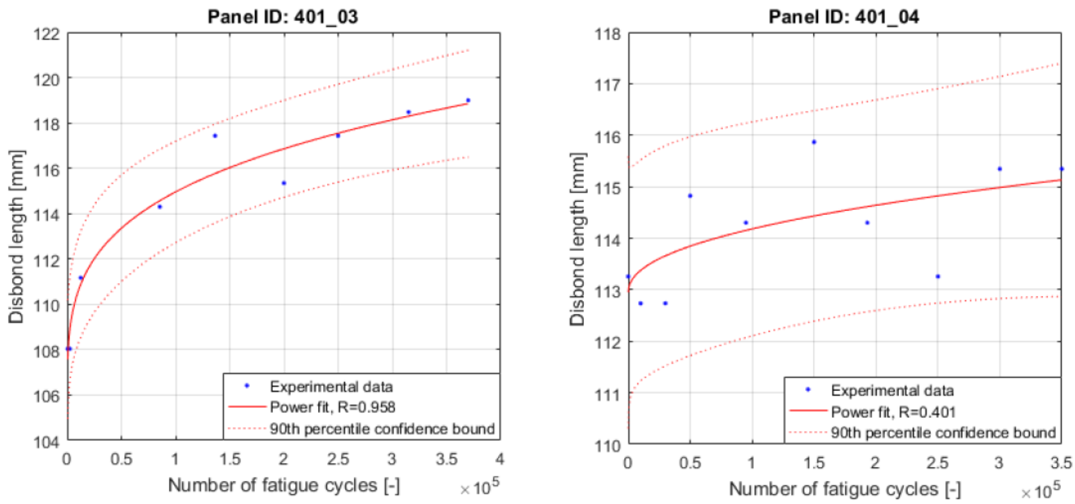

Figure 8-12 - Example of disbond length measurements under fatigue loading.

Strain Rate Effects on the Intralaminar Fracture Toughness of Composite Laminates Subjected to Compressive Loads (Ref. [27])

This paper presents an experimental and numerical study focused on the mode-I intralaminar toughness characterization of a woven carbon/epoxy composite loaded in compression and subjected to high strain rates. Simulations for a non-standardized Single Edge Notch Bending (SENB) and DEN were carried out using a continuum damage mechanics based failure model implemented as an user defined material model within ABAQUS software. A Finite Element Model was used in order to produce an optimal specimen for intralaminar fracture toughness tests. A new data reduction scheme based on the numerical evaluation of the strain energy release rate using the J-integral method is proposed to determine the stress intensity factor for composites. The proposed methodology accounts for finite geometry and material anisotropy effects.

The dynamic tests were carried out for the DEN specimen at strain rates of 560s^{-1}, 690s^{-1}, 770s^{-1} using an adapted version of the Split Hopkinson Pressure Bar. A high-speed camera was used for monitoring the crack propagation. A scanning electron microscope (SEM) was used to aid the fractographic analyses on the damaged surface of the tested samples searching for the possible failures mechanisms within the material. The experimental results indicated that the composite laminates studied herein are very sensitive to the strain rate effects.

Strain Rate Effects on the Intralaminar Fracture Toughness of Composite Laminates Subjected to Tensile Loads (Ref. [28])

This paper presents a numerical and experimental study on the intralaminar tensile fracture toughness of carbon fiber reinforced composite subjected to high strain rates. As there is no standardized testing procedures for intralaminar fracture toughness characterization of composites at high strain rates, there is a clear need to design specimen geometries, testing apparatus and data reduction schemes that allows the characterization of the fracture toughness of composites in the dynamic regime.

Initially numerical studies were performed based on finite element simulations in order to investigate the viability of its construction for different testing configurations to characterize the intralaminar toughness of composite laminates. A comparative study is presented showing the advantages and disadvantages of each testing configuration. A new data reduction scheme based on modifications in the ASTM standard, accounting for material anisotropy and specimen finite geometry effects is suggested.

Experimental tests were carried out, using the proposed specimen configuration at different strain rates in order to investigate the strain rate effects using a modified version of the Split Hopkinson Pressure bar. Fractography analyses using Scanning Electron Microscopy (SEM) have been also performed in order to investigate the strain rate effects on the failures mechanisms of the composite material studied herein.

The two papers above discussed are very closely related. In the previous ICAF review (Ref. [2]), the numerical results (that were obtained preliminarly) were presented, while this year the tests for validation are also included.

Some selected information from both papers is presented below. Figure 8-13 presents an overview of the Hopkinson bar used for the tests and the related instrumentation.

Figure 8-14 and Figure 8-15 bring a compilation of the numerical models, analysis results, experimental setup and test specimens and the correlation between analysis and experiments in terms of the fracture toughness under dynamic loading conditions.

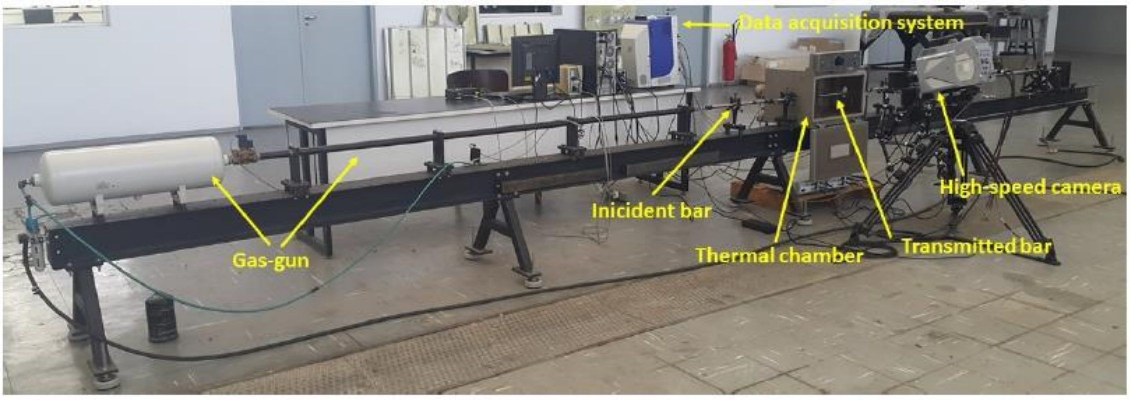

Figure 8-13 - Experimental setup for tests in the dynamic regime.

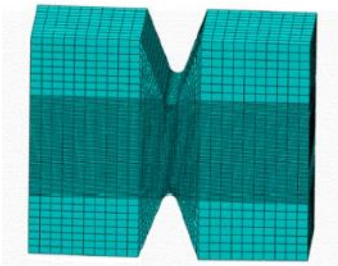

(a) DEN Specimen FEM mesh

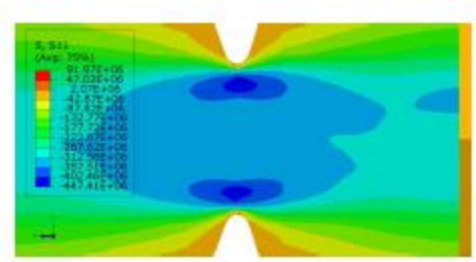

(b) Compression stress field at crack tip

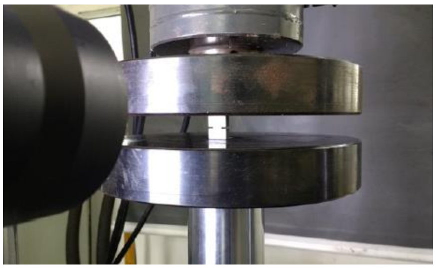

(c) Setup for quase-static tests

(d) Actual dynamic test specimen

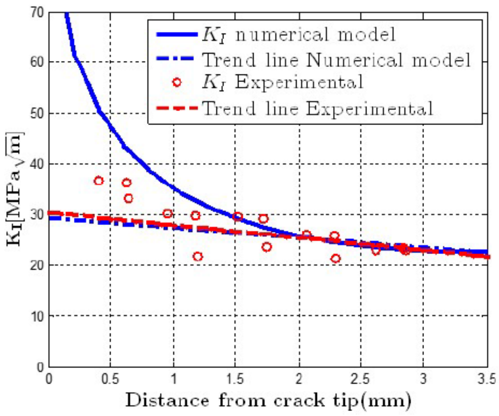

(e) Kc estimation from quase-static tests

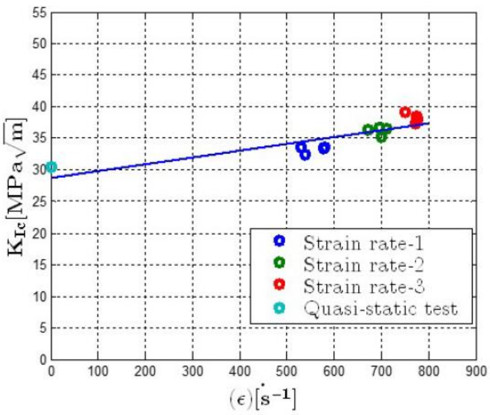

(f) Experimental dynamic fracture toughness

Figure 8-14 – Selected information about FEM modeling and analysis, experimental setup and test specimen and numerical and experimental results from Reference [27].

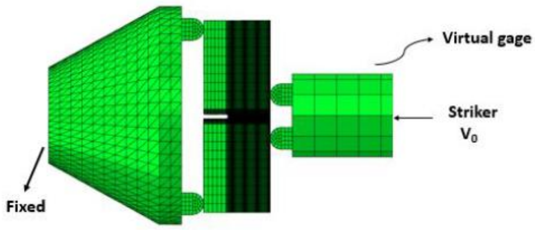

(a) SENB Specimen FEM mesh

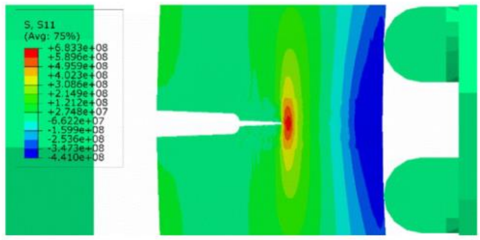

(b) Compression stress field at crack tip

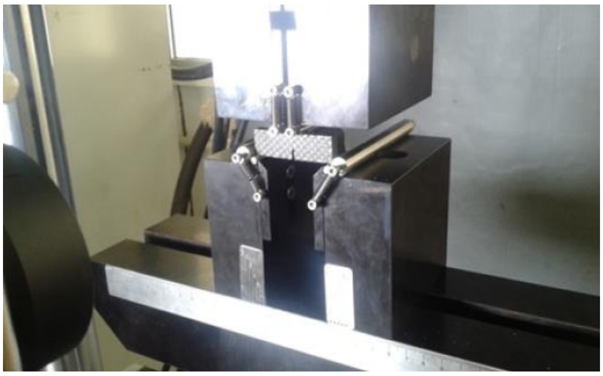

(c) Setup for quase-static tests

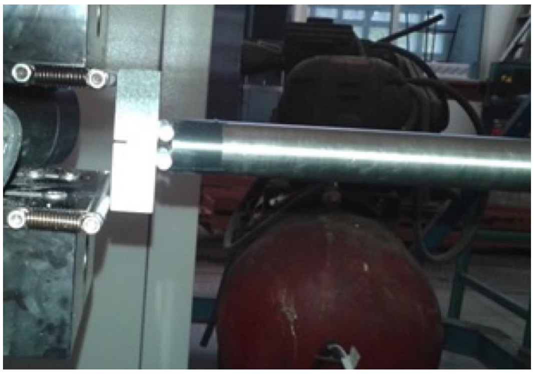

(d) Dynamic test specimen

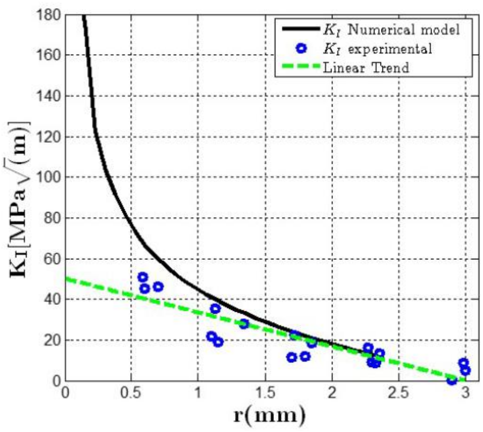

(e) Kc estimation from quase-static tests

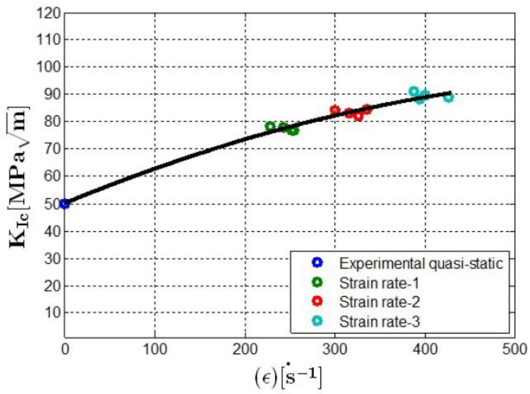

(f) Experimental dynamic fracture toughness

Figure 8-15 - Selected information about FEM modeling and analysis, experimental setup and test specimen and numerical and experimental results from Reference [28].

Hygrothermal Effects on Interlaminar Fracture Toughness of Composite Joints (Ref. [29])

Mode I Interlaminar Fracture Toughness Analysis of Co-Bonded and Secondary Bonded Carbon Fiber Reinforced Composites Joints (Ref. [30])

This work is driven by the need aerospace industry has to establish design allowables in damage tolerance analyses and to use composite in elongated aircraft wings. The main purposes of the work were to evaluate three different manufacturing processes to adhesively bond carbon/epoxy composite laminates (T800/3900-2) and to assess how hygrothermal aging affects their behavior.

The dissertation investigates the fracture behavior of three types of carbon/epoxy composite joints, named co-cure, co-bonding and secondary bonding, and how aging affects their properties. Two campaigns were conducted: one to be the reference, performed at room conditions, and one to evaluate the influence of temperature and moisture.

Fracture toughness was assessed through a set of mechanical tests carried out under pure Mode I (Double Cantilever Beam), pure Mode II (Four Point Bend End Notched Flexure) and Mixed-mode I/II at 35%, 50% and 75% of Mode II (Mixed Mode Bending) in order to obtain the failure envelope corresponding to each bonding technology. The mechanical tests showed that co-cure presented the lowest values of fracture toughness at ambient conditions under any failure mode, while co-bonding and secondary bonding alternated as the highest fracture toughness during mixed-mode tests, with co-bonding ending up as the highest under pure Mode II. For the aged set, however, co-cure presented by far the highest fracture toughness under pure Mode II, while secondary bonding was the toughest under mixed-mode tests and all three technologies were almost equal under pure Mode I.

Fractography analysis was performed in tested specimens to determine the failure mechanisms involved during fracture process and how temperature and moisture affected it, showing that the different values of fracture toughness resulted from a change in failure mode derived from the hygrothermal influence. Quantitatively, DMA and DSC tests determined that matrix and adhesive had their glass transition temperature lowered 20°C in average by the aging process, explaining the different results between dry and aged sets of tests, proving that the extreme ambient conditions cannot be neglected during project concept.

Figure 8.16 shows an overview of the apparatuses used in the mechanical tests performed in the work. Table 8-1 and Table 8-2 present the summary of results for each bonding technology appraised from all failure modes under RTA and ETW conditions respectively.

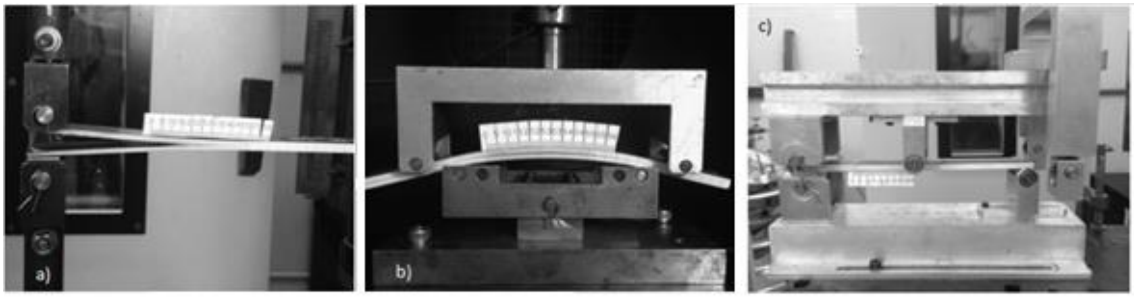

Figure 8-16 - Apparatuses used in the mechanical tests performed in this work. a) Characterization of Mode I fracture toughness - DCB test; b) Characterization of Mode II fracture toughness - 4ENF test and; c) Characterization of Mixed Mode I-Mode II fracture toughness - MMB test.

Table 8-1 - Summary of results for each bonding technology appraised from all failure modes under RTA condition.

	Co-Cure				
	Propagation	Failure Mode	GIc [N/mm]	GIIc [N/mm]	GT [N/mm]
Mode I	Unstable/Stable	Interlaminar	0.15-0.21	-	0.15-0.21
Mixed-Mode: 35%	Stable	Interlaminar	0.12-0.20	0.06-0.1	0.18-0.30
Mixed-Mode: 50%	Stable	Interlaminar	0.08-0.12	0.08-0.12	0.16-0.24
Mixed-Mode: 75%	Unstable/Stable	Interlaminar	0.06-0.08	0.18-0.22	0.24-0.30
Mode II	Stable	Interlaminar	-	0.70-0.91	0.70-0.92
	Co-Bonded				
	Propagation	Failure Mode	GIc [N/mm]	GIIc [N/mm]	GT [N/mm]
Mode I	Unstable/Stick-Slip	Cohesive/Interlaminar	0.24-0.30	-	0.24-0.30
Mixed-Mode: 35%	Unstable/Stable	Interlaminar	0.13-0.25	0.07-0.13	0.20-0.38
Mixed-Mode: 50%	Unstable/Stable	Interlaminar	0.09-0.15	0.10-0.16	0.19-0.31
Mixed-Mode: 75%	Unstable/Stable	Interlaminar	0.08-0.18	0.23-0.53	0.31-0.71
Mode II	Stable	Light-Fiber-Tear	-	6.00-8.01	6.00-8.02
	Secondary Bonded				
	Propagation	Failure Mode	GIc [N/mm]	GIIc [N/mm]	GT [N/mm]
Mode I	Unstable/Stable	Cohesive/Interlaminar	0.15-0.35	-	0.15-0.35
Mixed-Mode: 35%	Unstable/Stable	Interlaminar	0.32-0.44	0.17-0.23	0.49-0.67
Mixed-Mode: 50%	Unstable	Interlaminar	0.36-0.56	0.34-0.54	0.70-1.10
Mixed-Mode: 75%	Unstable	Interlaminar	0.10-0.28	0.31-0.81	0.41-1.09
Mode II	Stable/Unstable	Mixed*/Light-Fiber-Tear	-	5.45-6.56	5.45-6.57
	* *Mixed* refers to a fracture that propagates jumping, alternating between interfaces				

Table 8-2 - Summary of results for each bonding technology appraised from all failure modes under ETW condition.

	Co-Cure				
	Propagation	Failure Mode	GIc [N/mm]	GIIc [N/mm]	GT [N/mm]
Mode I	Stable	Interlaminar	0.08-0.14	-	0.08-0.14
Mixed-Mode: 35%	Stable	Interlaminar	0.05-0.17	0.06-0.12	0.11-0.29
Mixed-Mode: 50%	Stable	Interlaminar	0.14-0.18	0.13-0.17	0.27-0.35
Mixed-Mode: 75%	Stable/Unstable	Interlaminar	0.90-0.11	0.24-0.30	0.33-0.41
Mode II	Stable	Interlaminar	-	1.84-2.24	1.84-2.25
	Co-Bonded				
	Propagation	Failure Mode	GIc [N/mm]	GIIc [N/mm]	GT [N/mm]
Mode I	Stable	Light-Fiber-Tear/Interlaminar	0.10-0.14	-	0.10-0.14
Mixed-Mode: 35%	Stable	Interlaminar	0.12-0.22	0.06-0.12	0.18-0.34
Mixed-Mode: 50%	Stable	Light-Fiber-Tear/Interlaminar	0.17-0.23	0.17-0.23	0.34-0.46
Mixed-Mode: 75%	Stable/Unstable	Interlaminar	0.07-0.11	0.22-0.3	0.29-0.41
Mode II	Stable	Light-Fiber-Tear/Mixed*	-	0.53-0.61	0.53-0.62
	Secondary Bonded				
	Propagation	Failure Mode	GIc [N/mm]	GIIc [N/mm]	GT [N/mm]
Mode I	Stick-Slip	Light-Fiber-Tear	0.01-0.15	-	0.01-0.15
Mixed-Mode: 35%	Stable	Light-Fiber-Tear/Interlaminar/Cohesive	0.14-0.34	0.13-0.21	0.27-0.55
Mixed-Mode: 50%	Stable	Light-Fiber-Tear/Interlaminar/Cohesive	0.14-0.34	0.14-0.32	0.28-0.66
Mixed-Mode: 75%	Stable	Interlaminar/Cohesive	0.15-0.23	0.44-0.64	0.59-0.87
Mode II	Stable	Mixed*	-	0.28-0.4	0.28-0.5
	* *Mixed* refers to a fracture that propagates jumping, alternating between interfaces				

Hygrothermal Effects on the Fatigue Delamination Growth Onset in Composite Joints (Ref. [31])

Experimental Characterization of Mode I Fatigue Delamination Growth Onset in Composite Joints: A Comparative Study (Ref. [32])

In this work the effect of hygrothermal pre-conditioning on the fatigue delamination growth onset of bonded joints under pure Mode I and II was investigated. The fatigue tests were conducted on CFRP epoxy joints with an epoxy interleaf that was subjected to a relative humidity (RH) of 90% and at a temperature of 80°C until steady state saturation. For both loading configurations, three types of joining techniques were evaluated: co-curing, co-bonding and secondary bonding, see Figure 8-17. The co-bonded (CB) and secondary bonded (SB) specimens contained an epoxy adhesive film, while the co-cured (CC) specimens were only comprised by fibers and resin. The Mode I and II G-N curves were obtained using double cantilever beam (DCB) and three point bend end-notched flexure (3-ENF) testing, respectively. Through the G-N curves, the threshold (Gth) value of each bonding technology was estimated and compared with dry specimens.

Finally, the strain energy release rate (SERR) results were related with the joint´s failure mechanism through a fractographic analysis. Under both loading modes, the adhesive joints experienced a significant decrease in their Gth values in comparison with the dry joints. Water uptake degrades the adhesive and adhesive/substrate interface and causes the polyester net´s swelling, which favors the water diffusion through the laminate.

Some important conclusions drawn from this work are:

- For Mode I loadings, the CC aged joints experienced a Gth increase of 17.4% in comparison with the dry joints due to the increase of the interleaf plastic deformation. While, under Mode II loadings, the CC aged joints present a slight decrease of 1%.

- For Mode I loading, the aged CB joints present a better fatigue delamination growth onset than the aged CC and SB joints, while, for Mode II the aged CC joints exhibited a Gth value approximately 2 and 4 times higher than the aged CB and SB joints, respectively.

Figure 8-18 shows as an example the test setup for Mode I. Additionally, some selected results from this work are presented here. Figure 8-19 and Figure 8-20 show the Mode I and Mode II G-N curves for CC, CB and SB joints. Figure 8-21 shows the Mode II G-N curves for specimens with and without an environmental pre-conditioning.

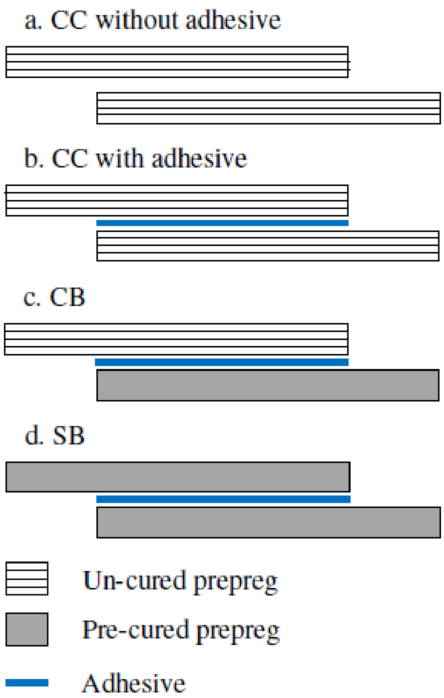

Figure 8-17 - Schematic of main manufacturing process of bonded joints.

Figure 8-18 - Mode I fatigue delamination tests set-up.

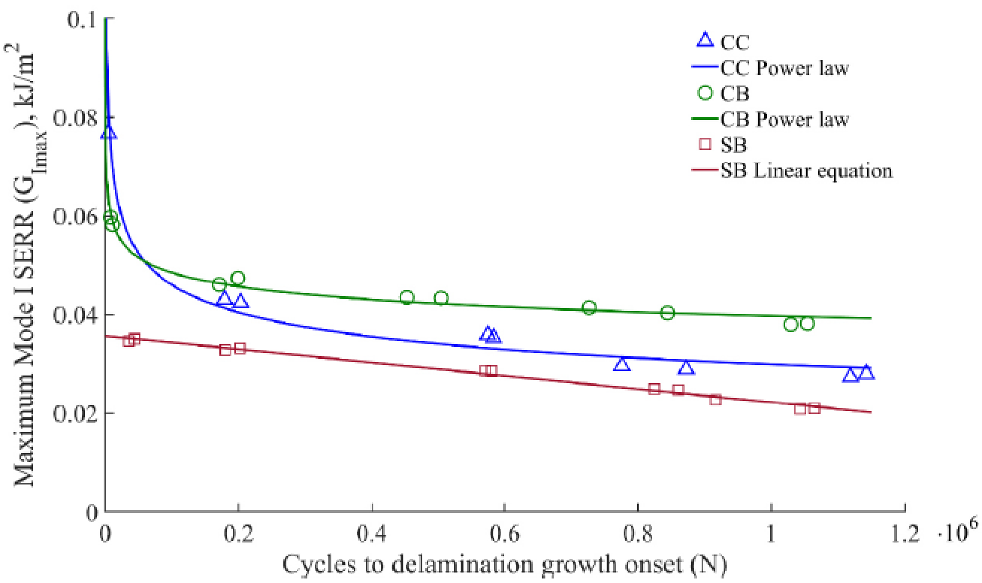

Figure 8-19 - Mode I G-N curve for CC, CB and SB joints.

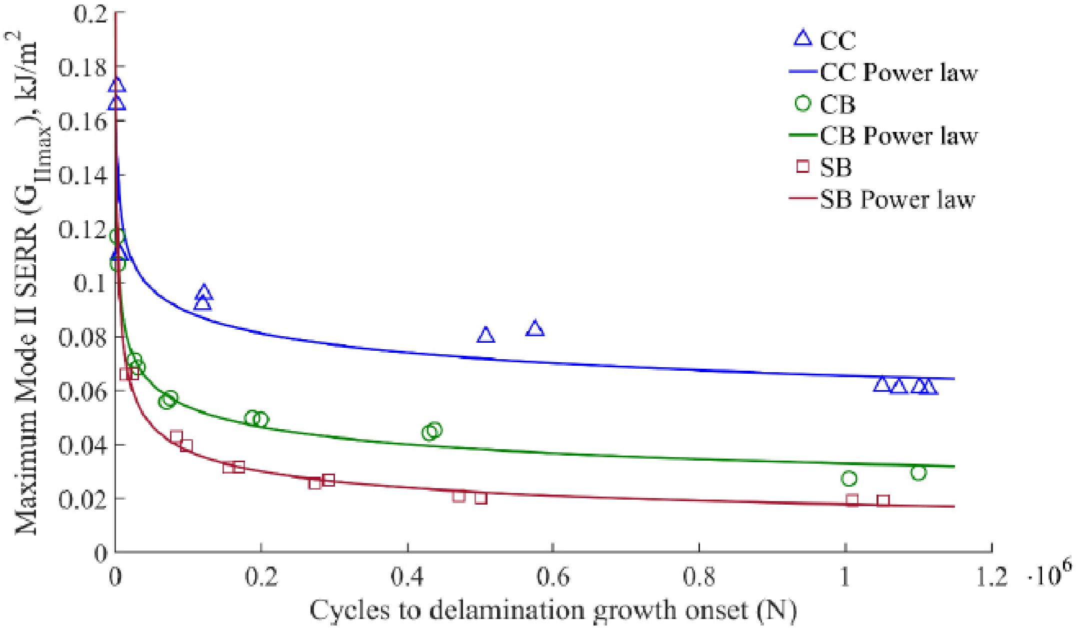

Figure 8-20 - Mode II G-N curve for CC, CB and SB joints.

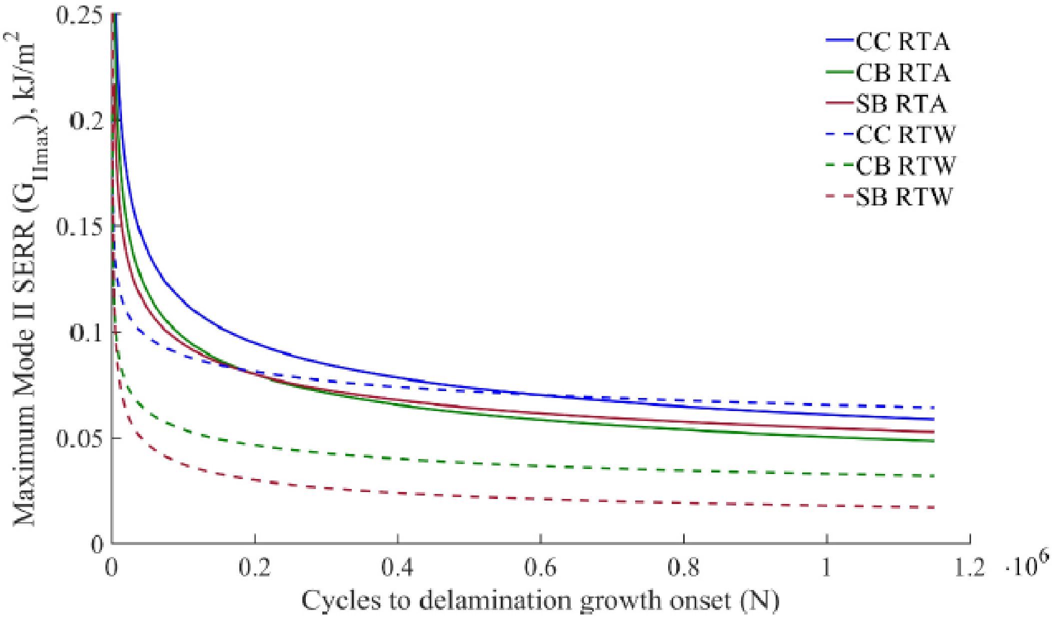

Figure 8-21 - Mode II G-N curves for specimens with and without an environmental pre-conditioning.

Experimental Characterization of Fatigue Delamination Growth Onset in Composite Joints Tested at Room Temperature Ambient Condition (RTA) (Ref. [33])

Structural Behavior of Secondary-bonded Composite Joints Subjected to Mode II Fatigue Induced Delamination (Ref. [34])

The aeronautical industry has strongly employed composite materials for the construction of aircraft since this class of materials allows the use of different types of matrix and reinforcement, resulting in high performance materials with improved mechanical and physical properties, such as low density, higher mechanical resistance and high effciency, key factors for use in the aeronautical sector. Despite these advantages, these materials are prone to interlaminar damage, especially under cyclic loading conditions. Several techniques are being researched in order to replace the conventional composite parts joining, especially rivets and screws because these mechanical procedures usually involves high energy needs to attach and can cause stress concentrators that could probably start defects and a reduction in fatigue life.

This work evaluated the structural behavior of three composite joint technologies, named as co-cure (CC), co-bonding (CB) and secondary bonding (SB), with the objective of obtaining the G-N_f curves, in terms of the strain energy release rate (G-SERR) versus number of cycles (N_f). Samples were submitted to Mode I fatigue tests using the Double Cantilever Beam and Mode II were performed with three-point bending End Notched Flexure (3-ENF).

The results show that the adhesive improves the threshold energy release rate value (Gth) for Mode I fatigue test, consequently the fatigue life behavior for the different joints respected the following order: similar G - N_f behaviour was found for co-bonded and secondary bonded joints with G values slightly higher than co-cured joints. For specimens submitted to Mode II, the results show a reduction on Gth for secondary-bonded and co-bonded composite joints, when compared to co-cured joints, where no adhesive is used.

Fractographic analyses were also performed in order to identify the main failure mechanisms related to each joining technology under Mode I and Mode II fatigue induced delamination.

Figure 8-22 shows the test setup, and Figure 8-23 shows the summary of all experimental results obtained for the three bonding technologies and delamination modes.

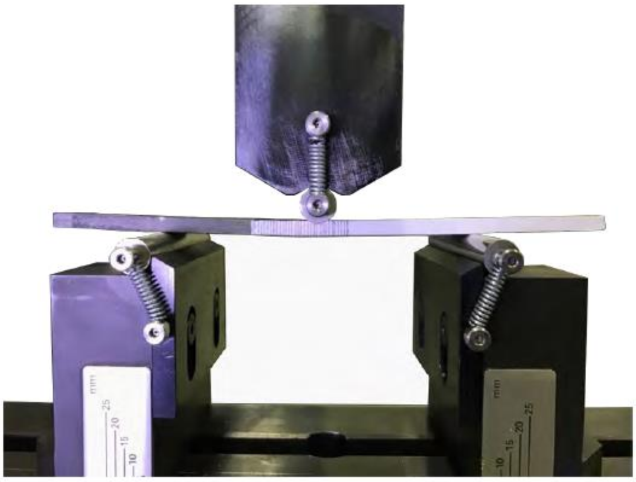

Figure 8-22 - 3-ENF setup fatigue test.

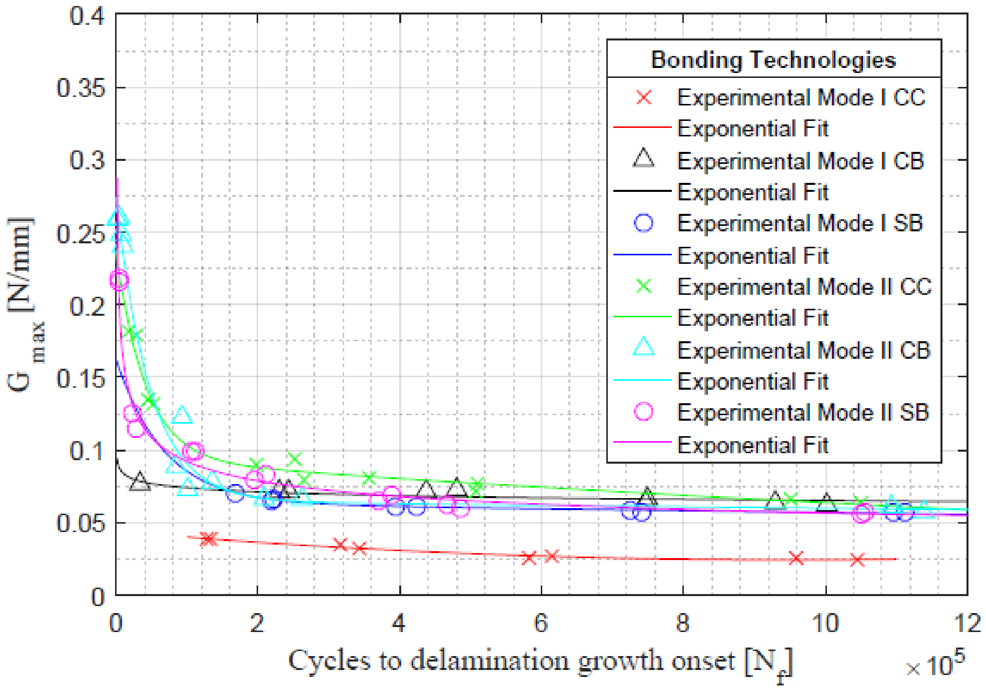

Figure 8-23 - Comparison between G-Nf curves for Mode I and II of all joint samples.

Fractographic Analysis of Adhesive by Bonded Technologies Applied to Advanced Composite Aerostructures (Ref. [35])

Adhesive bonding technologies for thermosetting polymer composites have been applied in several industrial sectors due to their excellent mechanical behavior (high strength-to-weight ratio, damage tolerance, and fatigue resistance). The great advantage of this technology compared to traditional mechanical fasteners is that the use of adhesive joints does not induce damage by delamination in the material during the joining process, as occurs when drilling holes for the assembly by rivets or bolts. Furthermore, the adhesive bonding results a more distributed loading transferring with a smaller addition of material weight.

The overall structural performance of the bonded joint depends on several factors related to the joint manufacturing process, such as surface preparation procedure, type of adhesive and aging effects. For this reason, there is a clear need to better understand how the behavior of joints can be affected by these factors as well as the causes of eventual failures in order to improve the design and performance.

Within this context, this work presents the application of Scanning Electron Microscopy (SEM) technique to perform the fractographic analysis in three different joint types namely, co-cured (CC), co-bonded (CB), and secondary bonded (SB), which were subjected to Mode I and Mode II interlaminar fracture toughness tests under both Room Temperature Ambient (RTA) and Elevated Temperature Wet (ETW) conditions.

The fracture surfaces of samples submitted to each loading condition were evaluated regarding their failure aspects, which were in turn associated with the mechanical behavior observed when submitted to the different loading modes and environmental conditioning.

A detailed fractographic characterization of the composite joints fracture surface was carried out, correlating their specific behavior, type of processing and conditioning, thus validating the use of the joints for conditions similar to those of real application.

In this work, it was observed that the CB composite joints presents higher fracture toughness when subjected to environmental conditioning in comparison to the other type of joints studied herein, due to the type of adhesion between the laminates and laminate/adhesive interfaces, mechanical interlocking and chemical bonding during the manufacturing process. The CC joints showed a good performance under Mode II delamination loading at ETW conditioning due to thermoplastic particles that enhance the joint toughness. The SB joint presented the worst performance to conditioning in both loading conditions.

In conclusion, CB joints were considered to be the best configuration bonded joints, followed by CC joints and finally SB joints.

The following Tables (Table 8-3 and Table 8-4) and Figures (from Figure 8-24 to Figure 8-29) show the summaries of all failure modes identified and mapped along the work, for CC, CB and SB joints and for Modes I and II. The dissertation contains inumerous pictures with the SEM fractographic analysis performed and the failure mechanisms described in detail.

Table 8-3 - Summary of failure modes observed in composite joints subjected to Mode I delamination

Nº	FAILURE ASPECT	Abv	CC		CB		SB	
			RTA	ETW	RTA	ETW	RTA	ETW
1	Broke fibers	BRF	○	• •	•	• •	• •	• •
2	Cleavage by fiber bridging	CFB	• •	•	○	○	○	• • •
3	Cusps (fiber region)	CFR	•	○	•	•	•	○
4	Cusps (matrix region)	CMR	○	○	○	•	○	•
5	Debris	DBR	○	○	○	○	○	• • •
6	Failure in two planes	FTP	-	-	-	-	○	• • •
7	Failure occured by Polyester net node	FPN	-	-	•	○	• • •	•
8	Feather	FTH	○	○	•	•	•	• •
9	Fiber bridging	FIB	• • •	• • •	• •	• • •	• •	• • •
10	Fiber imprint	FII	• • •	• • •	• •	• • •	• •	• • •
11	Loose particle	LPT	-	• • *	-	• • *	-	• • *
12	Microcracks	MCR	○	• • *	○	• *	•	•
13	Particle deformed	PDF	• • •**	•	•	•	•	•
14	Particle pullout	PPO	• • •**	○	•	○	•	•
15	Peel ply (Adhesive failure)	PPA	-	-	•	• • *	•	• •
16	Peel ply (Cohesive failure)	PPC	-	-	•	• *	•	•
17	Resin deformation (plasticization)	RDF	-	• •	-	• •	-	○
18	Ribbon	RBB	○	○	•	○	○	○
19	River lines	RIL	• • •	○	• •	○	•	• •
20	Roughness appearance on the adhesive	RAA	-	-	•	• • *	• •	•
21	Scarp on the adhesive	SAD	-	-	• •	• *	• •	•
22	Scarp on the resin	SRS	○	○	•	• *	•	•
23	Smooth appearance on the adhesive	SAA	-	-	• • •	• *	• •	• *
24	Texturized microflow	TMF	• •	○	•	•	○	•

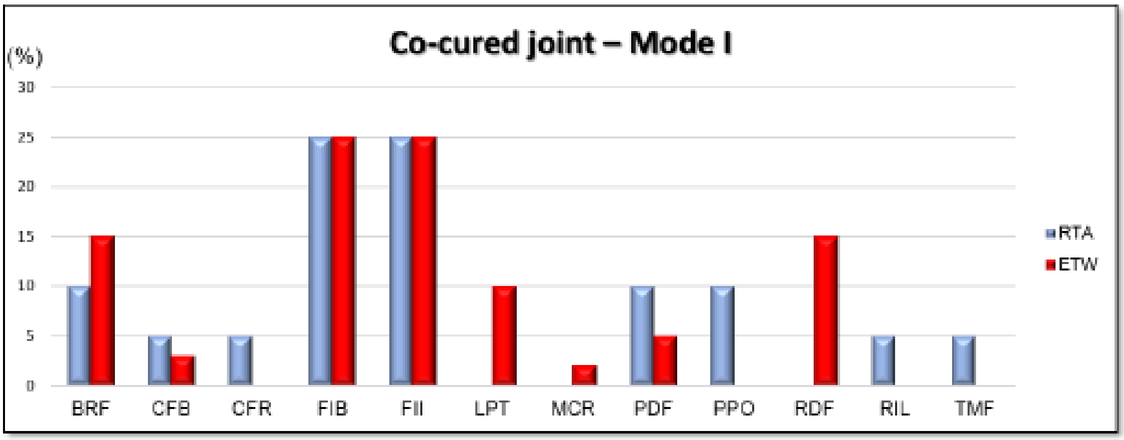

Figure 8-24 - Comparison of failures aspects observed in co-cured specimens tested under Mode I loading at RTA and ETW conditions.

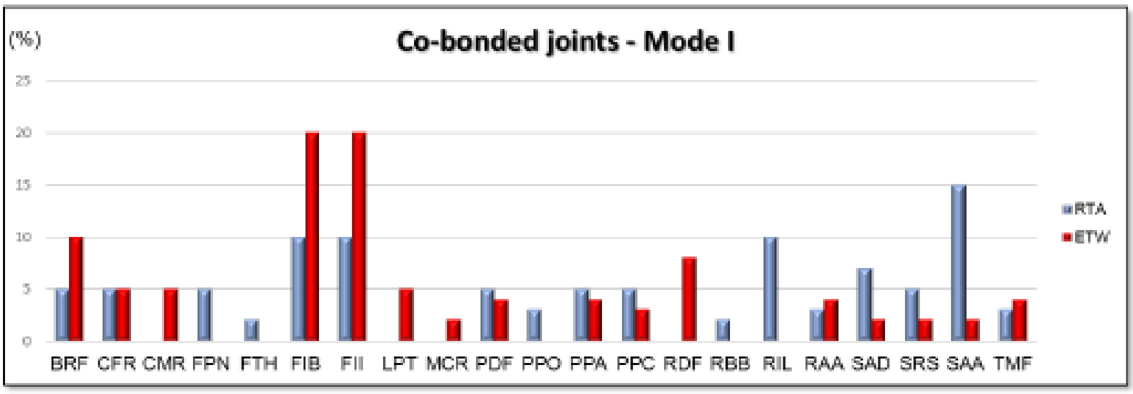

Figure 8-25 - Comparison of failures aspects observed in co-bonded joints tested under Mode I loading at RTA and ETW conditions.

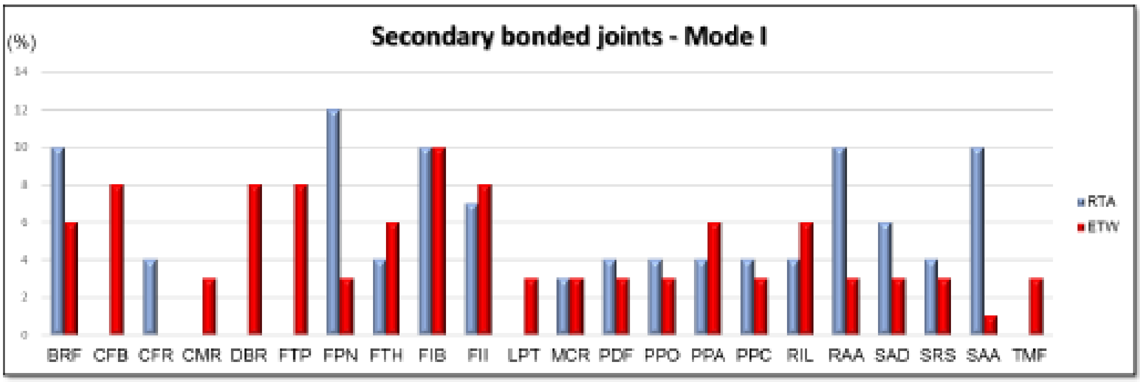

Figure 8-26 - Comparison of failures aspects observed in secondary bonded joints tested under Mode I loading at RTA and ETW conditions.

Table 8-4 - Summary of failure modes observed in composite joints subjected to Mode II delamination

Nº	FAILURE ASPECT	Abv	CC		CB		SB	
			RTA	ETW	RTA	ETW	RTA	ETW
1	Broke fibers	BRF	• •	• •	○	• • •	•	-
2	Cleavage	CLV	•	•	○	○	• • •	-
3	Cusps (fiber region)	CFR	• • •	• • •	• •	•	• • •	-
4	Cusps (matrix region)	CMR	• • •	• •	○	○	•	-
5	Debris	DBR	• •	• •	•	• • •	• •	•
6	Failure in two planes	FTP	-	-	-	-	•	○
7	Failure occured by Polyester net	FPN	-	-	• • •	• • •	• • •	• • •
8	Feather	FTH	•	-	○	-	• • •	-
9	Fiber bridging	FIB	•	•	○	• •	•	-
10	Fiber imprint	FII	• • •	• • •	• • •	• • •	• • •	○
11	Gouges	GGS	○	○	•	•	• • •	-
12	Loose particle	LPT	○	•*	•*	• •	○	•
13	Microcracks	MCR	○	•	•	• •*	• • •	•
14	Particle deformed	PDF	• • •*	-	•	•	• •	•
15	Particle In a flat shape	PFS	-	•	-	• • •	-	-
16	Particle in high deformation	PHD	○	• • •	• • •*	○	-	-
17	Particle partially bonded to adhesive	PBA	-	-	• •	• •	-	-
19	Particle pullout	PPO	• •	-	○	○	•	
20	Peel ply (Adhesive failure)	PPA	-	-	○	• • •	• • •	• • •
21	Peel ply (Cohesive failure)	PPC	-	-	○	• •	•	• • •
22	Resin deformation (plasticization)	RDF	-	• • •	-	○	-	-
24	River lines	RIL	•	•	○	•	• • •	-
25	Rollers	RLL	-	-	-	○	-	• • •
26	Roughness appearance on the adhesive	RAA	-	-	• • •	• • •	• • •	• • •
27	Scarp on the adhesive	SAD	-	-	•	○	•	-
28	Scarp on the resin	SRS	•	•	○	○	•	-
29	Texturized microflow	TMF	•	• • •	•	○	•	-

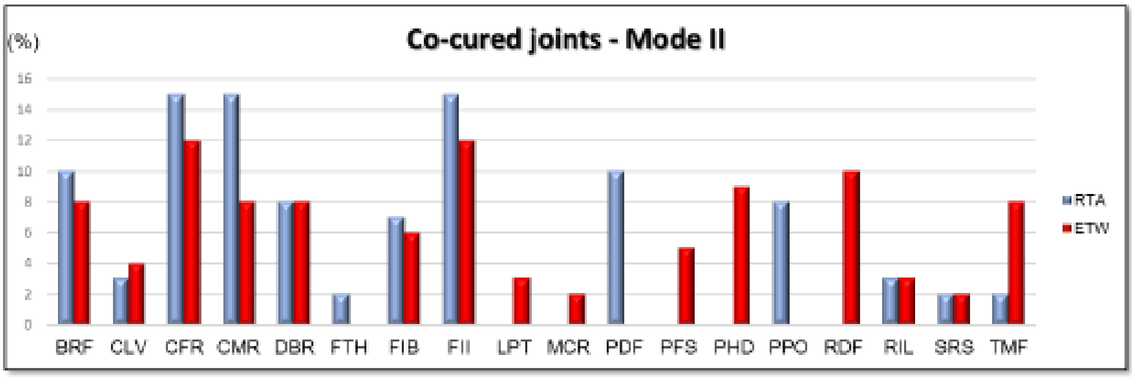

Figure 8-27 - Comparison of failures aspect between RTA and ETW conditioning of co-cured joints under Mode II delamination.

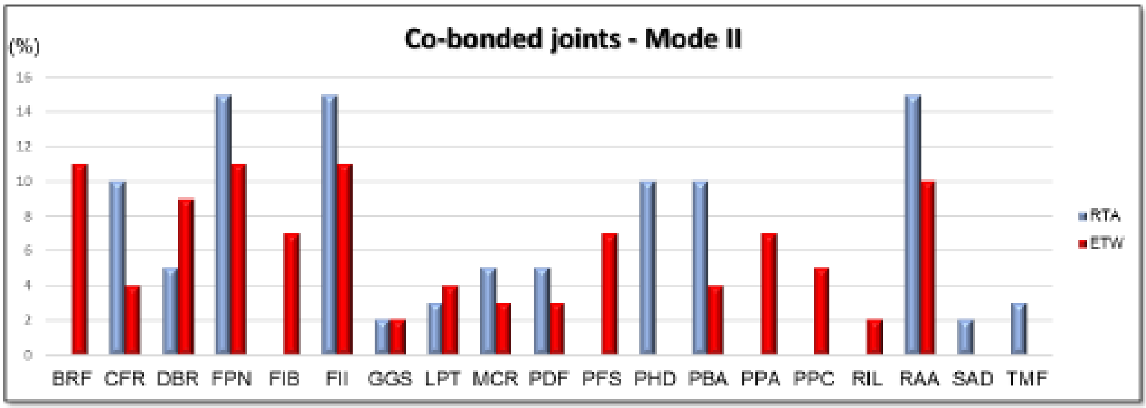

Figure 8-28 - Comparison of failures aspect between RTA and ETW conditioning of co-bonded joints under Mode II delamination.

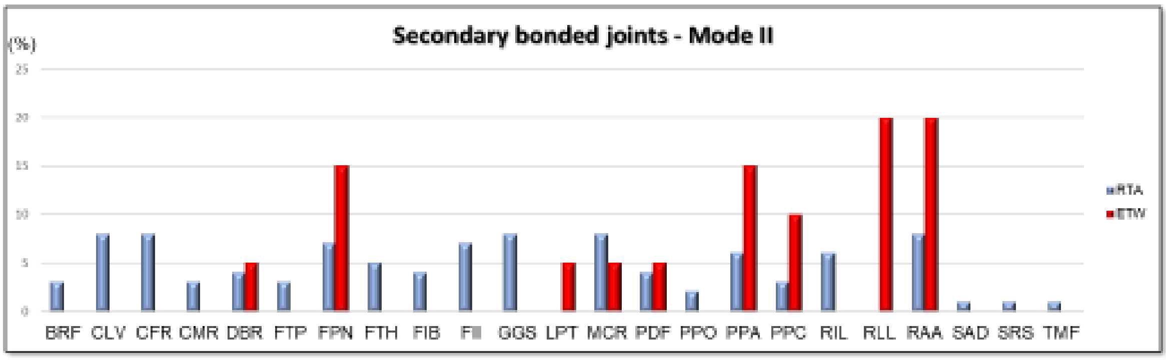

Figure 8-29 - Comparison of failures aspect between RTA and ETW conditioning of secondary bonded joints under Mode II delamination.

Translaminar Fracture Toughness and Fatigue Crack Growth Characterization of Carbon-Epoxy Plain Weave Laminates (Ref. [36])

An experimental investigation of Mode-I translaminar fracture toughness and fatigue crack growth behavior of a carbon fiber-epoxy plain weave laminate manufactured by resin infusion under flexible tooling (RIFT) is presented along this work. Pre-cracked compact tension (CT) specimens were used to perform both quasi-static and fatigue tests.

Different data reduction techniques for fracture toughness calculation were used and compared with each other. The ASTM E399 test method was modified to account for the material orthotropy and specimen geometry effects using a correction function based on a numerical evaluation of the strain energy release rate.

The proposed modification shows good agreement against other experimental methods found in the literature and its application was validated for fatigue tests. Fatigue testing shows that failure in undesired modes is likely to occur prior to translaminar fracture, which was attributed to a higher tensile fatigue threshold than compression or shear fatigue threshold presented by the composite in analysis. Increasing the specimens' initial notch length was a solution for avoiding these types of failure.

The experimental results were compiled in the form of a Paris curve, and their particularities were discussed. A fractographic analysis was carried out to define damage patterns and its evolution process in both types of tests.

The use of compact tension specimens proved itself to be challenging for materials that presents better fatigue performance in tension than in shear or compression, since the specimen design causes relatively high shear and compressive stresses to occur in critical regions, leading to failure in undesired modes. A modification on the initial notch length was made to avoid these types of failure, although an alternative solution would be designing a specimen with greater thickness at the weaker areas to mitigate this problem.

Fatigue crack growth results showed an apparent restrain-release behavior, with sudden crack growth rate variations, possibly related to local resistance variations inside the laminate, as was later shown by fractographic analysis of the fracture surfaces. Although fatigue crack propagation was marked with discontinuities, an overall behavior could be represented by a Paris law curve, that reasonably fitted the propagation data.

The fractographic analysis revealed distinct characteristics for each loading type, proving main damage mechanisms to have a completely different development: for monotonic fracture abrupt fiber bundle rupture and splitting occurs, while in fatigue a gradual damage process takes place, where matrix cracking between fibers act together with breakage of little branches of separated fibers at each cycle, justifying its propagation for loads lower than critical.

Figure 8-30 shows schematically the resin infusion process. Figure 8-31 shows the CT specimen dimensions, the FEM model developed and the experimental setup that was used for fracture toughness and fatigue crack growth tests. Figure 8-32 shows the experimental energy release rate obtained by four different methods that were considered in this study. Figure 8-33 shows the fatigue crack growth rate curves obtained though the tests.

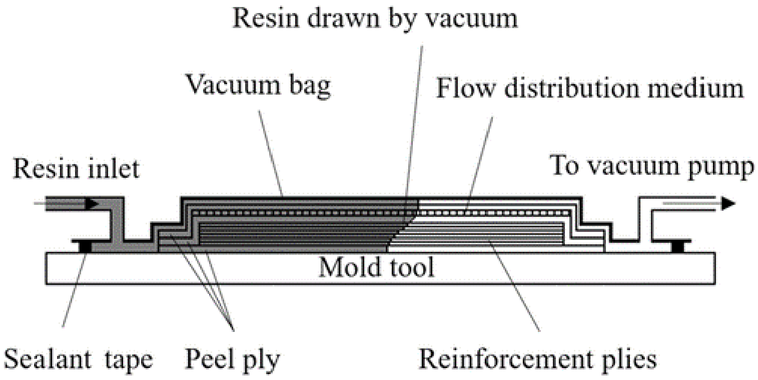

Figure 8-30 - Resin infusion process (schematic).

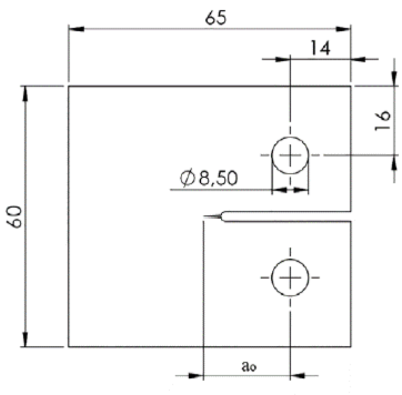

Specimen dimensions in mm

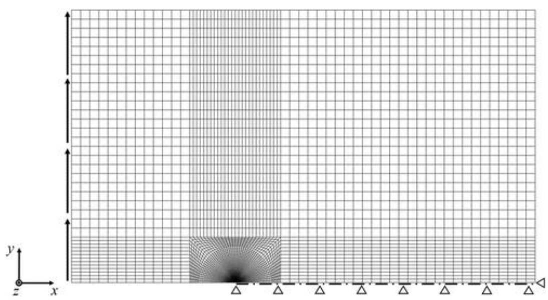

FEM model of CT specimen

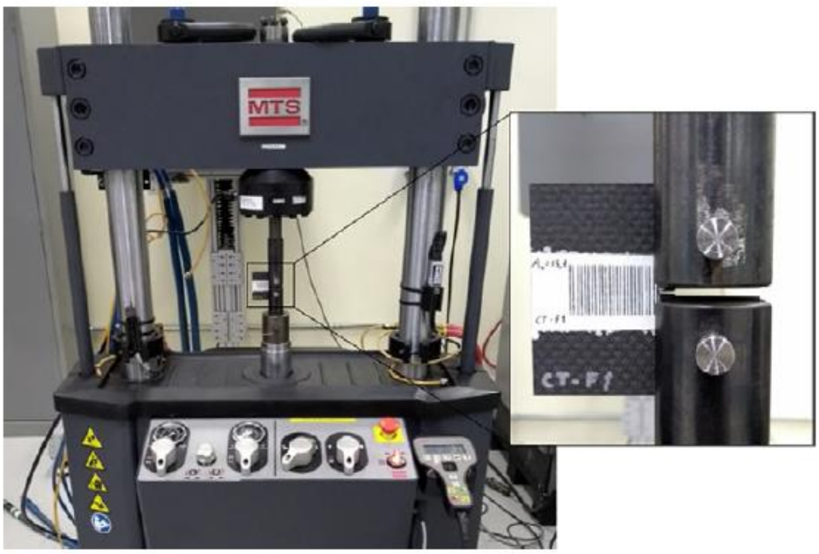

Figure 8-31 – Specimen dimensions, FEM model and experimental setup for the toughness and fatigue crack growth tests.

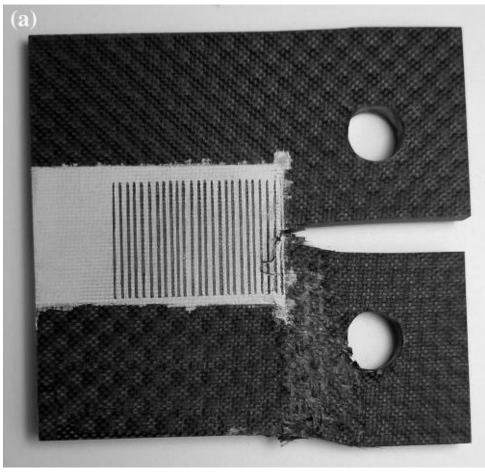

Undesired failure modes obtained during fatigue testing

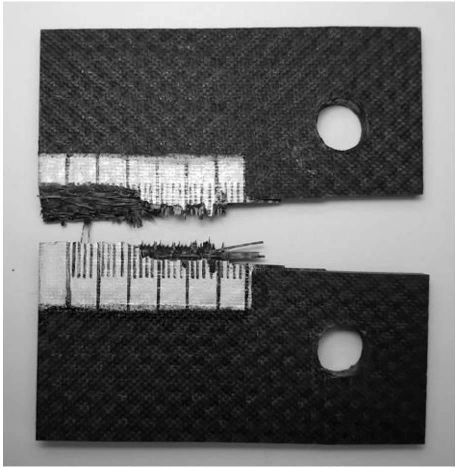

Correct failure aspect of mode-I fatigue crack growth

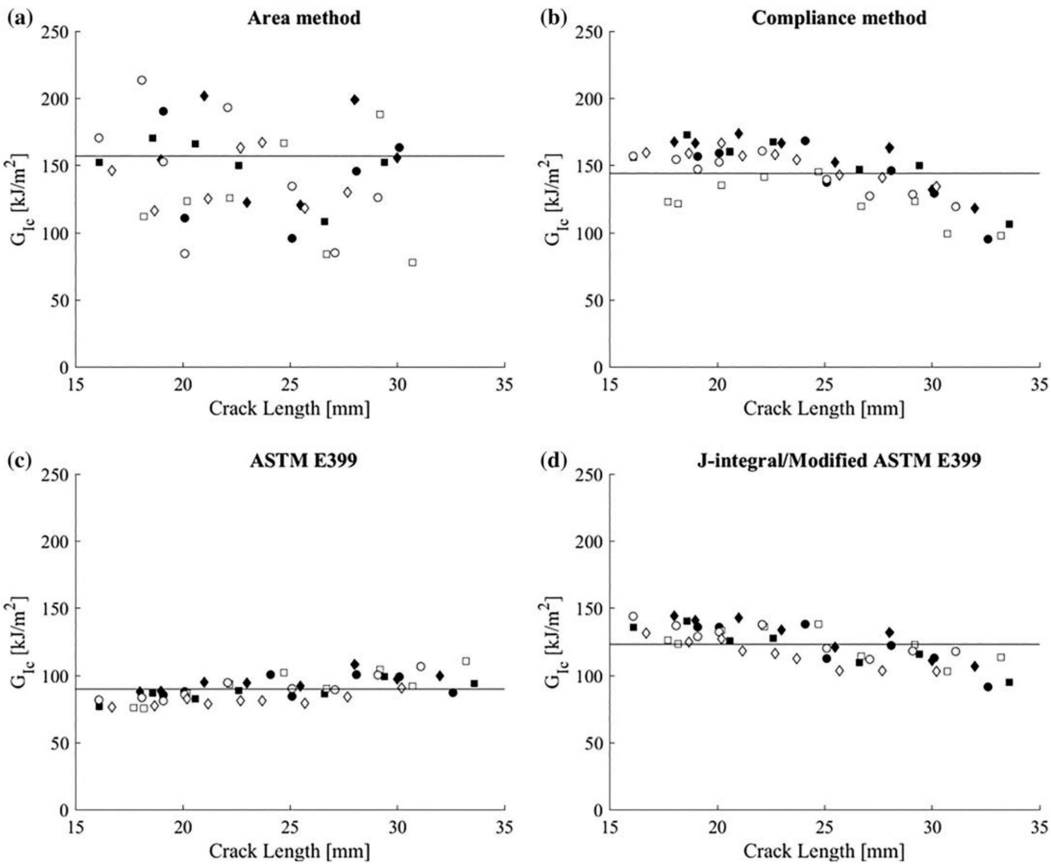

Figure 8-32 - Experimental energy release rate calculated by (a) area method, (b) compliance method, (c) standard method and (d) J-integral/modified standard method.

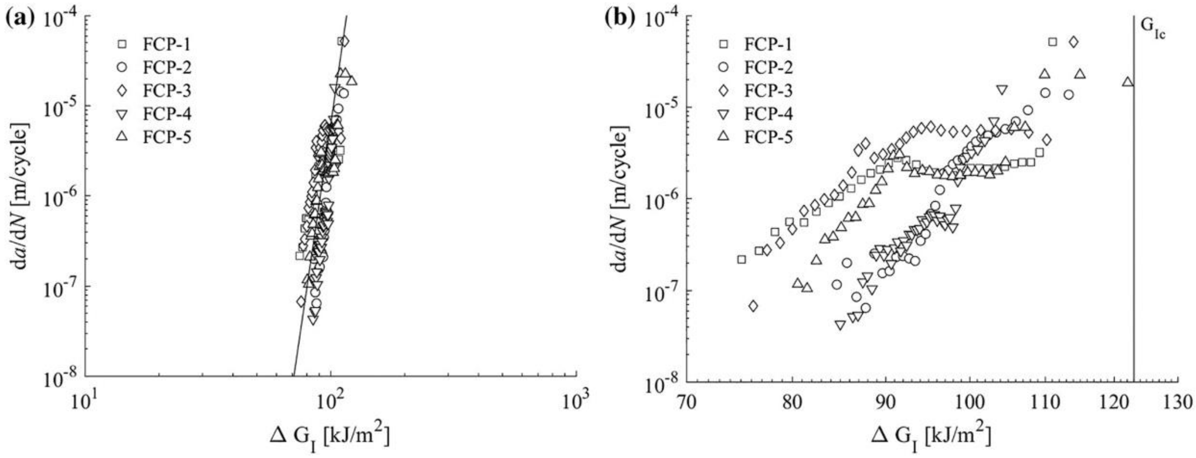

Figure 8-33 - Fatigue crack growth rate curves: (a) general and (b) specific shape.

Interlaminar Crack Onset in Co-cured and Co-bonded Composite Joints under Mode I Cyclic Loading (Ref [37])

Composite joints exhibit different behavior in regard to delamination resistance when dealing with fatigue phenomenon. This research work focuses on an investigation to understand the failure mechanisms on the interfacial strength domain for delamination onset in cocured (CC) and cobonded joints. The analysis was based on strain energy release rate versus number of cycles plots that were obtained from fatigue tests in mode I with a stress ratio R = 0.1. The analysis encompassed from the microscopic to mesoscopic level obtained from scanning electron microscopic, and the images processed to extract the most relevant fracture patterns. The main difference between the two technologies was the stress concentration at the crack tip in which the cobonded joint presents a fabric carrier that blunts the adhesive layer, then delaying the delamination.

In order to develop this work, similarity of damage mechanisms steps in either static or fatigue loadings in a mesoscopic scale was taken into account. Analysis of cracked surface of specimens tested under Mode I static delamination was carried out, considering the difficult task in determining the reasons of damage initiation in barely developed cracked specimens tested under cyclic fatigue loading. The shapes of the G-N curves obtained for each type of composite joint studied herein were explained with the aid of qualitative and quantitative fractographic analyses. Many of the quality concerns of the adhesive joints were treated and discussed in this paper in order to help designers selecting an appropriate type of adhesive joint for a given structural application.

The composite joints studied in this work were composed of unidirectional prepreg layers, which consist of T800 carbon fibers embedded in an epoxy matrix 3900-2C produced by Toray. The prepreg layers were stacked with a thin Teflon film inserted in the midplane of the laminate, in which the film induces a sharp crack for the subsequent interlaminar fatigue tests.

This paper provides important information and guidelines to aid designers in the selection of the best composite joint for high-performance structural applications.

Figure 8-34 shows the G-N curves obtained in Mode I of both joint technologies. Figure 8-35 shows the fracture surfaces for the CB and the CC joint respectively.

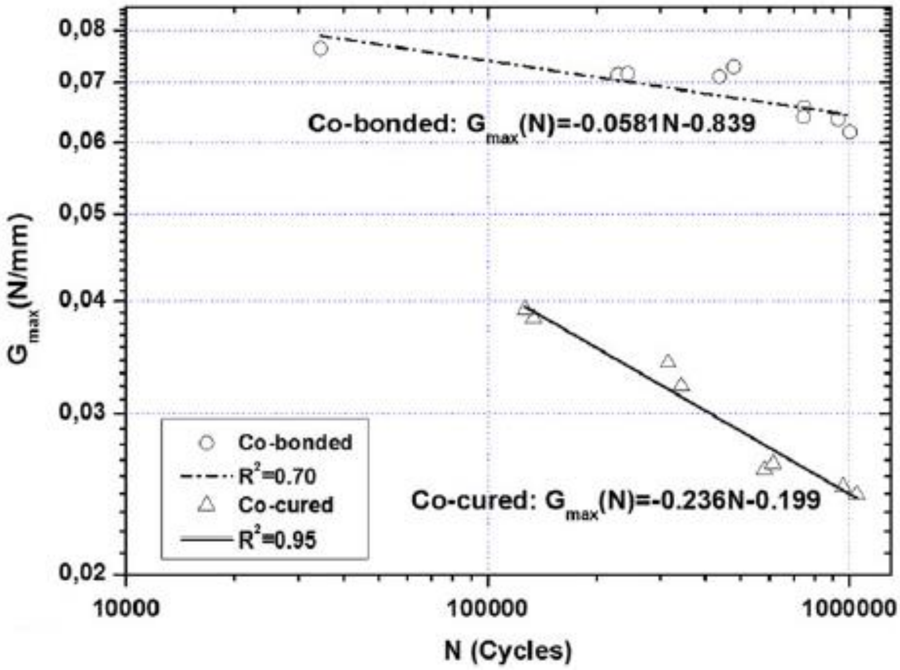

Figure 8-34 - G-N curves in Mode I of both joint technologies.

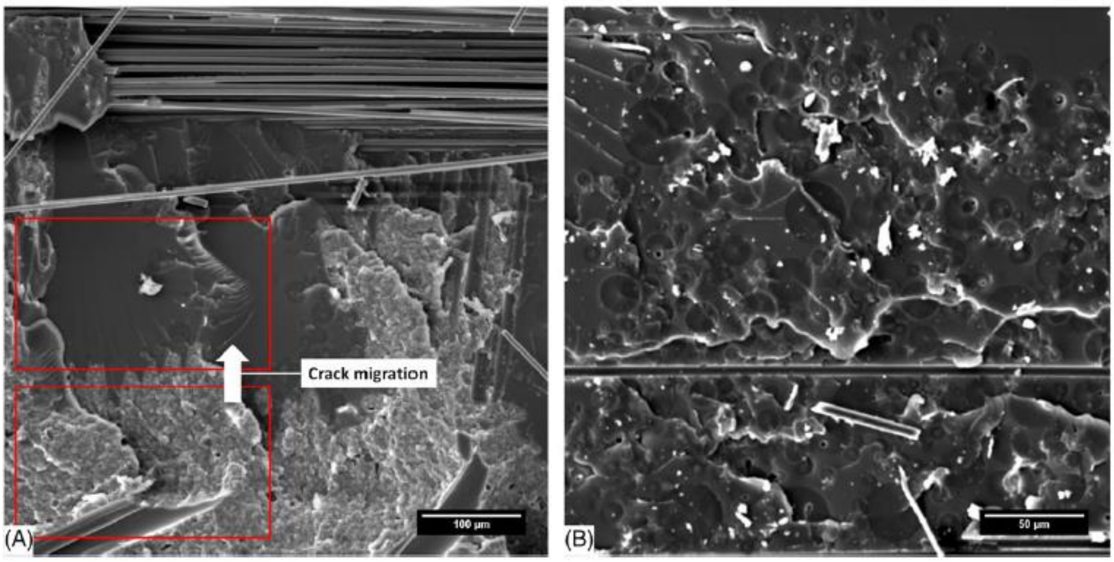

Figure 8-35 - Fracture surface in (a) CB joint and (b) CC joint.

The Role of Stitch Yarn on the Delamination Resistance in Non-crimp Fabric: Chemical and Physical Interpretation (Ref. [38])

In a 3D preform, the out-of-plane reinforcement is effective for decelerating or suppressing the delamination process as the non-crimp fabric does not connect the neighboring laminae effectively. Hence, the interlaminar strength of the stitched laminae is supposed to behave in the same way as a regular unidirectional composite. In order to determine whether or not the stitched yarns contribute to the interlaminar fracture toughness, this study determinated the delamination resistance of a quasi-isotropic laminate. The analysis was based on interlaminar fracture toughness (GIc) and propagation energy curve in tests conducted in Mode I opening with double cantilever beam specimen geometry.

The results of fracture toughness as well as strain energy for propagation were compared to their fracture surface. A decrease in the propagation energy prevailed in the surface because the stitch yarn replaced the carbon fiber/epoxy interface, which has better chemical affinities, i.e., covalent bonds.

Figure 8-36 is a SEM fractography showing details of general fracture in NCF (non-crimp fabrics) composites.

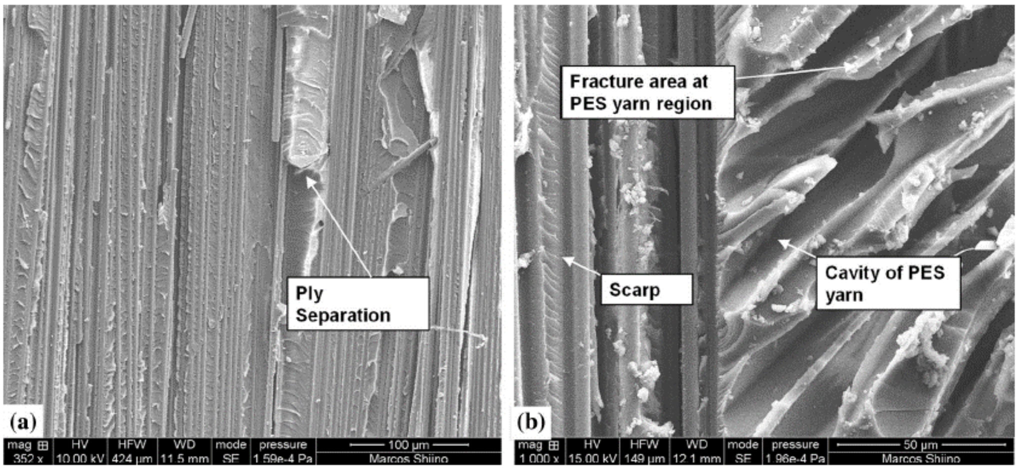

Figure 8-36 - Details of general fracture in NCF composites.

A Numerical-Experimental Evaluation of the Fatigue Strain Limits of CFRP Subjected to Dynamic Compression Loads (Ref. [39])

The use of composite materials in the most varied industrial sectors has increased considerably in recent years, especially those made of carbon fiber/epoxy resin. For this reason, the use of these materials need a better understanding of their mechanical behavior, especially when submitted to cyclical load requests, especially about compression, which is the object of study of this work.

Residual strength degradation in CFRP is evaluated by numerical models and experimental tests relating the residual strength to the applied fatigue cycles and the maximum stress. The present work proposes to characterize the static and fatigue mechanical properties in compression of a carbon fiber/epoxy resin composite, used in the aeronautical industry, to present a mathematical model to determine the residual strength.

The experimental methodology for strain limit evaluation has involved the residual strength after the fatigue test limited to 120,000 or 240,000 cycles, considering frequency of 12 Hz and stress ratio R=10 in different strain levels.

This study establishes that the strain limit corresponds to deformation in which the residual strength becomes equal to the design stress (stress reduced statically to the B – basis value).

Lastly, the adjusted mathematical model for determining the residual strength and the finite element simulations showed consistent results when compared with experimental tests. This study shows the relevance of the allowable levels determined from static strength to the onset of abrupt failure as a function of increasing maximum fatigue stress level that is a significant finding for the fatigue design community.

Figure 8-37 and Figure 8-38 show a flowchart of the numerical and experimental procedure and a flowchart of the methodology for strain limit determination. Figure 8-39 and Figure 8-40 show the numerical model and specimen details and the strain obtained from the analysis considering failure after 120,000 and 240,000 cycles applied.

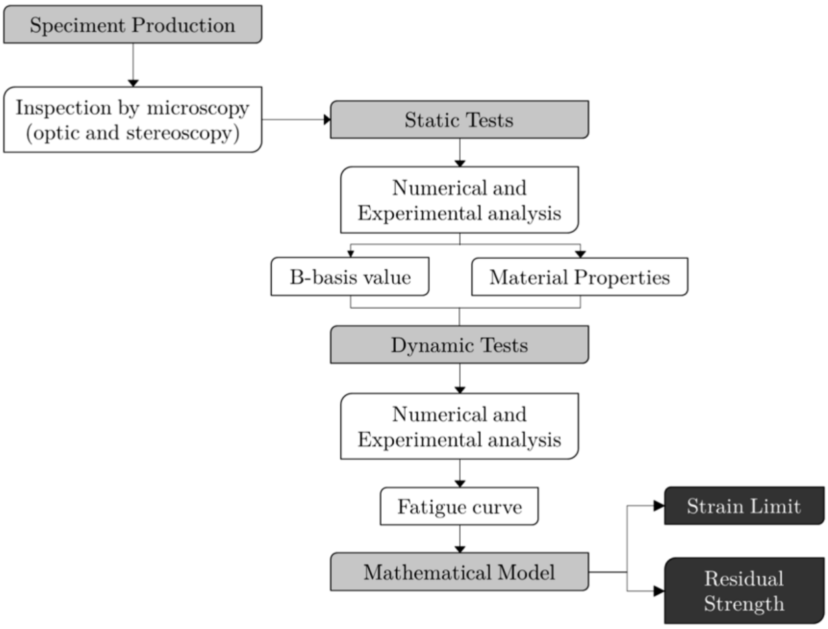

Figure 8-37 - General flowchart of the numerical and experimental procedure.

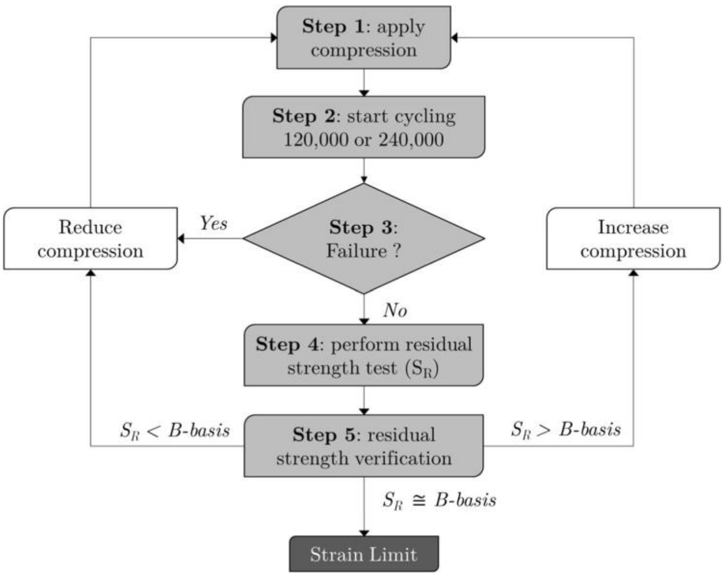

Figure 8-38 - Flowchart of the methodology for strain limit determination.

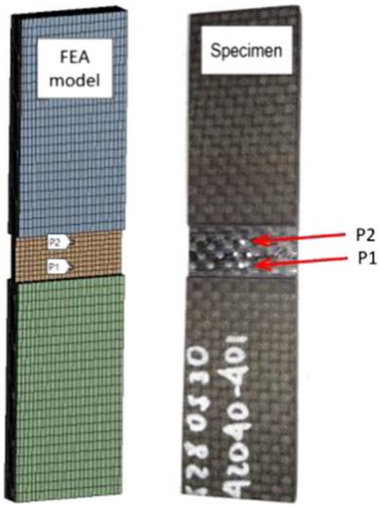

Figure 8-39 - Model and specimen details and the measured points P1 and P2 in the most loaded region.

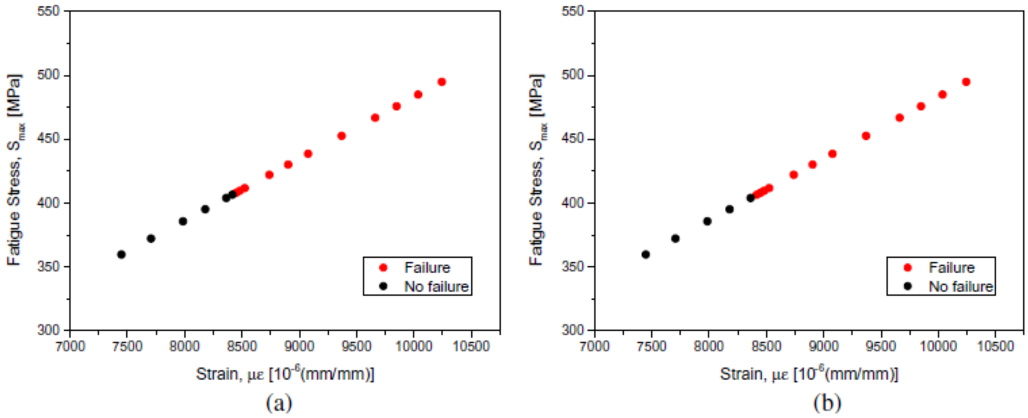

Figure 8-40 - Maximum strain considering failure of the material obtained numerically for (a) 120,000 and (b) 240,000 cycles.

9. COMPOSITE MATERIALS - STRUCTURES

Embraer 175-E2 (Second Generation) – composite horizontal empennage development

Embraer is currently developing a re-engined version (E2) named E-175, with significant gains in performance. Amongst its primary structural components, the E-175 will employ a CFRP horizontal stabilizer. Design features of such component play an important role on its structural behavior and, as such, their influence must be characterized through tests within a building block approach. The tests comprising this building block are performed in different structural levels, from coupons (material tests, including lamina and laminate allowables), passing through subcomponent level (including evaluation of damage scenarios on reinforced composite panels), up to full-scale test of the horizontal stabilizer component. E-175 E2 prototype is under production and scheduled for first flight in 2019.

Figure 9-1 shows the prototype empennage assembly.

Figure 9-1 – E-175 E2 horizontal empennage.

10. HYBRID STRUCTURES

Ultrasonic Joining of Through-the-thickness Reinforced Metal-Composite Hybrid Structures (Ref. [40])

A Review on Direct Assembly of Through-the-Thickness Reinforced Metal–Polymer Composite Hybrid Structures (Ref. [41])

This doctoral thesis aims at introducing Ultrasonic Joining (U-Joining), a new joining concept (co-invented by the author and patented by HZG, US 9,925,717 B2, 2018), to produce metal-composite overlap joints that have improved out-of-plane strength. U-Joining uses ultrasonic energy to join metallic parts with integrated pins – manufactured in this work by metal injection molding (MIM) - to fiber-reinforced thermoplastic composites. Joining is accomplished by two major bonding mechanisms that are activated by ultrasonic frictional heating: mechanical interlocking and adhesion forces. The first results from a through-the-thickness reinforcement (TTR) effect between metallic pins and the composite, wherein adhesive forces are formed at the metal-composite interface after joint consolidation of the softened polymeric matrix. A case-study joint on the aircraft material combination of glass-fiber reinforced polyetherimide laminate (GF-PEI) and MIM-structured Ti-6Al-4V was chosen to evaluate the process feasibility and joint properties.

The hybrid joint's global mechanical performance was assessed by single lap shear and fatigue tests. A significant increase in ultimate lap shear force, ULSF) and toughness were observed, compared to non-reinforced reference joints, with final failure by shearing of the metallic pins. Therefore, it is possible to conclude that through-the-thickness reinforcement effectively improved the load transfer capability between metal and composite in the U-Joining joints. Moreover, the S-N curves obtained indicated outstanding results in accordance with aircraft standard procedure, and the hybrid joints produced reached their fatigue limits (i.e. 106 cycles) with loading levels corresponding to 30% of ULSF.

For understanding and optimization of the U-Joining process parameters a Box-Behnken design of experiments was carried out. The individual and combined effects of each joining parameter on the ULSF were evaluated with a response surfaces method and analysis of variance. As a result, a set of optimized joining parameters were obtained to produce sound joints with above-average ULSF. This PhD work therefore succeeds in introducing and scientifically describing an alternative joining approach for metal-composite hybrid structures with TTR, addressing its fundamental characteristics and joint properties at coupon level. In addition, the results of this work contribute to filling knowledge gaps with regards to process, microstructure and mechanical performance correlations in the direct assembly of hybrid joints.

Some selected information from both works is shown in the following pages. Figure 10-1 shows the U-Joining test specimen geometry and Figure 10-2 outlines the U-joining fatigue test setup. Figure 10-3 presents the fatigue life data for a U-Joining joint and fitted S-N curves. Figure 10-4 presents an schematic illustration of the U-Joining joint, and an illustration of the proposed crack growth mechanism under cyclic loading.

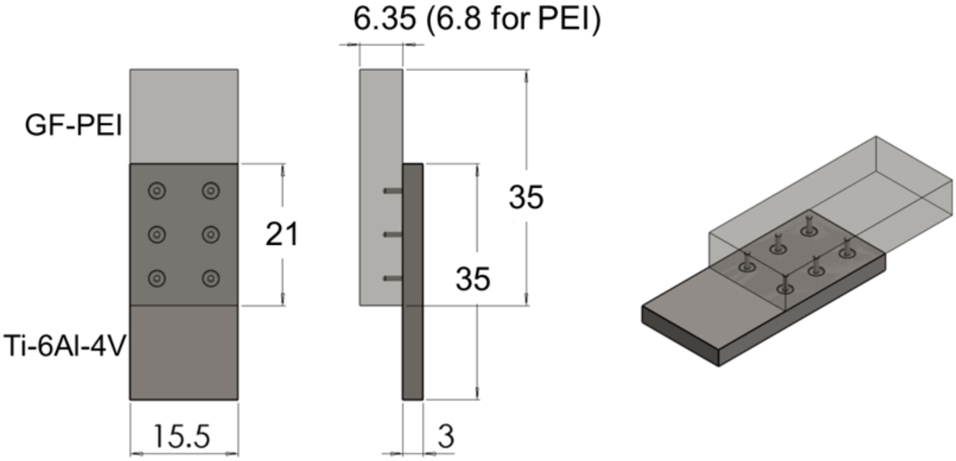

Figure 10-1 – U-Joining joint specimen geometry (dimensions in mm).

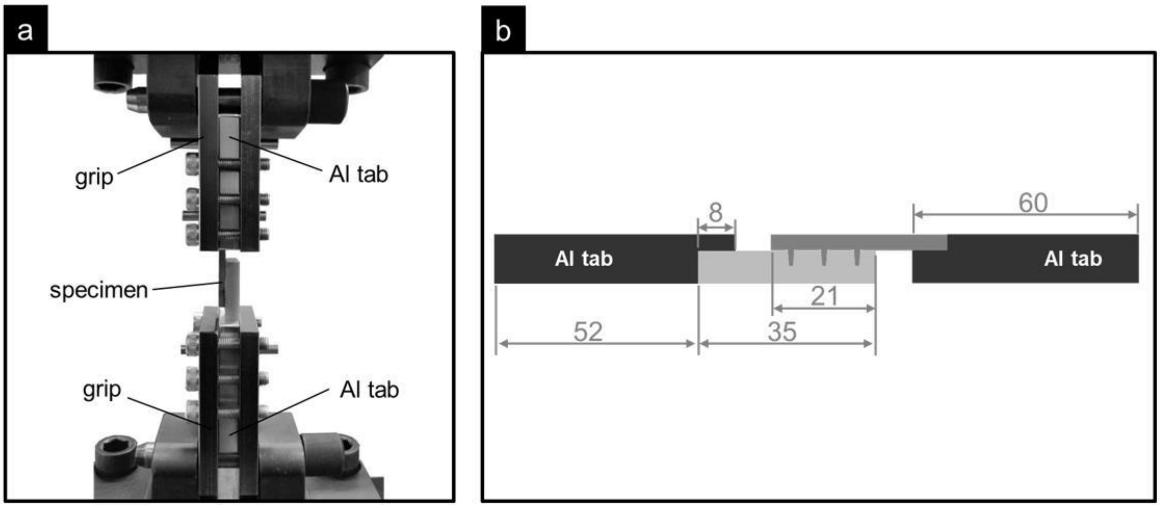

Figure 10-2 – U-joining fatigue test setup.

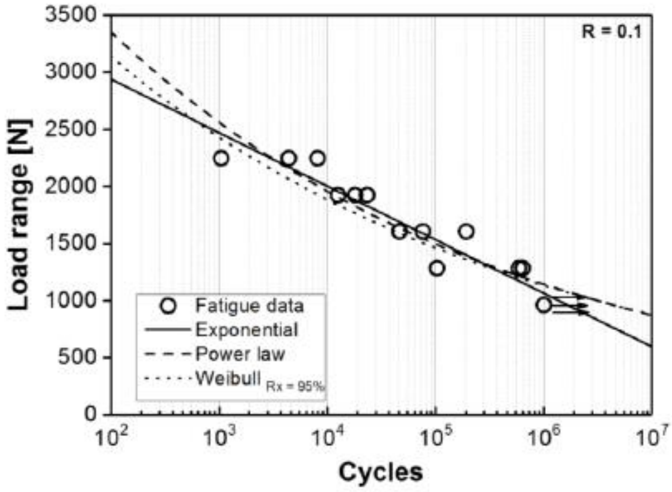

Figure 10-3 – Fatigue life scatter plots for a U-Joining joint and fitted S-N curves according to the exponential, power law, and two-parameter Weibull (reliability level 95%) models.

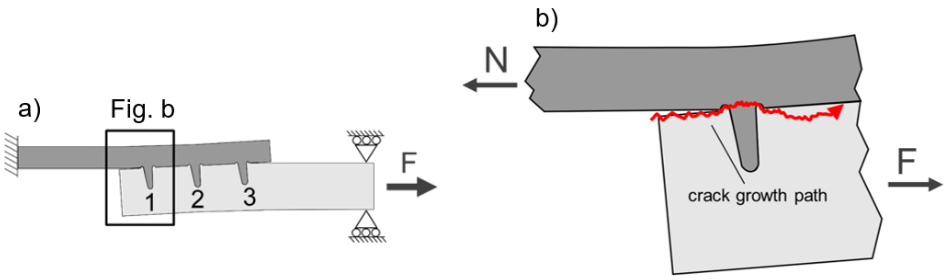

Figure 10-4 – (a) Schematic illustration of the U-Joining joint, (b) illustration of the proposed crack growth mechanism under cyclic loading.

11. STRUCTURAL HEALTH MONITORING

During this period there were contributions on Structural Health Monitoring (SHM) mainly from the University of São Paulo (Professor Volnei Tita and his team), from the University of Itajubá (Professor Antonio Ancelotti and his team) and from Embraer, who worked in partnerships with Sandia National Laboratories and the University of Rio Grande do Sul (URGS). Many SHM technologies being developed are focusing in composite materials.

Structural Health Monitoring of Sandwich Structures Based on Dynamic Analysis (Refs. [42] and [43])

This work aims to contribute to the development of SHM systems based on vibration methods to be applied on sandwich structures. The main objective is focused on experimental damage identification via changes in the Frequency Response Function (FRF) with the usage of damage metrics. Specimens of sandwich structures made from skins of epoxy resin reinforced by glass fiber and a core of PVC foam were manufactured.

First, preliminary nondamped Finite Element (FE) models are developed, and results obtained are used to define the frequency range of interest for the experimental procedure. After that, vibration experimental analyses are carried out on undamaged specimens. The natural frequencies are compared to the preliminary FE results.

Second, experimental analyses are performed on damaged specimens with and without piezoelectric sensors. Then, damage metric values are calculated based on FRFs for damaged and undamaged structures, which were obtained from experimental and FE analyses (with damping effects).

In addition, a new procedure is proposed to improve the quality of results provided by the damage metric. It is shown that the new procedure is very effective to identify the damage using both amplitude and phase from FRFs.

Finally, the potential and limitations of the FE model to predict damage metric values, comparing to experimental data is discussed.

Figure 11-1, Figure 11-2 and Figure 11-3 show some details about the test setup and specimen and about the FE model that was developed.

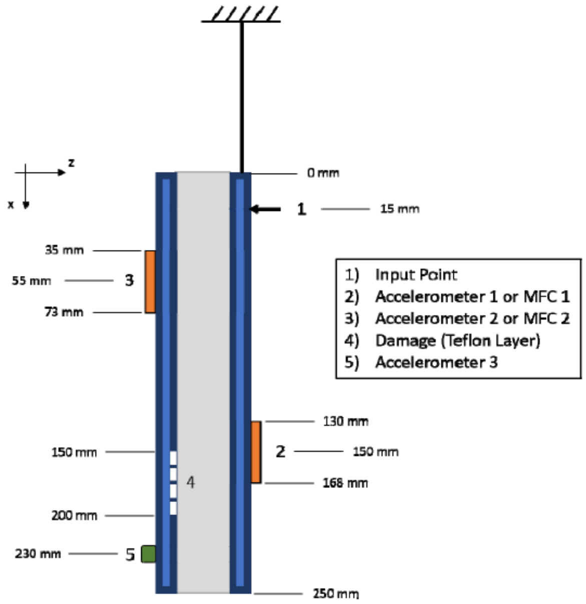

Figure 11-1 - Schematic representation of the sandwich structure specimens (out of scale).

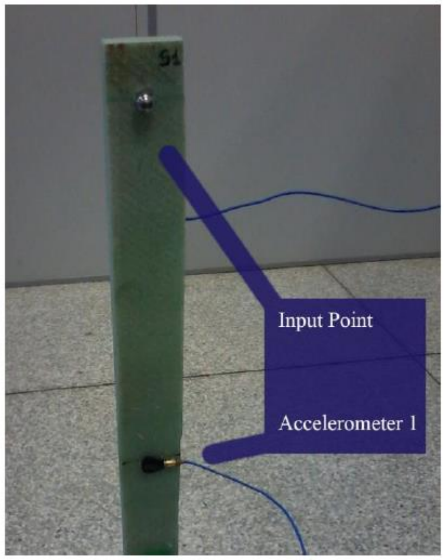

Figure 11-2 - Details of the experimental set-up for free-free condition of sandwich structure: input and output points.

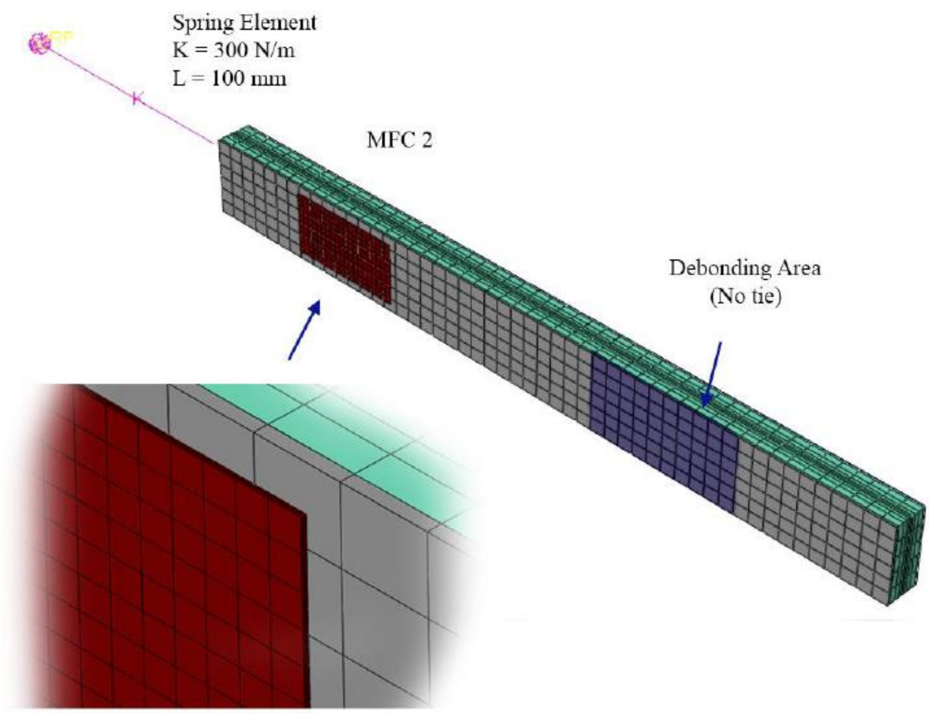

Figure 11-3 - Finite Element model for the sandwich structure corresponding to specimen S2P2.

Figure 11-4 shows the non-rigid modal shapes for the undamaged sandwich structure. Figure 11-5 and Figure 11-6 show the frequency responses for the undamaged and damaged structures obtained from tests and from analysis respectively.

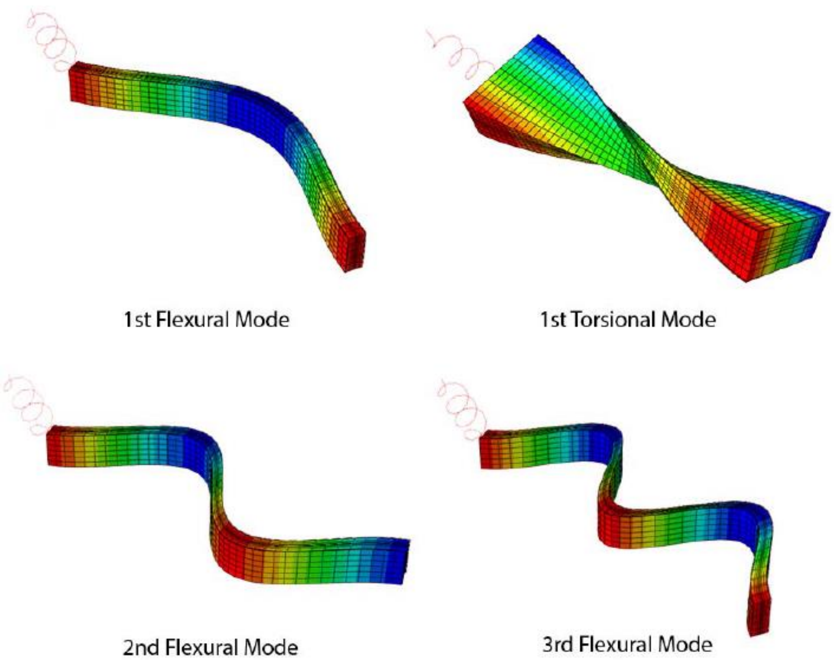

Figure 11-4 - Non-rigid modal shapes for the undamaged sandwich structure.

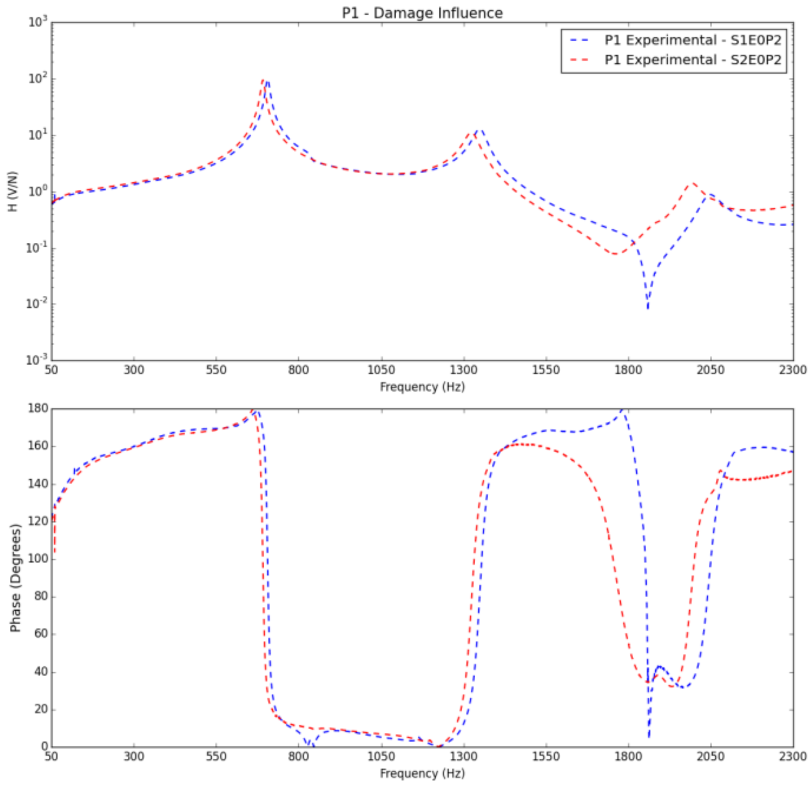

Figure 11-5 - Experimental results – influence of the damage.

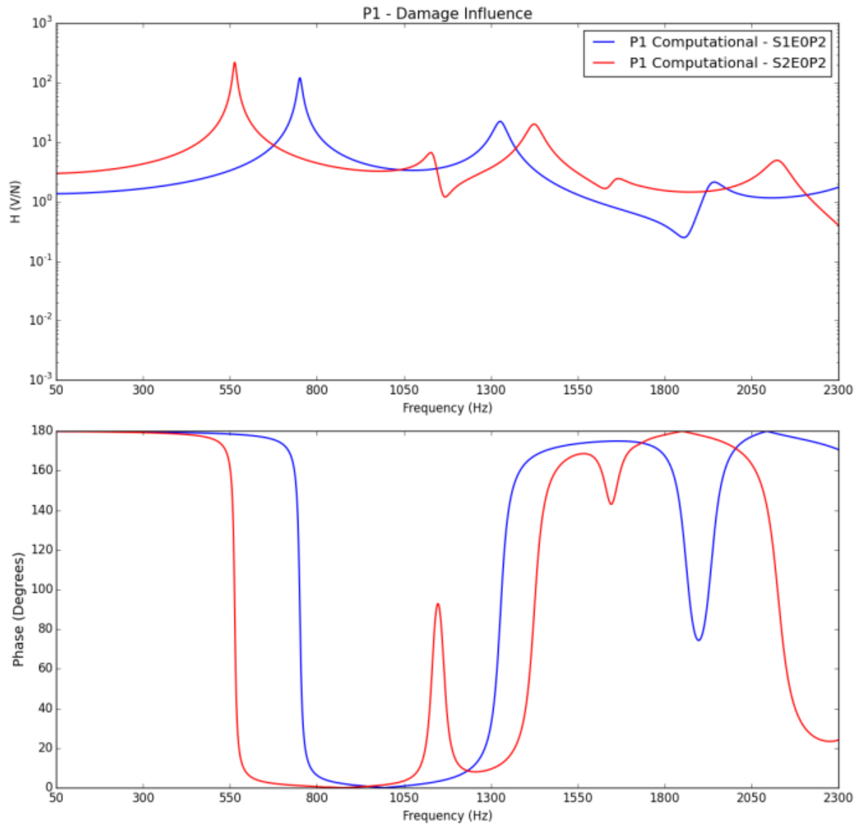

Figure 11-6 - Computational results – influence of the damage.

The computational analysis did not properly represent the damage in the structure due to the absence of contact model for simulating the debonded region. Thus, the damage effect in the dynamic signature that is observed in the computational specimens is much greater than the experimental ones.

Figure 11-7 presents a comparison between experimental and computational results for the specimen named S1P2.

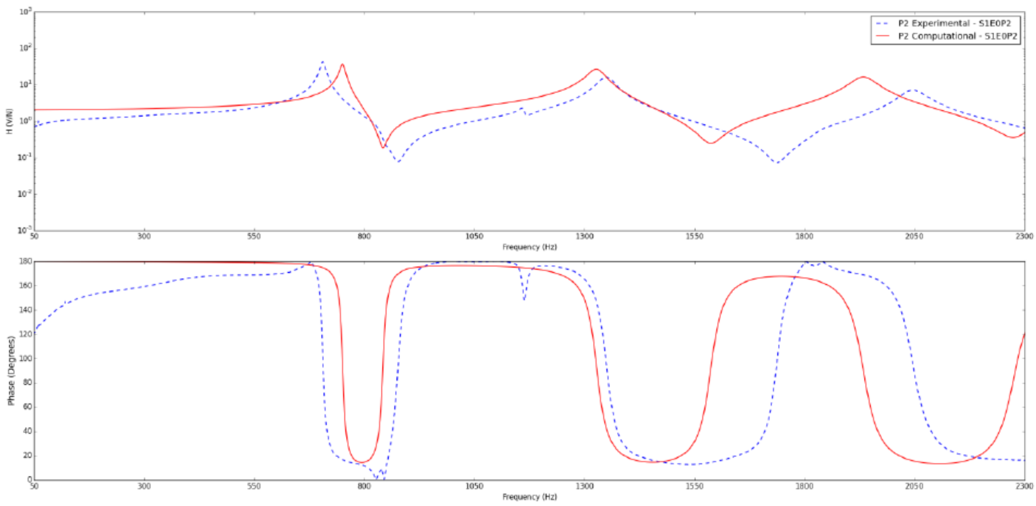

Figure 11-7 - Computational vs. Experimental results for specimen S1P2.

Structural Health Monitoring of Thin Thermoplastic Composite Plates Via Vibration Based Method (Ref. [44])

This work presents the results of a study on Structural Health Monitoring via vibration based method in a Carbon Fiber Reinforced Polymer (CFRP) plate.

First, a model of an intact and perfect flat plate is built in finite elements and a modal analysis is carried out. A new simulation is done then using the measurements of the specimen, which presents some curvature rather than being a perfect flat surface, and the impact of the curvature in the modal response of the plate is investigated. Later, an experimental impact test is performed in the intact plate and the results are compared with the numerical ones. Finally, a modal simulation of the intact plate and another one with a controlled damage is performed.

The Frequency Response Functions (FRF) obtained from the simulations are used to quantify the damage by means of a damage metric from the literature.

Some selected results from this work are shown below. Figure 11.8 shows the experimental setup and specimen

Figure 11-9 presents the mode shape comparison for the second vibrational mode for a flat (ideal) surface and for a deformed (3D) surface.

The results from the modal simulation of the 3D surface compared against the perfect flat CFRP plate show that the plate's curvature has a strong effect in the first vibrational mode, increasing its natural frequency in almost 60% when compared to what would be expected in a flat plate. Table 11-1 and Table 11-2 show the measured differences for both conditions and the comparison between the experimental and numerical results obtained for the plate tested.

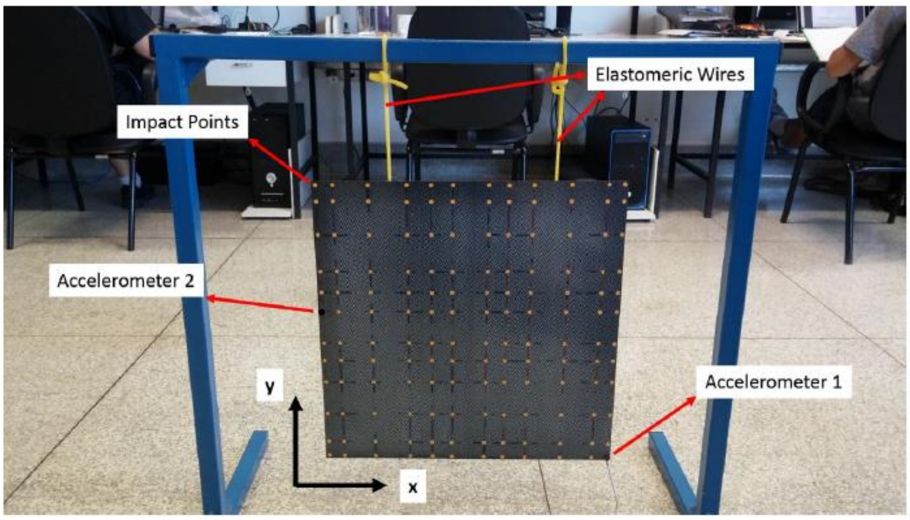

Figure 11-8 - Experimental setup for the CFRP plate under analysis.

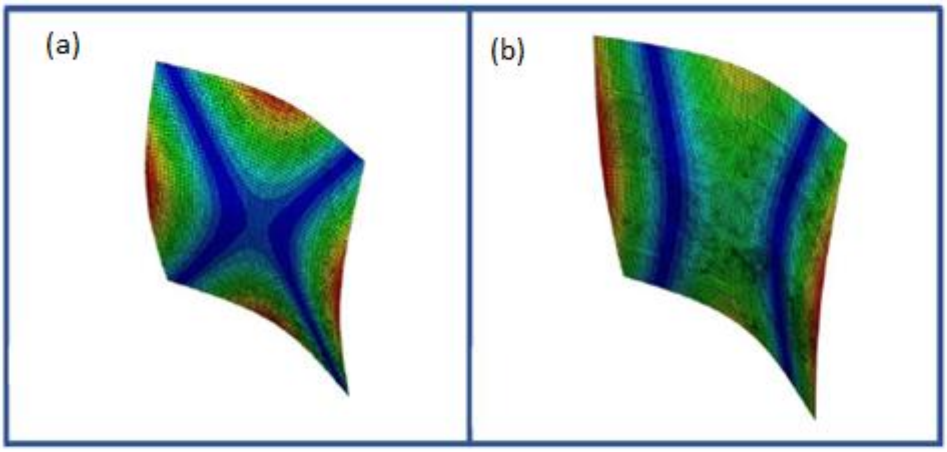

Figure 11-9 - Mode shape comparison for the second vibrational mode. a) flat surface. b) 3D surface.

Table 11-1 - Natural frequencies for the flat (ideal) and curved (real) plate, obtained from numerical analysis.

Mode	Flat Surface Frequency [Hz]	3D Surface Frequency [Hz]
1st Mode	19.15	30.40
2nd Mode	64.47	63.06
3rd Mode	67.26	65.68
4th Mode	76.01	76.86
5th Mode	76.66	78.09
6th Mode	122.28	121.26

Table 11-2 - Comparison between numerical and experimental natural frequencies for the plate.

Numerical Natural Frequency [Hz]	Experimental Natural Frequency [Hz]	Error $\left\|\frac{NNF-ENF}{NNF}\right\|$
30.40	30.88	1.58 %
63.06	61.99	1.70%
65.68	-	-
76.86	76.14	0.94%
78.09	82.80	6.03%
121.26	127.29	4.97 %

Reliability of Lamb Wave SHM Systems: influence of Hydrostatic Pressure and Mechanical Loading (Ref. [45])

Structural Health Monitoring (SHM) systems have the potential to change maintenance paradigms in several areas, including aerospace. Lamb wave-based technologies are promising candidates since they provide coverage of a relatively large area with a reduced number of sensors and may allow both detection and localization of damage in the structure. However, the reliability of these systems under severe operational conditions still needs to be carefully investigated.

In this work, results of two evaluations, which are part of a larger study on the reliability of Lamb Wave SHM systems, are presented. In the first evaluation, four different levels of hydrostatic pressure were applied on small aluminium panels instrumented with piezoelectric sensors. Results show that simple surface contact with fluid has a significantly higher influence on signal attenuation than increases in pressure, see Figure 11-10. It is also clear that, as expected, each mode generated by the piezoelectric sensors is attenuated differently by the fluid.

In the second experiment, similar specimens were subjected to static loading, including four levels under tension and one level in compression. Results show that signal amplitude is strongly influenced by the applied load, with the lowest amplitude level seen for the compression cycle and the greatest for the highest tension load. The influence of loading on baseline subtraction and other signal processing methods is analysed. Figure 11-11 shows the comparison of the amplitude of the first wave packet of four samples analyzed when subjected to different load levels.

It is expected that these findings, when associated with other more substantial results to be generated through this reliability evaluation program, will help manufacturers to increase their confidence in using such systems in real operational conditions.

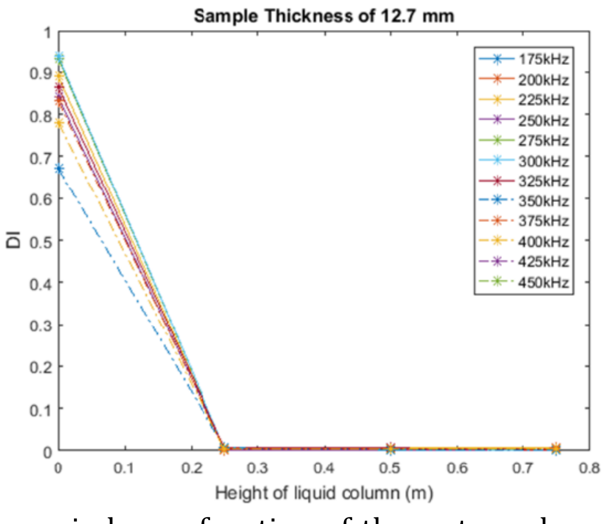

Figure 11-10 - Damage index as function of the water column height. There is a significant difference in the DI when there is water and when there is no water. The reference was taken with a 0.25m water column.

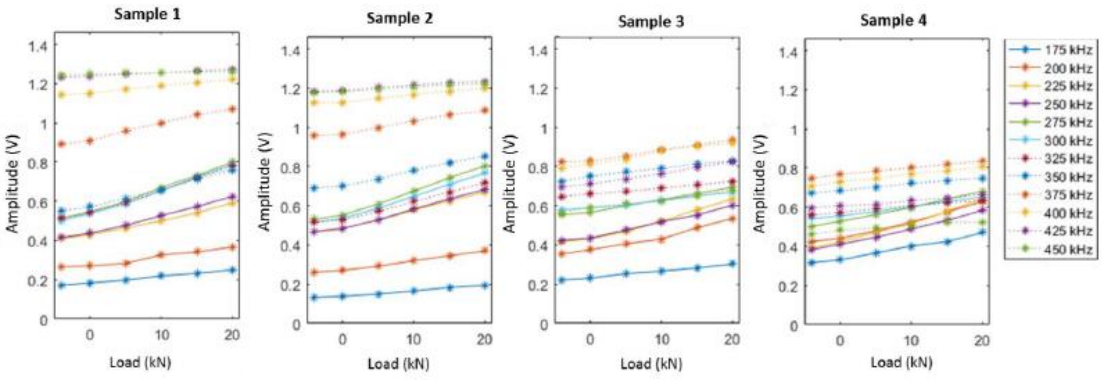

Figure 11-11 - Comparison of the amplitude of the first wave packet of four samples analyzed for different levels for the applied load.

Advancements on the Adoption of SHM Damage Detection Technologies into Embraer Aircraft Maintenance Procedures (Ref. [46])

SHM Qualification Process and the Future of Aircraft Maintenance (Ref. [47])

Corrosion Detection in Aeronautical Structures Using Lamb Waves System for SHM (Ref. [48])

Structural Health Monitoring (SHM) is a tool that has the potential to revolutionize aircraft maintenance. When compared to current Non Destructive Test (NDT) technologies, SHM can reduce the amount of time and burden of the inspection tasks, it can provide facilitated structural damage detection in areas with restricted access with early detection of flaws, and also allow the reduction of maintenance costs due to less time-consuming and less complex maintenance procedures.

There are two different types of application for SHM technologies, Scheduled Structural Health Monitoring (S-SHM) and Automated Structural Health Monitoring (A-SHM), which are commonly recognized by the SHM community. Installation, integration and operation requirements depend on each type of application. Aircraft industry requires reliable SHM systems. In order to determine systems' reliability, Embraer selected two different SHM technologies for a more in-depth study.

These two SHM technologies were extensively investigated through ground tests with metallic and composites structural components and assemblies and through tests on-board of a flight test aircraft. After demonstrating strong results on ground tests and in the flight test aircraft, Embraer decided to develop a project using the S-SHM approach for the qualification of Comparative Vacuum Monitoring (CVM) and Lamb Waves (LW) technologies and to validate the performance of such systems in real-life operational environment. This project included laboratory tests for the assessment of detection capabilities and tests with systems installed on a number of operator's aircraft to check operational behavior.

Detection capability was demonstrated in terms of Probability of Detection (POD) according to the One-Sided Tolerance Interval methodology. SHM sensors and cables were installed into five aircraft operated by an airline, and were periodically assessed, demonstrating their survivability and durability in real operational environment.

A formal process for S-SHM implementation was established, allowing the next steps for SHM damage detection systems application. Reliable SHM systems will allow time and cost reduction of structural inspections without affecting, or affecting positively aircraft safety.

These three references present more details about the above described SHM technologies and their validation and implementation. Additionally, references about Embraer experience with SHM may be found in References [1] and [2].

Structural Health Monitoring with Augmented Reality for Aircraft Maintenance (Ref. [49])

The Structural Health Monitoring (SHM) has a great potential to reduce the costs of the current aeronautical maintenance procedures that are done through Non-Destructive Testing (NDT). These tasks use to be complex, as they are normally done in areas with restrict access that demand the disassembly of several parts of the aircraft.

With the SHM trustworthy systems, it is possible to evaluate the current conditions of the structure without the need of disassembly and thus inform the maintenance company about the presence and location of a structural failure.

Another technology that has shown great potential of use in the aeronautical industry is the Augmented Reality (AR). The integration of the real world with the virtual world allows the time reduction in tasks of manufacturing, maintenance, and training.

This paper shows that, when SHM and AR are combined, the data about the structure - obtained by the SHM technology - can be shown in real time without the need of disassembly, thus reducing the maintenance costs and the "human factors" risks during an inspection.

Figure 11-12 and Figure 11-13 show the overview of the proposed application (Embraer patent US20170322119 A1).

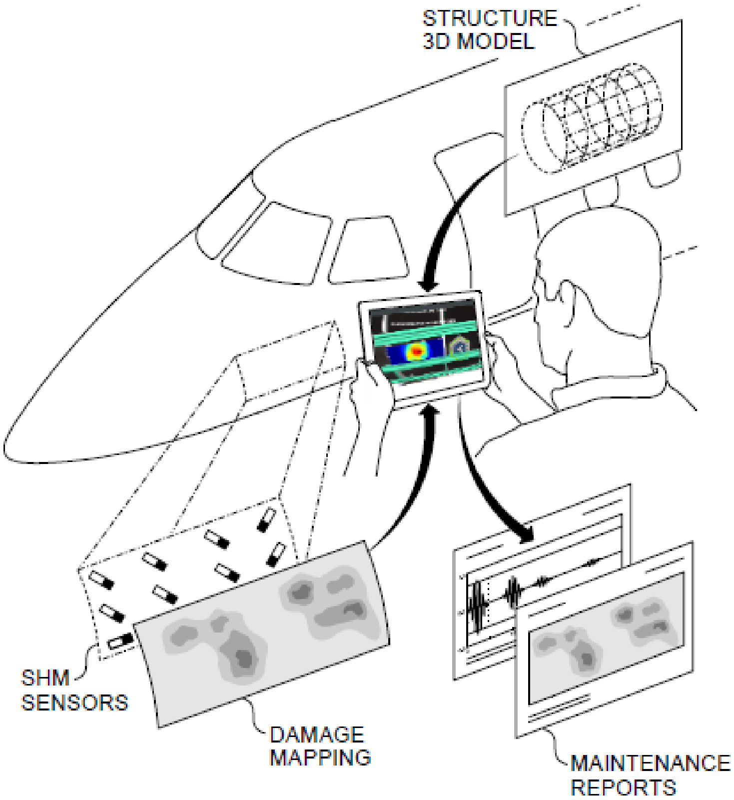

Figure 11-12 - Simplified proposal of a system using SHM enhanced by AR.

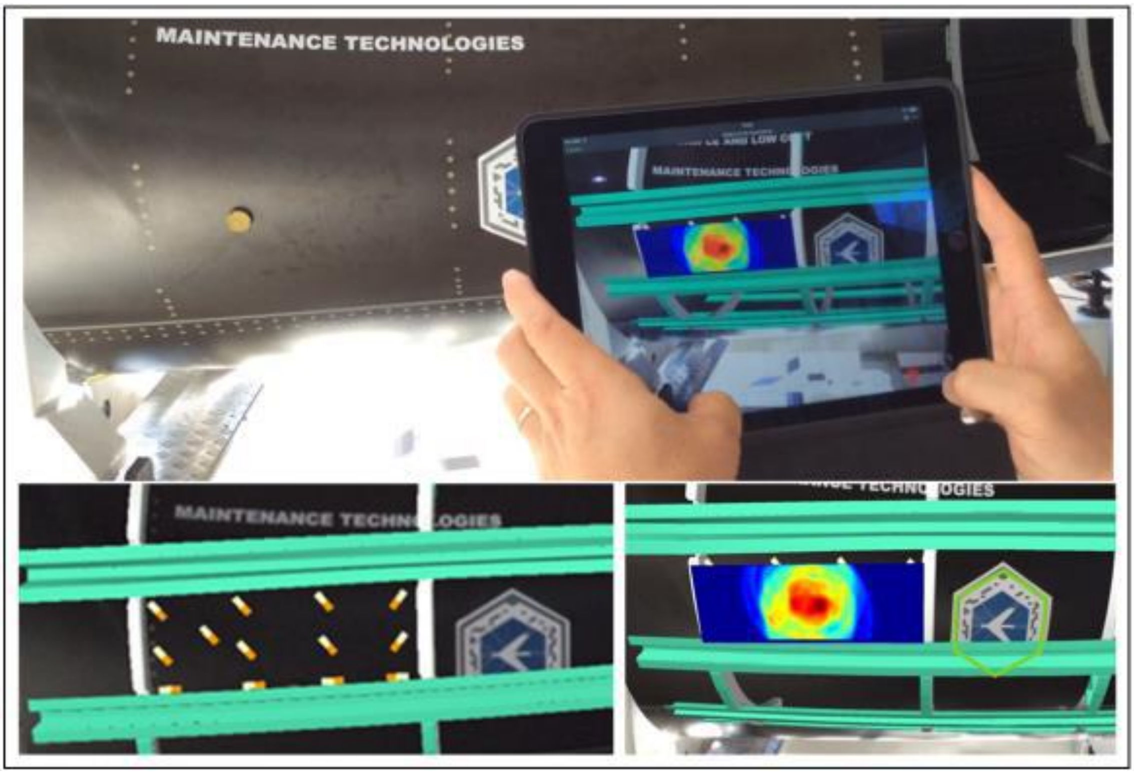

Figure 11-13 - Example of a non-need disassembly to perform a maintenance procedure with SHM with AR.

An Estimate of the Location of Multiple Delaminations on Aeronautical CFRP Plates Using Modal Data Inverse Problem (Ref. [50])

With the increase in the use of composite materials, especially in the aeronautical industry, it is essential that a complete evaluation of the mechanical performance of such structures be undertaken, especially with regard to structural integrity. To assist in this task, structural health monitoring methodologies are employed in order to minimize time and maintenance costs, and errors arising principally from human factors, and which can occasionally result from the failure to properly evaluate the aircraft conditions through inspections.

This study addresses the use of an inverse method for delamination identification in carbon fiber reinforced polymers plates. First, the direct problem was modeled via a finite element method in order to obtain a faithful model that represented the real case studied. The inverse problem was solved by minimizing an objective function through genetic algorithms. Modal responses of delaminated plates are able to identify the possible location of multiple delaminations in laminated plates since the structural matrices are changed as a function of the induced damage.

Numerical and experimental results showed excellent identification of small delaminations, reducing the initial search area by up to 96%, which can lead to savings in time and costs for the aeronautical industry.

Some selected information about the modeling, analysis, tests performed and test results are presented below. Figure 11-14 shows the modeling scheme and the damage assumption. Figure 11-15 shows the plates tested - two plates, one with damages and the other without damages. Figure 11-16 and Figure 11-17 show the frequency responses measured and the damage indications respectively.

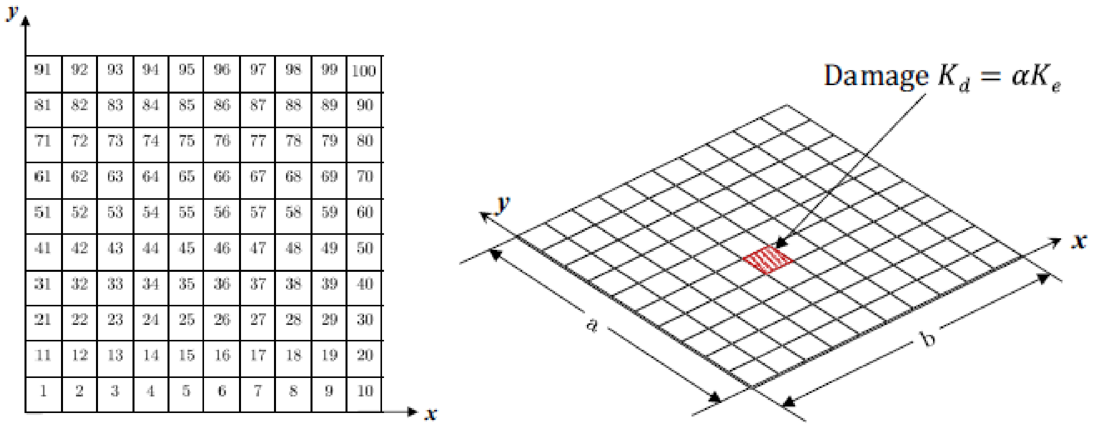

(a) (b)

Figure 11-14 - Modeling of the structure damaged by FEM and system of reference of the elements. a Numbering of elements. b Damage inserted by local reduction of stiffness.

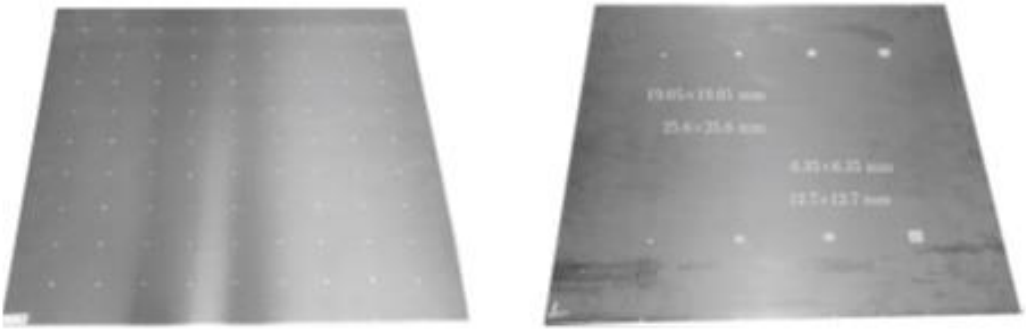

(a) (b)

Figure 11-15 - Test structures used in this work, provided by Embraer. a) plate without damage. b) plate with damage.

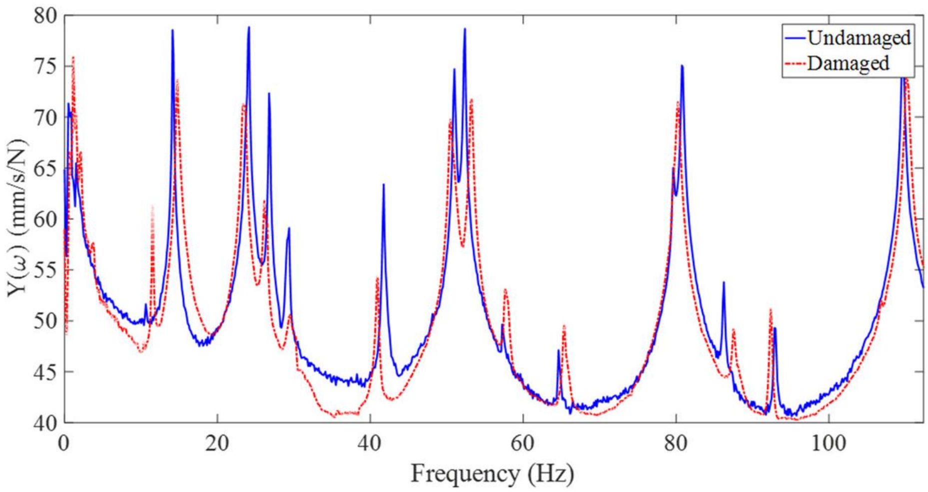

Figure 11-16 - Frequency response function for study boards. FRF from the both plates, undamaged and damaged (average of 121 values for the FRF for each state taken individually).

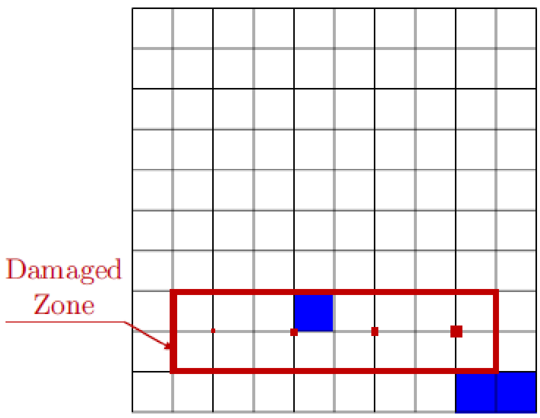

Figure 11-17 - Final result of the identification of damages with possible location of the damage (s) (where blue boxes indicate the damage detected and red boxes indicate the positions of the actual damages).

A Sunflower Optimization (SFO) Algorithm Applied to Damage Identification on Laminated Composite Plates (Ref. [51])

The need for global damage detection methods that can be applied in complex structures has led to the development of methods that examine the structural dynamic behavior. The damage detection problem can be considered as a inverse problem with minimization of a objective function. For those reasons, a new nature-inspired optimization method based on sunflowers' motion is introduced.

The proposed sunflower optimization algorithm (SFO) technique is a population-based iterative heuristic global optimization algorithm for multi-modal problems. Compared to traditional algorithms, SFO employs terms as root velocity and pollination providing robustness. The new method is then applied in an inverse problem of structural damage detection in composite laminated plates.

Figure 11-18 shows schematically the damage applied on the plate, and Figure 11-19 presents the resulting structural damage detection in composite plate using a genetic algorithm (GA) and the sunflower optimization algorithm (SFO).

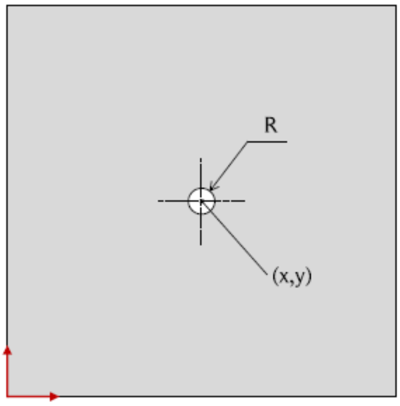

Figure 11-18 - Damage modeling on the plate considering three variables in the inverse problem.

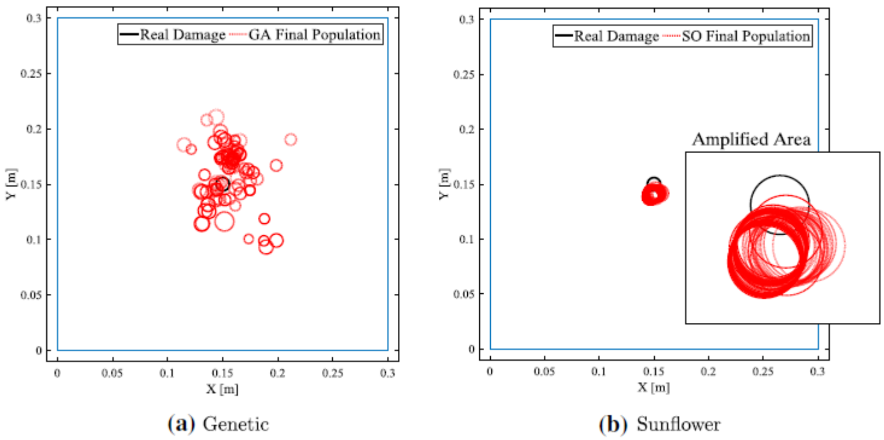

Figure 11-19 - Structural damage (holes) detection in composite plate using GA and SFO algorithm.

12. RELIABILITY AND RISK ANALYSIS

Aircraft Structural Inspections Definition Considering Probabilistic Analysis of Failures Based on Variability of Crack Growth Parameters and Probability of Detection (Ref. [52])

This work proposes a new methodology to calculate the risk/reliability of structural components and to determine inspections plans based on a probabilistic approach accounting for the variability of crack growth parameters and inspections methods' probability of detection.

An optimization process selects the inspection plan with the lowest cost attending the specified structural reliability requirements (maximum Cumulative Probability of Failure (CPOF) or its inverse, minimum Reliability (R); and maximum Single Flight Probability of Failure (SFPOF)).

A bibliographic review is presented exposing the basic concepts that fundaments this work and current probabilistic methodologies applied to aircraft structures are indicated. Each input variability modelling is discussed based on available data in literature. Monte Carlo method with Latin Hypercube Sampling is used for the probabilistic crack growth calculation. In order to reduce the number of runs to achieve a desired confidence level, Beta distribution is considered to construct a confidence band given a specified confidence level for any number (N) of Monte Carlo simulations. modeFrontier® Multi-Objective Genetic Algorithm II (MOGA II) is used for the optimization process. An example of application is presented for a typical aircraft shear joint where the results of traditional deterministic methodology are compared with the ones from the proposed methodology along with further explored ideas.

The developed methodology is divided in two main modules: one to calculate a crack size vs flight cycle's databank taking into account the variability of each inputs; and other to calculate the probabilities of failure taking into account inspections methods and intervals. The second module has an optimization process to select the inspection plan with lowest cost that meets to a specified reliability level. Figure Figure 12-1 gives an overview of the process.

The results show a potential for cost reduction along with reliability increase. Some examples of are presented in Table 12-1 and Table 12-2. Customized inspection plans for different operator may also be generated. Finally, a test validation plan for the proposed methodology is briefly outlined for future works along with a list of some aspects and ideas to be further explored.

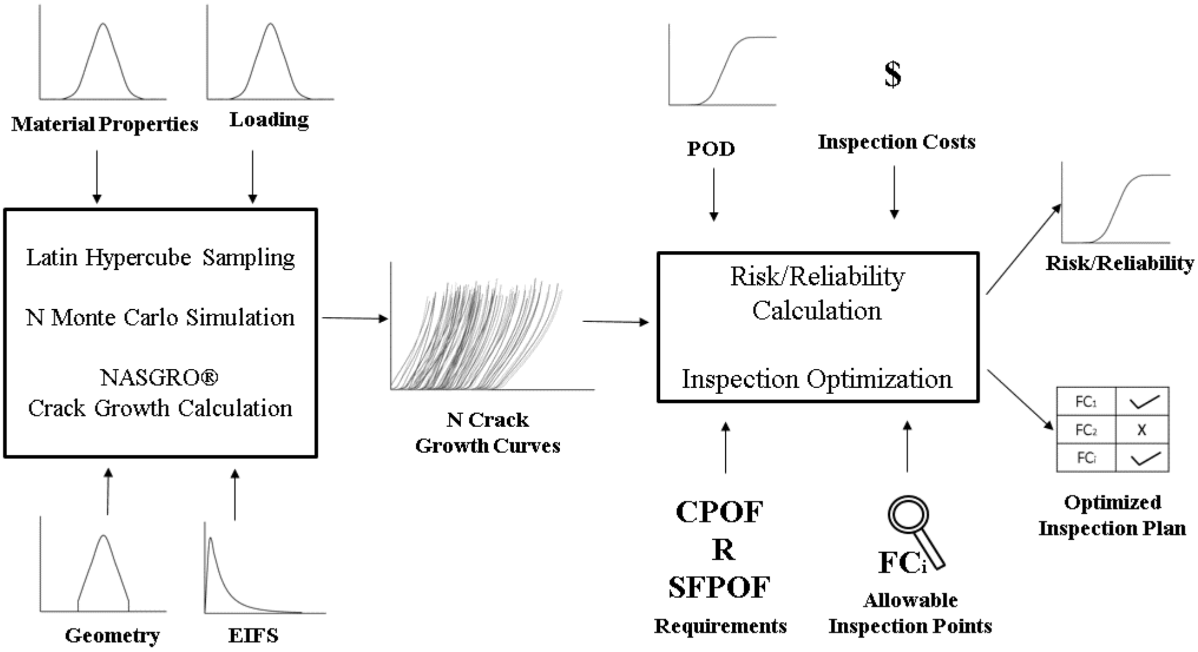

Figure 12-1 – Overview of the risk analysis process from Reference [52].

Table 12-1 – Results comparison from traditional inspection plan vs optimized inspection plan for reduced CPOF and SFPOF targets.

Calculation Process	Number of Inspections	Inspections Relative Cost	CPOF_DSG	Reliability_DSG	SFPOF
Traditional Inspections Calculation	6	8.49	5.525%	94.475%	$3.09.10^{-5}$
Probabilistic Propagation - Optimized Inspections	5	7.07	4.474%	95.526%	$2.73.10^{-5}$

Table 12-2 – Example of optimized inspection plan results by inspection method for reduced CPOF and SFPOF targets.

Method	Number of Inspections	Inspections Relative Cost	CPOF_DSG	Reliability_DSG	SFPOF
1 - Visual	15	15.00	10.816%	89.184%	$1.13.10^{-5}$
2- Eddy Current	5	7.07	4.474%	95.526%	$2.73.10^{-5}$
3- Ultrasonic	10	17.32	5.265%	94.735%	$8.73.10^{-6}$
4- Dye Penetrant	9	18.00	5.270%	94.730%	$6.41.10^{-6}$
5- X-ray	15	33.54	6.285%	93.715%	$6.80.10^{-6}$

13. LOADS

A Guidance to Derive Statistical Data for Asymmetrical Maneuvers on Transport Operation (Ref. [53])

The airplane fatigue design is based on a load history that shall represent in a reliable way the typical operational usage. To predict airplane operational loads is not an easy task, especially when the airplane design presents innovative features. In such situation, it is possible to derive loads from operational flights of similar airplanes. The flight parameters records obtained from prototype ferry flights are consolidated into a reduced information, which may be applied to an airplane design fatigue analysis. For cyclic loading conditions, such as gusts and maneuvers, the spectrum format is adopted, which consists of curves associating the parameter intensity to the exceedances (accumulated occurrences). The spectrum may be derived for different flight parameters and is treated in the aeronautical industry as an statistical representation of the data records. A good quality of the statistical data is the basis for a realistic fatigue loads, therefore, an assertive analysis and better structural dimensioning.

There are several statistical datasets presented in normative rules, like MIL, and FAA reports comprising flight loads data of commercial operation. These are references frequently adopted in the airplane design development, however there are few published statistical datasets on asymmetrical maneuvers. The loads spectra derived for these maneuvers may be essential for the design of certain components, such as control surfaces and its respective mechanisms.

In order to fill this lack, this work presents a guidance to derive maneuver statistical databank, indicating methods and criteria to process flight data, investigating and suggesting the better flight parameter to represent asymmetrical maneuvers. Moreover, presents normalized flight parameters spectra and discuss if the reduction of the flight data into a multi-parameter statistical data may lead to a generic statistical database that may be representative for different airplanes.

The generation of a statistical databank to represent these maneuvers for airplanes with variable dimensions and structural configurations may enable its re-use for future aeronautical structural designs.

The full investigation will be presented during the 30th ICAF Symposium.

14. AIRWORTHINESS

Widespread Fatigue Damage Evaluation for Multi Elements Based on a Probabilistic Approach (Ref. [55])

In order to obtain a Type Certificate for civil transport category aircraft the Applicant must to comply with some design rules - airworthiness requirements. Among those, the one associated with structural fatigue (§25.571), whose main objective is related to prevent a catastrophic event, from structural damage, during the operational life of the aircraft. That section requires special attention for Widespread Fatigue Damage (WFD). For that, the design approval holder (DAH) must establish a Limit of Validity (LOV) of the engineering data that supports the structural maintenance program. Up to the LOV, DAH must demonstrate that the aircraft will be free from WFD. A Widespread Fatigue condition can be originated from: Multi Site Damage (MSD), Multi Element Damage (MED) or a combination of both. The objective of this work is to propose a probabilistic approach to define maintenance actions to prevent widespread fatigue damage condition from Multi Element Damage up to the LOV.

To support establishment of the LOV, the DAH must demonstrate by test evidence and analysis at a minimum and, if available, service experience or by service experience plus teardown inspection results of high-time airplanes, that WFD will not occur in that airplane up to the LOV.

For any susceptible structural area, it is not a question of whether WFD will occur, but when it will occur. This "when" is called WFD Average Behavior (WFD_{AVE}), which is the point when, without intervention, half of the airplanes in a fleet would have experienced WFD in the considered area.

The main sources of engineering data to support the WFD_{AVE} are laboratory fatigue tests (full-scale fatigue tests, components tests, and teardown) and service experience. This work intends to propose an approach to establish the WFD_{AVE} for a MED scenario for a WFD_{SS} based on these sources of data.

Once WFD_{AVE} is determined, the maintenance actions (ISP- Inspection Start Point and/or SMP-Structural Modification Point) are established based on this value.

Methodology

In order to define the WFD_{AVE} is necessary to know when (in Flight Cycles, FC or Flight Hours, FH) the structure achieve the minimum residual strength - as per §25.571(b). This is an important step for MED, i.e. to evaluate the size of simultaneous cracks in its elements the structure can withstand. For the sake of clarity, a typical frame construction of five elements is considered herein, which WFD condition is established when three of these five frames are failed, independent of position.

The typical fatigue life, considered as 50% unreliability, of each frame is typically obtained from Full-Scale Fatigue Tests or Service Experience findings. In case there is no findings for one or more frames, the total cycles of FSFT is considered as the typical life for it. It is considered the fatigue behavior of elements follow a 2-parameter Weibull Distribution.

For each element, from its typical life it is generated random values based on Weibull distribution for that shape (β) and characteristic life (η).

In the assumed example (five frames), the WFD condition is established when three of this five frames are failed, independent of position. For each random set of lives, one WFD_{AVEi} is determined at the moment of three frames are failed. The WFD_{AVE} for the WFD_{SS} is defined as the moment when 50% of the airplanes in a fleet would have experienced WFD in the considered area, i.e. the moment of the fleet (in our case, the distribution of WFD_{AVEi}) reaches 50% of unreliability.

The resulting distribution of WFD_{AVE} does not necessarily follow Weibull with knowledge β as single fatigue behavior of each element. Therefore, ISP and SMP will not be defined as 1/3 and 1/2 of WFD_{AVE}, but by reliability of 1% and 5% respectively.

Results

It is assumed, arbitrary, typical lives from five elements (five frames in a row). These values may come from any source of Engineering data (Testing or Service Experience), and are assumed to already have considered any kind of adjustment. In resume, it is the time to failure of each structure.

It was considered in this example 3,000 simulations. Table 14-1 shows the first five for better comprehension – the three first failed frames, that indicates the WFD condition, are highlighted.

From the cumulative distribution it is possible to determine the WFD_{AVE}, and then the necessary maintenance actions ($ISP=N_{01}$ and $SMP=N_{05}$, in case structure is inspectable) - see Figure 14-1. The WFD_{AVE}, ISP, and SMP are defined considering the point in time immediately below the thresholds (50%, 1%, 5% for WFD_{AVE}, ISP, and SMP respectively).

Conclusions

A simple probabilistic approach for definition of WFD average behavior for MED scenarios was proposed.

The probabilistic fatigue behavior of MED scenario (herein, considered three of five frames failed) is not the same of individual one. The results demonstrate that the shape factor (for MED Weibull) is strongly dependent on the variability of the individual fatigue lives – the more variability in individual fatigue lives, the lower the shape factor. The principal effect of this is that to define maintenance actions using guidance of AC 120-104 usually results in conservative values – however in case of high dispersion this behavior might not be true.

The interaction between cracks in different elements was not considered. In case this influence cannot be neglected some reductions factors at individual lives must be considered.

This work will be presented as a poster paper during the 30th ICAF Symposium.

Table 14-1 - Determination of WFD_{AVEi}.

Simulation #	Random Lives for element *i*					WFD_{AVE}^{i}
	1	2	3	4	5	
1	102873	77094	226756	126598	**103691**	**103691**
2	61808	27824	167482	120718	77168	**77168**
3	73971	58339	**111873**	164892	120340	**111873**
4	29930	51749	235489	101060	134871	**101060**
5	105485	65053	225997	**141707**	147155	**141707**

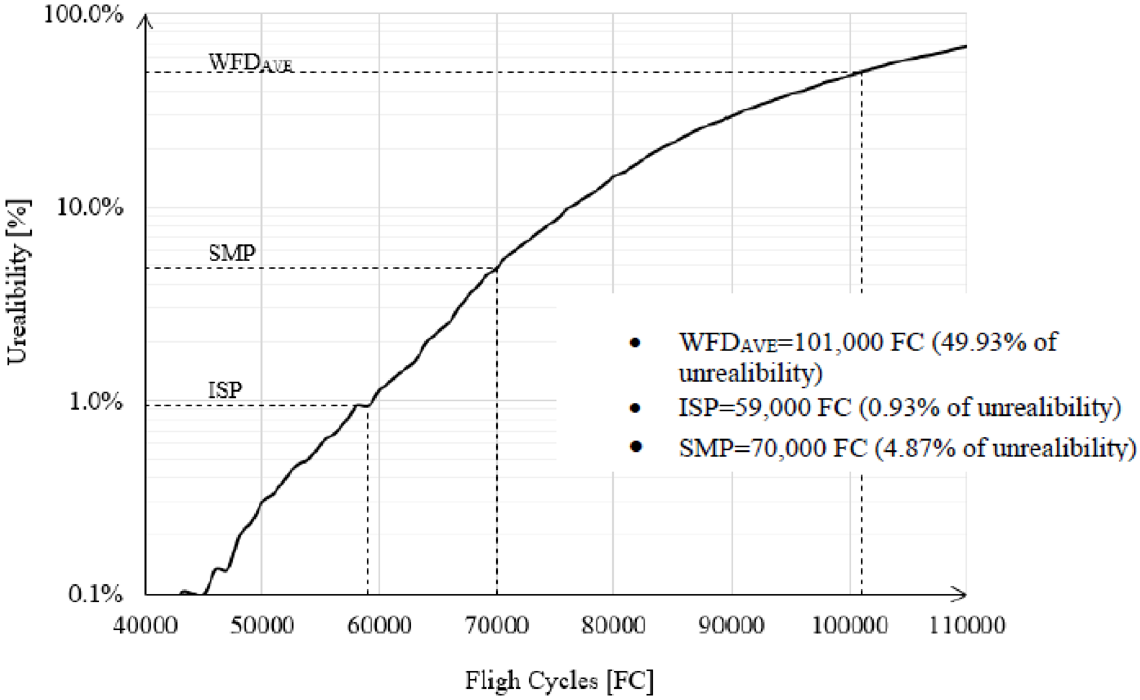

Figure 14-1 - Cumulative distribution of WFD_{AVEi}.

15. MISCELLANEOUS

The PROF Project (Refs. [56] and [57])

Embraer is one of the members of an international fatigue research project called Prediction of Fatigue in Engineering Alloys (PROF) under development in the Netherlands Aerospace Centre (NLR). Others members are Fokker, Airbus, Wartsila, Royal Netherlands Air Force, Delft University of Technology and Lloyd's Register. This four year project started in July 2016 and the objective of the project is to improve the prediction of fatigue in aluminum and other engineering alloys by the application of a more physics based approach. The main deliverable is the physical prediction model for fatigue crack growth under constant and variable amplitude fatigue that contributes to a better understanding of metallic material behavior and improved fatigue resistance. Furthermore, the physical prediction model allows obtaining accurate crack growth rates and, consequently, determining with more reliability the influence in fatigue crack growth rate of some factors like temperature, humidity and frequency.

More information about the progress of the PROF project will be presented in the National Review of the Netherlands.

MACMS 2017

At the end of 2017, in the University of São Paulo, Campus of São Carlos, it was held the MACMS 2017 - Meeting on Aeronautical Composite Materials and Structures. Despite of being a meeting with a wider scope including design, engineering and manufacturing technologies related to composite materials, many papers presented during that event were related to fatigue, damage tolerance, structural health monitoring and structural integrity of structures with composite materials, including works from brazilian researchers and works developed by researchers from foreign institutions.

The proceedings from MACMS 2017 were made available for downloading from the University of São Paulo website. The related link is shown in Ref. [58].

16. REFERENCES

1. Chaves, C. E., *A Review of Aeronautical Fatigue Investigations in Brazil*, International Committee on Aeronautical Fatigue and Structural Integrity (ICAF), Helsinki – Finland – June, 2015.

2. Chaves, C. E., *A Review of Aeronautical Fatigue Investigations in Brazil,* International Committee on Aeronautical Fatigue and Structural Integrity (ICAF), Nagoya - Japan – June, 2017.

3. Donadon, M.V., Arbelo, M.A., Castro, S.G.P., Shiino, M.Y., Amaro, L., Montestruque, C.V., Rizzi, P., A *Multiaxial Fatigue Damage Model for Isotropic Materials*, presented during the ICAF 2019 Symposium, Krakow, Poland.

4. Oliveira, L.A., Donadon, M.V., Arbelo, M.A., *Fatigue-driven Delamination in Composites and Adhesives*, presented during the ICAF 2019 Symposium, Krakow, Poland.

5. Dugdale, D., *Yielding of Steel Sheets Containing Slits*. Journal of the Mechanics and Physics of Solids 1960;8:100-104.

6. Blanco, N., Gamstedt, E.K., Asp, L.E., Costa, J., *Mixed-mode Delamination Growth in Carbon–Fibre Composite Laminates under Cyclic Loading*. International Journal of Solids and Structures, 2004;41:4219-4235.

7. Donadon, M.V., de Almeida, S.F.M., Arbelo, M.A., de Faria, A.R. *A Three-Dimensional Ply Failure Model for Composite Structures in Carbon–fibre Composite Laminates Under Cyclic Loading*. International Journal of Aerospace Engineering 2009.

8. Asp, L.E., Sjögren, A., Greenhalgh, E.S., *Delamination Growth and Thresholds in a Carbon/Epoxy Composite Under Fatigue Loading*. Journal of Composites Technology & Research 2001;23(2):55–68.

9. Marcolin, M. L., *A Numerical Tool for Fatigue Induced Failure Analysis in the Frequency Domain*, MSc Dissertation, ITA, 2018.

10. Angelo, M.V., Ribeiro, M.L., Tita, V., *A Computational Framework for Predicting Onset and Crack Propagation in Composite Structures via EXtended Finite Element Method (XFEM)*, Latin American Journal of Solids and Structures, 2018.

11. Angelo, M.V., *Análise Quase-Estática de Estruturas Escalonadas Laminadas em Material Compósito via Modelo Fenomenológico de Falhas e Elementos Finitos Estendidos: Desenvolvimento de uma Ferramenta Computacional*, PhD Thesis, University of São Paulo, 2018.

12. Jamali, J. *Mechanistic Failure Criterion for Unidirectional and Random Fibre Polymer Composites*. The University of Western Ontario, 2014.

13. Sartorato, M., *Micro and Macroscale Analyses for Prognosis of Composite Structures: A new Physics Based Multiscale Methodology*, PhD Thesis, University of São Paulo, 2018.

14. Sá, M.V.C., Ferreira, J.L.A., da Silva, C.R.M., Araújo, J.A., *The Role of the Shear and Normal Stress Gradients on Life Estimation of Notched Al7050-T7451 Under Multiaxial Loadings*, Theoretical and Applied Fracture Mechanics 97 (2018) 38–47.

15. Pereira, G.S., Teixeira, G.B., Bose Filho, W.W., *Microstructural and Mechanical Characterization of WE43 Magnesium Alloy*, 25th ABCM International Congress of Mechanical Engineering, Uberlândia, Brazil, 2019.

16. Araújo, J.A., Almeida, G.M.J., Ferreira, J.L.A. , da Silva, C.R.M., Castro, F.C., *Early Cracking Orientation Under High Stress Gradients: The Fretting Case*, International Journal of Fatigue 100 (2017) 611–618.

17. Araújo, J.A., Susmel, L., Pires, M.S.T., Castro, F.C., *A Multiaxial Stress-based Critical Distance Methodology to Estimate Fretting Fatigue Life*, Tribology International 108 (2017) 2–6.

18. Carpinteri, A., Ronchei, C., Spagnoli, A., Vantadori, S., *On the use of the Prismatic Hull Method in a Critical Plane-based Multiaxial Fatigue Criterion*, International Journal of Fatigue 68 (2014) 159–167.

19. Lima, M.S.F., Carvalho, S.M. , Siqueira, R.H.M., Cunha, M.C., Gonçalves, C.M., Godefroid, L.B., *Laser-induced Heating for Enhanced Fatigue Life of Aerospace Aluminum Alloys*, Journal of the Brazilian Society of Mechanical Sciences and Engineering.

20. Cunha, M.C., *Tratamento Superficial a Laser para Modificação da Velocidade de Propagação de Trincas por Fadiga em Ligas de Alumínio Aeronáutico*, MSc Dissertation, ITA, 2018.

21. Carvalho, A.L.M., Martins, J.P., Pereira, V.F., Fernandez, F.F., *Application of Friction Surfacing to the Production of Aluminum Coatings on the Aeronautical Alloys*, 17th MRS Meeting, Natal - RN, Brazil, September 2018.

22. Mendonça, W.R.P., Silva, D.F.N.R., *Analysis Prediction and Correlation of Fiber Metal Laminate (FML) Crack Propagation in Semi-wing Full-scale Test*, ICAF 2019, Krakow, Poland.

23. Felix, P.H. W., *Crack Growth Analysis of Panels with Different Construction Methodologies*, ITA, 2019 (not available for public release).

24. Bakuckas, Jr., J.G., Stonaker, K., Stanley, D., Tian, Y., Kulak, M., Chang, P.Y., Freisthler, M., Rodrigues, M.R.B., Chaves, C.E., Fanton, F., *Assessment of Emerging Metallic Structures Technology through Test and Analysis of Fuselage Structure*, ICAF 2019, Krakow, Poland.

25. Van den Akker, B., *Durability of Co-bonded Stiffened CFRP Panels Subjected to Post-bucking Fatigu*e, MSc Dissertation, ITA, 2018.

26. Cederløf, D.J.H., *Durability of Stiffened CFRP Panels with Initial Delaminations*, MSc Dissertation, TU Delft, 2018.

27. Leite, B.M., Leite, L.F.M., Reis, V.L., Donadon, M.V., Silveira, N.N.A., *Strain Rate Effects on the Intralaminar Fracture Toughness of Composite Laminates Subjected to Compressive Loads*, Composite Structures, Volume 186, 15 February 2018, Pages 94-105.

28. Leite, L.F.M., Leite, B.M., Reis, V.L., Silveira, N.N.A., Donadon, M.V., Strain Rate *Effects on the Intralaminar Fracture Toughness of Composite Laminates Subjected to Tensile Loads*, Composite Structures, Volume 201, 1 October 2018, Pages 455-467.

29. Brito, C. B. G., *Hygrothermal Effects on Interlaminar Fracture Toughness of Composite Joints*, MSc Dissertation, ITA, 2017.

30. Brito, C.B.G, Contini, R.C.M.S., Gouvêa, R.F., Oliveira, A. S., Arbelo, M.A., Donadon, M.V., *Mode I Interlaminar Fracture Toughness Analysis of Co-Bonded and Secondary Bonded Carbon Fiber Reinforced Composites Joints*, Materials Research. 2017; 20 (Suppl. 2): 873-882.

31. Ramírez, F.M.G., *Hygrothermal Effects on the Fatigue Delamination Growth Onset in Composite Joints*, MSc Dissertation, ITA, 2018.

32. Ramírez, F.M.G., Garpelli, F.P., Sales, R.C.M., Cândido, G.M., Arbelo, M.A., Donadon, M.V., *Experimental Characterization of Mode I Fatigue Delamination Growth Onset in Composite Joints: A Comparative Study*, Materials and Design 160 (2018) 906-914.

33. Garpelli, F.P., *Experimental Characterization of Fatigue Delamination Growth Onset in Composite Joints Tested at Room Temperature Ambient Condition (RTA)*, MSc Dissertation, ITA, 2018.

34. Garpelli, F.P., Ramírez, F.M.G., Resende, H.B., Donadon, M.V., *Structural Behavior of Secondary-bonded Composite Joints Subjected to Mode II Fatigue Induced Delamination*, 39th Risø International Symposium on Materials Science, IOP Conf. Series: Materials Science and Engineering 388 (2018).

35. Silveira, N.N.A., *Fractographic Analysis of Adhesive by Bonded Technologies Applied to Advanced Composite Aerostructures*, MSc Dissertation, ITA, 2018.

36. Souza, R.R.R., Nascimento Jr., S.L., Silveira, N.A., Arbelo, M.A., Donadon, M.V., *Translaminar Fracture Toughness and Fatigue Crack Growth Characterization of Carbon-Epoxy Plain Weave Laminates*, Polymer Composites, 2019.

37. Shiino, M.Y., Ramírez, F.M.G., Garpelli, F.P., Silveira, N.N.A., Sales, R.C.M., Donadon, M.V., *Interlaminar Crack Onset in Co-cured and Co-bonded Composite Joints under Mode I Cyclic Loading*. Fatigue and Fracture of Engineering Materials and Structures, 2019;42:752–763.

38. Shiino, M.Y., Pelosi, T.S., Cioffi, M.O.H., Donadon, M.V., *The Role of Stitch Yarn on the Delamination Resistance in Non-crimp Fabric: Chemical and Physical Interpretation*, Journal of Materials Engineering and Performance 978 - Volume 26(3), 2017.

39. Souza, A., Gomes, G.F., Isaías, J.C., Ancelotti Jr., A.C., *A Numerical-Experimental Evaluation of the Fatigue Strain Limits of CFRP Subjected to Dynamic Compression Loads*, The International Journal of Advanced Manufacturing Technology (2019).

40. Feistauer, E.E., *Ultrasonic Joining of Through-the-thickness Reinforced Metal-Composite Hybrid Structures*, PhD Thesis, Technical University of Hamburg, 2018.

41. Feistauer, E.E., Santos, J.F., Amancio-Filho, S.T., *A Review on Direct Assembly of Through-the-Thickness Reinforced Metal–Polymer Composite Hybrid Structures*, Polymer Engineering & Science, 2018.

42. Marques, D., Flor, F.R., Medeiros, R., Pagani Jr., C.C., Tita, V., *Structural Health Monitoring of Sandwich Structures*, MECSOL 2017, Joinville - SC, Brazil.

43. Marques, D., Flor, F.R., Medeiros, R., Pagani Jr., C.C., Tita, V., *Structural Health Monitoring of Sandwich Structures Based on Dynamic Analysis*, Latin American Journal of Solids and Structures, 2018.

44. Marques, D., Ferreira, A.J.M., Tita, V., *Structural Health Monitoring of Thin Thermoplastic Composite Plates Via Vibration Based Method*, Meeting on Aeronautical Composite Materials and Structures - MACMS 2017.

45. Dorneles, L., Oliveira, H., Clarke, T., Dotta, F., Tamba, A., Rulli, R.P., *Reliability of Lamb Wave SHM Systems: influence of Hydrostatic Pressure and Mechanical Loading*, 7th Asia-Pacific Workshop on Structural Health Monitoring November 12-15, 2018 Hong Kong SAR, P.R. China.

46. Rulli, R.P., Dotta, F., Prado, G.O.C, Roach, D., Rice, T., *Advancements on the Adoption of SHM Damage Detection Technologies into Embraer Aircraft Maintenance Procedures*, presented in the 11th Workshop of Structural Health Monitoring, IWSHM 2017, Stanford - CA, USA.

47. Dotta, F., Silva, P.A., Vieira, L.C., Tamba, A.K.F., Prado, G.O.C., Roach, D., Rice, T., *SHM Qualification Process and the Future of Aircraft Maintenance*, presented in the 31st Congress of the International Concil of the Aeronautical Sciences, ICAS 2018, Belo Horizonte, Brazil.

48. Tamba, A.K.F., Vieira, L.C., Prado, G.O.C., Dotta, F., Rulli, R.P., Silva, P.A., Cunha, R.R., Costa, J.P., *Corrosion Detection in Aeronautical Structures Using Lamb Waves System for SHM,* presented in the 31st Congress of the International Concil of the Aeronautical Sciences, ICAS 2018, Belo Horizonte, Brazil.

49. Prado, G.O.C., Silva, P.A., Simomura, F.M., Pereira, K.L.O., *Structural Health Monitoring with Augmented Reality for Aircraft Maintenance*, presented in the 31st Congress of the International Concil of the Aeronautical Sciences, ICAS 2018, Belo Horizonte, Brazil.

50. Gomes, G.F., Almeida, F.A., Cunha Jr., S.S., Ancelotti Jr., A.C., *An Estimate of the Location of Multiple Delaminations on Aeronautical CFRP Plates Using Modal Data Inverse Problem*, The International Journal of Advanced Manufacturing Technology (2018) 99:1155–1174.

51. Gomes, G.F., Cunha Jr., S.S., Ancelotti Jr., A.C., *A Sunflower Optimization (SFO) Algorithm Applied to Damage Identification on Laminated Composite Plates*, Engineering with Computers, 2018.

52. Oliveira, M.C.C.Z., *Aircraft Structural Inspections Definition Considering Probabilistic Analysis of Failures Based on Variability of Crack Growth Parameters and Probability of Detection*, MSc Dissertation, 2018.

53. Mattos, J.D., Peixoto, D.S., Machado, F., *A Guidance to Derive Statistical Data for Asymmetrical Maneuvers on Transport Operation*, ICAF 2019, Krakow, Poland.

54. Ximenes, I.B.O., Mattos, D.F.V., Bürger, D., Ribeiro, F.N., *Load Spectrum for a Fatigue Life Test of a Landing Gear: a Case Study*, ICAF 2019, Krakow, Poland.

55. Hernandes, F., *Widespread Fatigue Damage Evaluation for Multi Elements* Based on a Probabilistic Approach, ICAF 2019, Krakow, Poland.

56. Amsterdam, E., Prediction of Fatigue in Engineering Alloys (PROF), NLR Proposal, July. 2016.

57. New Partnership on Research of Aluminium and Steel – NLR website https://www.nlr.org/news/new-partnership-on-research-of-fatigue-of-aluminium-and-steel/

58. MACMS 2017, Meeting on Aeronautical Composite Materials & Structures http://www.biblioteca.eesc.usp.br/images/soac/macms/anaisEletronicosMacms2017.pdf (accessed in April, 2019).